FUNDAMENTALS OF SPUTTER DEPOSITION

Ivan Petrov
Materials Research Laboratory, University of Illinois at Urbana-Champaign, USA
Department of Physics, Chemistry, and Biology, Linköping University, Sweden

petrov@illinois.edu

RWTH Aachen University
February 10, 2025

REVIEW ARTICLE

Review Article: Tracing the recorded history of thin-film sputter deposition: From the 1800s to 2017

J. E. Greene[a)]
D. B. Willett Professor of Materials Science and Physics, University of Illinois, Urbana, Illinois, 61801; Tage Erlander Professor of Physics, Linköping University, Linköping, Sweden, 58183, Sweden; and University Professor of Materials Science, National Taiwan University Science and Technology, Taipei City, 106, Taiwan

Citation: Journal of Vacuum Science & Technology A: Vacuum, Surfaces, and Films **35**, 05C204 (2017); doi: 10.1116/1.4998940
View online: https://doi.org/10.1116/1.4998940

526 references; open access

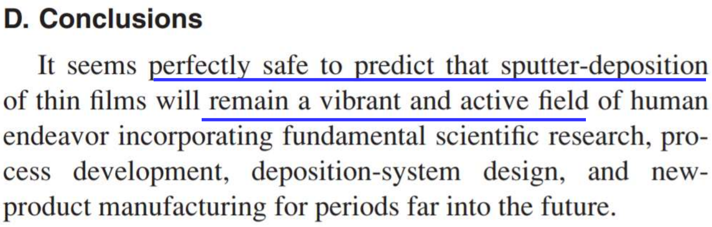

D. Conclusions

It seems perfectly safe to predict that sputter-deposition of thin films will remain a vibrant and active field of human endeavor incorporating fundamental scientific research, process development, deposition-system design, and new-product manufacturing for periods far into the future.

Sputter deposition

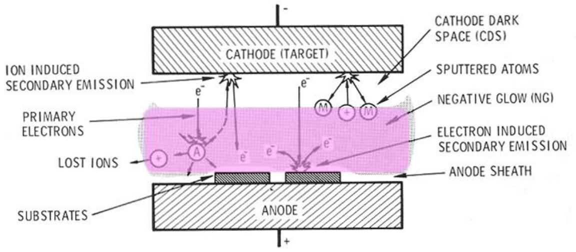

Basics:

- A voltage is applied across a rarified gas in a vacuum.
- Breakdown of the gas forms a glow discharge plasma.
- Positive ions from the plasma strike the negative electrode (cathode/target).
- Energy from the ions is transferred to target atoms.
- A few of these may escape from the target surface (they are sputtered).
- Sputtered atoms undergo collisions in the gas phase
- Some of the sputtered atoms reach the substrate
- The sputtered atoms condense on the substrate forming a film.

Sputter deposition

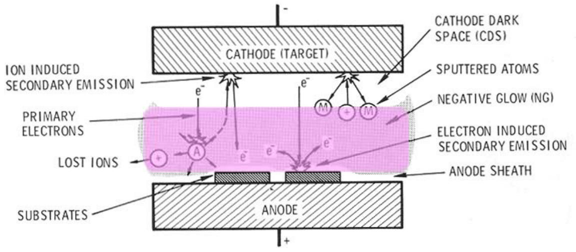

Important processes:

- Ion-solid interactions on the target.
- Plasma generation and discharge maintenance
- Collisions in the gas phase – ionization, scattering.
- Nucleation and film growth on the substrate.
- Use of ion solid interactions to modify film growth

Part 1. Fundamentals of Sputter Deposition

1.1 Elements of kinetic theory of gases
- Gas laws
- mean free path
- gas impingement rate

1.2 Elements of plasma physics
- Plasma probes
- Sheath width
- Penning ionization
- Electron energy distribution functions

1.3 Glow discharge maintenance
- Secondary ion-electron emission
- Electron ionization cross-sections

1.4 Sputtering yield
- Linear cascade model
- Correction for threshold effects
- Sputtering efficiency
- Energy of sputtered atoms
- Other energetic particles: backscattered ions and negative oxygen ions

1.5 Transport in the gas phase
- Thermalization
- Deposition rate calculation

1.6 Sputtering systems
- Magnetron sputtering
- Reactive sputtering

1.7 HIPIMS
- Source of metal ions
- Time separation between gas and metal ions
- High energy ions
- Lower deposition rates
- Bipolar HIPIMS
- Control of doubly charged ions

Elements of Kinetic Theory of Gases

For gas phase transport we need some basic formulas from the **kinetic theory of gases**

Mean free path $$\lambda = \frac{1}{\sqrt{2}\, n\, \sigma}$$

Gas density $$n = \frac{p}{kT}$$

Average velocity $$\bar{v} = \sqrt{\frac{8kT}{\pi m}}$$

Impinging gas flux on the walls $$J_g = \frac{n\bar{v}}{4} = \frac{p}{\sqrt{2\pi mkT}}$$

Modifications of these expressions are used in plasma physics

---

Kinetic theory of gases

provides microscopic picture of gas laws

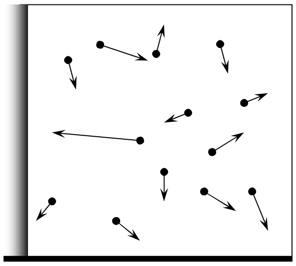

Assumptions:

- A gas consists of a large number of molecules;
- separations are large compared to molecule size
- Molecules move randomly with a distribution in velocities which remains constant
- Molecules obey Newton laws of motion.
- Elastic collisions between the molecules and between molecules and the walls; no forces otherwise.

Pressure of gas molecules

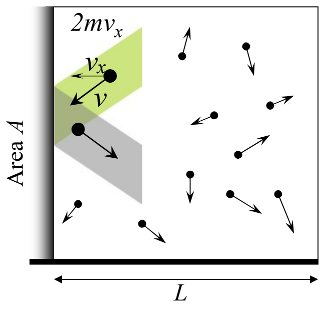

$n = \frac{N}{V}$

$p = F/A$ units [N/m^2] or [Pa]

Momentum change in one collision – $\Delta p = 2\,m\,v_x$
Time between collisions – $\Delta t = 2L/v_x$
Force by one molecule – $\Delta p/\Delta t = m\,v_x^2/L$
Force by N molecules – $N\,m\,v_x^2/L$
Pressure – $p = N\,m\,v_x^2/L\,A = n\,m\,v_x^2$

However, the average kinetic energy in x
$E = ½\,mv_x^2 = ½\,kT$

$$\boxed{p = n\,k\,T}$$

Ideal gas laws:
Boyle: p ~1/V
Charles: V ~ T
Gay-Lussac: p ~ T

N - number of molecules
V - volume (= *L x A*)
p - pressure
T - absolute temperature
m, v - mass and velocity of molecules
k - Boltzmann constant = 1.38 10 $^{-23}$ [J/K]

Velocity and energy distribution of gas molecules

Maxwell-Boltzmann distribution

Velocity

$$f(v) = 4\pi\,(\frac{m}{2\pi\,kT})^{\frac{3}{2}}\,\exp(-\frac{m}{2\,kT}v^2)\,v^2$$

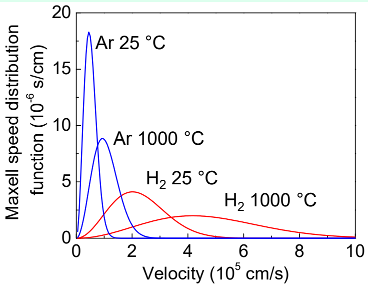

Energy

$$f(e) = 2\pi\,(\frac{1}{\pi\,kT})^{\frac{3}{2}}\,\exp(-\frac{e}{kT})\,\sqrt{e}$$

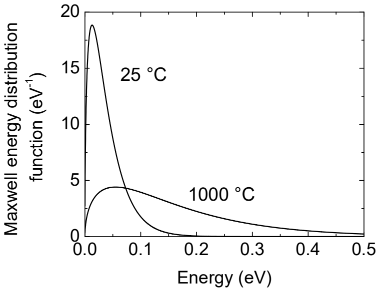

average

$$v_{av} = \sqrt{\frac{8}{\pi}}\sqrt{\frac{kT}{m}}$$

root-mean-square

$$v_{rms} = \sqrt{3}\,\sqrt{\frac{kT}{m}}$$

most probable

$$v_p = \sqrt{2}\,\sqrt{\frac{kT}{m}}$$

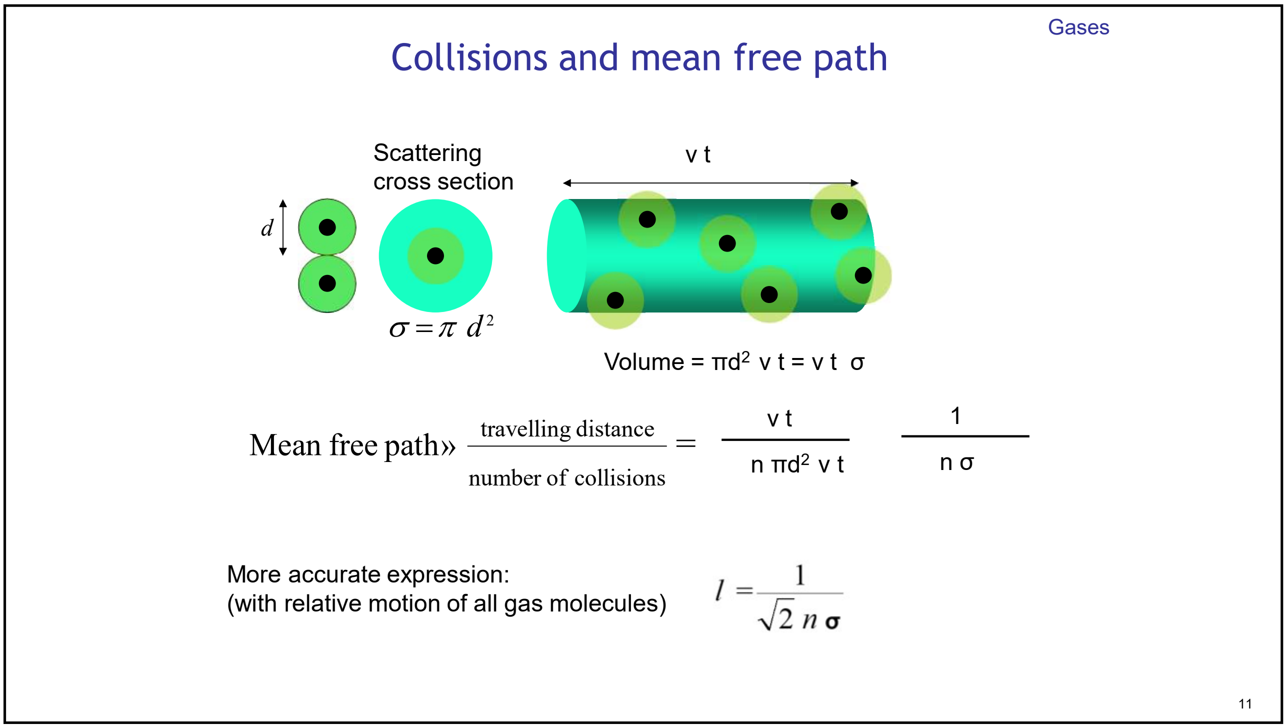

Collisions and mean free path

$\sigma = \pi\ d^2$

Volume = πd^2 v t = v t σ

Mean free path» $\dfrac{\text{travelling distance}}{\text{number of collisions}} = \dfrac{v\ t}{n\ \pi d^2\ v\ t} \quad \dfrac{1}{n\ \sigma}$

More accurate expression:
(with relative motion of all gas molecules)

$$l = \frac{1}{\sqrt{2}\ n\ \boldsymbol{\sigma}}$$

Some useful formulas from kinetic theory of gases

Mean free path $\lambda = \dfrac{1}{\sqrt{2}\ n\ \sigma}$

Gas density $n = \dfrac{p}{kT}$

Average velocity $\boldsymbol{\bar{v}} = \sqrt{\dfrac{\boldsymbol{8kT}}{\boldsymbol{\pi m}}}$

Impinging gas flux on the walls $J_g = \dfrac{n\bar{v}}{4} = \dfrac{p}{\sqrt{2\pi mkT}}$

Deposition flux
growth rate R [cm/s]
films density n_{dep} [at/cm^3]

$$J_{dep} = Rn_{dep}$$

Note: from the bottom two expressions one can calculate the expected contamination of the films due to residual gases from the background pressure and the deposition rate J_g/J_{dep}

Examples

	λ		J (cm^{-2} s^{-1})		t_{ML}
	25ºC	1000ºC	25ºC	1000ºC	25ºC
1 atm (10^5 Pa)	100 nm	400 nm	2.4 $\times 10^{23}$	1.2 $\times 10^{23}$	4 ns
1 Torr (133 Pa)	70 µm	300 µm	3.2 $\times 10^{20}$	1.6 $\times 10^{20}$	3.0µs
1 mTorr (0.133)	7 cm	30 cm	3.2 $\times 10^{17}$	1.6 $\times 10^{17}$	3.0 ms
10^{-6} Torr	70 m	300 m	3.2 $\times 10^{14}$	1.6 $\times 10^{14}$	3.0 s
10^{-11} Torr	7,000 km	30,000 km	3.2 $\times 10^{9}$	1.6 $\times 10^{9}$	84 hours

λ: mean free path

J: flux of the atoms on sample/walls

t_{ML}: time to form a monolayer (ML) at sticking probability of 1

diameter of a gas atom ~ 3 x 10 $^{-8}$ cm; area of a gas atom ~ 10^{-15} cm^2
one monolayer ~ 10^{15} atoms cm^{-2}

For comparison: Ti growth with 1 µm/h J_{Ti} = 1.6 x 10^{15} (cm^{-2} s^{-1})

Elements of Plasma Physics

Sputter deposition plasmas

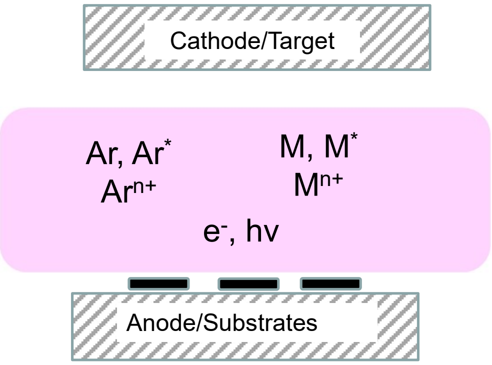

Many plasma particles:

- neutral atoms, gas and target
- electrons
- ions, gas and target
- excited atoms, gas and target
- plasma radiation

Which are most important plasma species for film growth?

↙ ↘

DCMS ↓ gas ions (thermal) ↙ $E_i = e(V_{plasma} - V_{bias})$

HIPIMS ↓ target ions (energetic) ↘ $E_i = e(V_{plasma} - V_{bias}) + \langle E_{gas\ phase} \rangle$

Plasma characterization by electrostatic probes

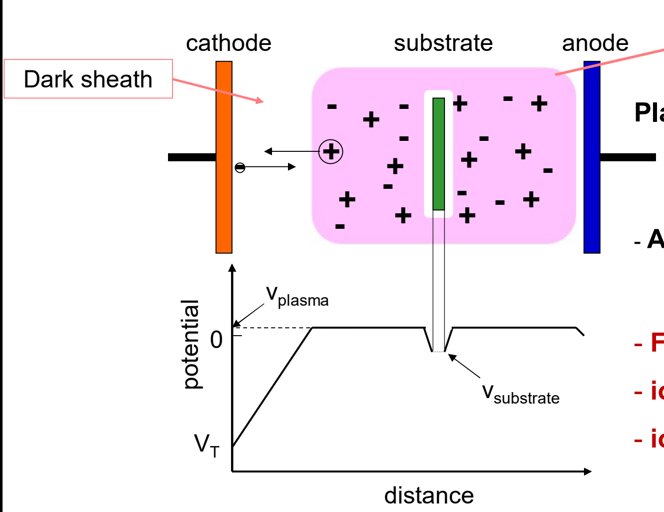

Plasma parameters

- Electron density & temperature : n_e, T_e
- Ion density & temperature : n_i, T_i
- Plasma potential : V_{plasma}

- **Assumptions**

- Singly charged ions : $n_e \approx n_i$
- Cold ions : $T_i \ll T_e$

- For film growth we need to know:

- ion flux J_i and

- ion energy $E_i \approx e(V_{substrate} - V_{plasma})$

Discharge

Why is the dark sheath dark?

Because electron leave the cathode with energy well above the maximum of the excitation cross section

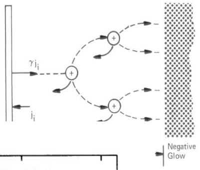

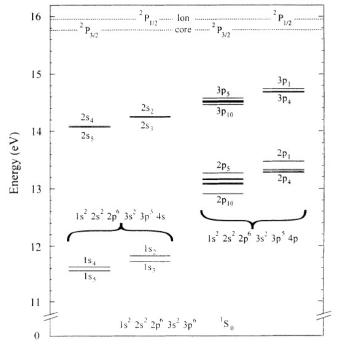

FIG. 1. Energy-level diagram of the argon atom. The Paschen notation ($1s_2$, $1s_3$, $1s_4$, and $1s_5$ and $2p_1, 2p_2, \ldots, 2p_{10}$) is used to label the energy levels associated with the $1s^22s^22p^63s^23p^54s$ and the $1s^22s^22p^63s^23p^54p$ configurations.

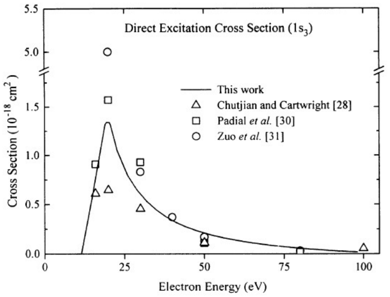

FIG. 13. Comparison of experimental and theoretical results for the energy dependence and magnitude of the direct excitation cross section for the $1s_3(J=0)$ metastable level.

PHYSICAL REVIEW A VOLUME 50, NUMBER 1 JULY 1994

Measurements of cross sections for electron-impact excitation into the metastable levels of argon and number densities of metastable argon atoms

R. Scott Schappe, M. Bruce Schulman,* L. W. Anderson, and Chun C. Lin
Department of Physics, University of Wisconsin, Madison, Wisconsin 53706

(Received 20 December 1993)

Sheath width between the plasma and a negatively biased electrode (target or substrate)

Plasma

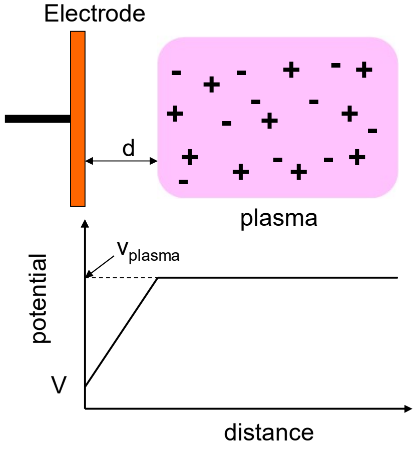

Child-Langmuir formula

$$d^2 = \frac{4\varepsilon_0}{9}\left(\frac{2e}{m}\right)^{1/2}\frac{V^{3/2}}{j}$$

V – bias voltage
j – ion current density
m – ion mass

$$for\quad Ar^+ \longrightarrow d^2[m^2] = \frac{4\times 8.854\times 10^{-12}}{9}\left(\frac{2\times 1.6\times 10^{-19}}{40\times 1.66\times 10^{-27}}\right)^{1/2}\frac{V^{3/2}[V]}{j\left[\frac{A}{m^2}\right]} = 8.64\times 10^{-9}\,\frac{V^{3/2}}{j}$$

Mean free path

$$\lambda = \frac{1}{\sqrt{2}\,n\,\sigma}$$

We use this expression to compare the sheath width with **the ion mean free path** and evaluate the energy of the impinging ions on the electrode (target or substrate)

Plasma parameters

- Electron density & temperature : n_e, T_e
- Ion density & temperature : n_i, T_i
- Plasma potential : V_{plasma}

- Assumptions

- Singly charged ions : $n_e \sim n_i$
- Cold ions : $T_i << T_e$

- For film growth we need ion flux J_i and ion energy $E_i \sim e(V_{substrate} - V_{plasma})$

- Fluxes (in analogy with the kinetic theory of gases)

$$J_{i,e} = \frac{n_{i,e}\overline{v_{i,e}}}{4} = \frac{n_{i,e}}{4}\sqrt{\frac{8kT_{i,e}}{\pi m_{i,e}}} = 0.4 n_{i,e}\sqrt{\frac{kT_{i,e}}{m_{i,e}}}$$

Bohm presheath

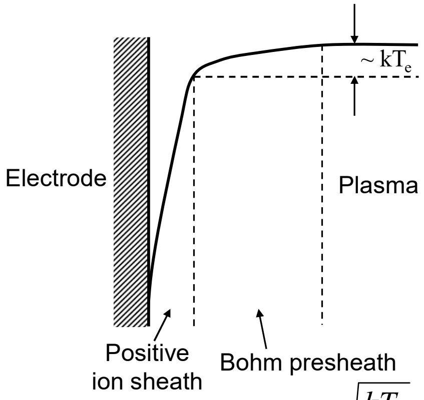

Ions at the edge of the sheath are accelerated to a velocity which depends on the electron temperature

$$v_i \sim \sqrt{\frac{kT_e}{m_i}}$$

$$J_i = 0.6 n_i \sqrt{\frac{kT_e}{m_i}} \longleftarrow \text{Electron temperature!!}$$

Ion flux is a function of the electron temperature T_e, not T_i

S D Baalrud and C C Hegna, Kinetic theory of the presheath and the Bohm criterion, Plasma Sources Sci. Technol. 20 (2011) 025013

Langmuir Probe Characteristics

small wire probe

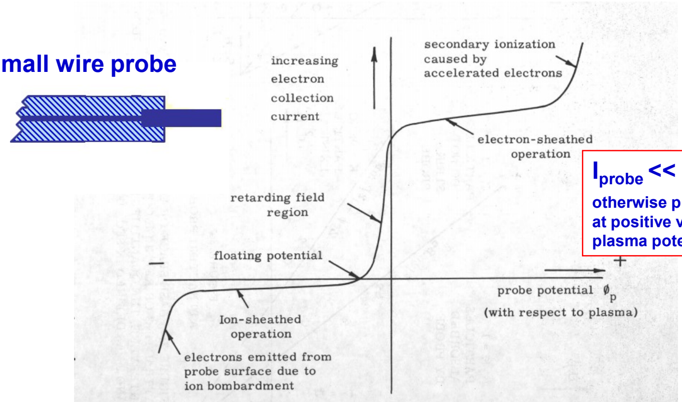

FIGURE 2

COMPLETE LANGMUIR PROBE CHARACTERISTIC.
(AFTER REF. 2) ION CURRENT EXAGGERATED.

$I_{probe} << I_{discharge}$

otherwise probe becomes an anode at positive voltages and affects the plasma potential

Laframboise, J.G.
University of Toronto, Institute of Aerospace Studies, Report No 100

Available to download – Google it.

Idealized Probe Characteristics

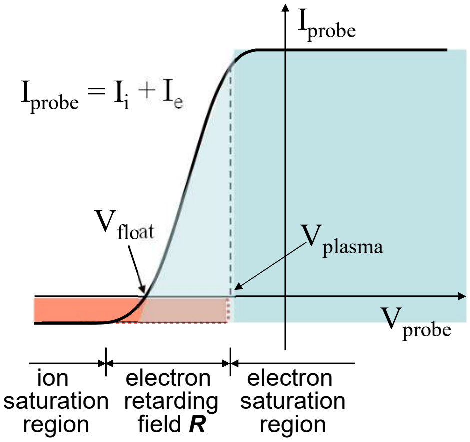

$V_{probe} > V_{plasma}$

$$I_e = I_e^{sat} = eJ_e = 0.4en_e\sqrt{\frac{kT_e}{m_e}}$$

$$I_i = 0$$

$V_{probe} \le V_{plasma}$

$$I_i = I_i^{sat} = eJ_i = 0.6en_i\sqrt{\frac{kT_e}{m_i}}$$

$$I_e = I_e^{sat} e^{-\frac{e(V_{probe}-V_{plasma})}{kT_e}}$$

$$\frac{I_e^{sat}}{I_i^{sat}} = \frac{0.4}{0.6}\sqrt{\frac{m_i}{m_e}} \quad >>1$$

Electrons much lighter; for Ar^+ the ratio is ~ 200

NB; magnetic field affects the motion of the electrons and this ratio could be smaller

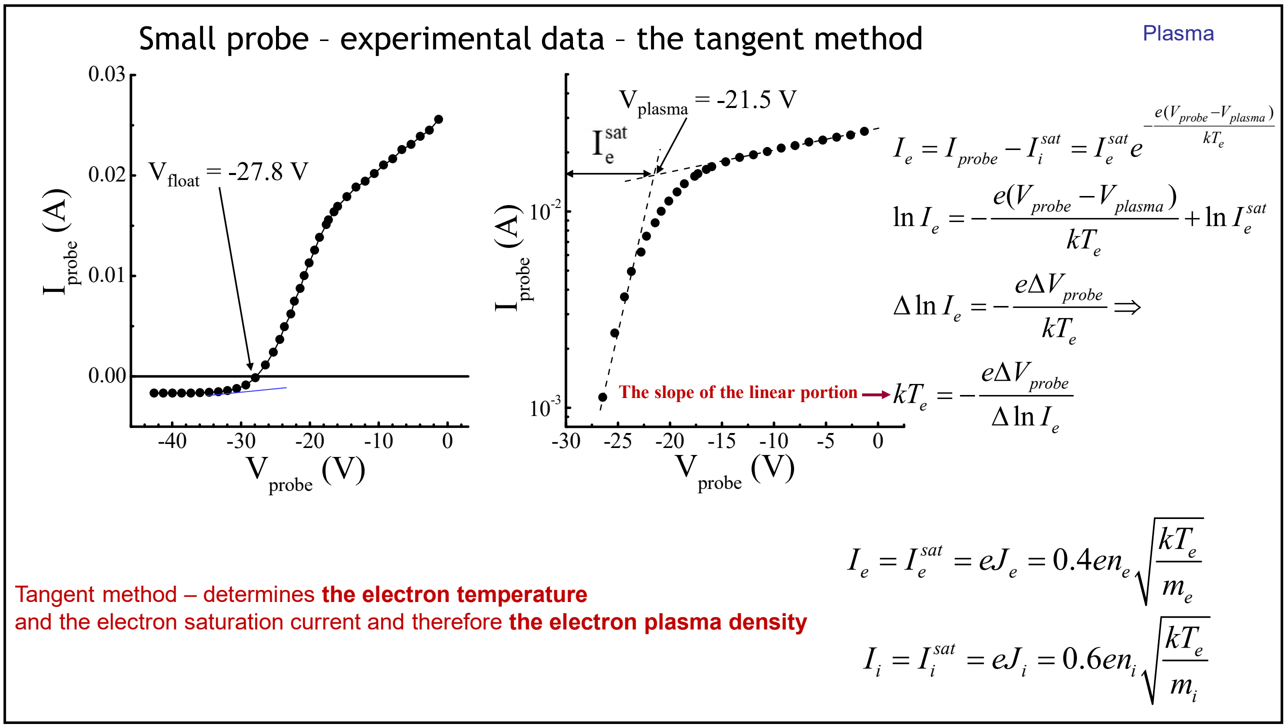

Small probe – experimental data – the tangent method

$$I_e = I_{probe} - I_i^{sat} = I_e^{sat} e^{-\frac{e(V_{probe}-V_{plasma})}{kT_e}}$$

$$\ln I_e = -\frac{e(V_{probe}-V_{plasma})}{kT_e} + \ln I_e^{sat}$$

$$\Delta \ln I_e = -\frac{e\Delta V_{probe}}{kT_e} \Rightarrow$$

The slope of the linear portion →

$$kT_e = -\frac{e\Delta V_{probe}}{\Delta \ln I_e}$$

$$I_e = I_e^{sat} = eJ_e = 0.4en_e\sqrt{\frac{kT_e}{m_e}}$$

$$I_i = I_i^{sat} = eJ_i = 0.6en_i\sqrt{\frac{kT_e}{m_i}}$$

Tangent method – determines **the electron temperature**
and the electron saturation current and therefore **the electron plasma density**

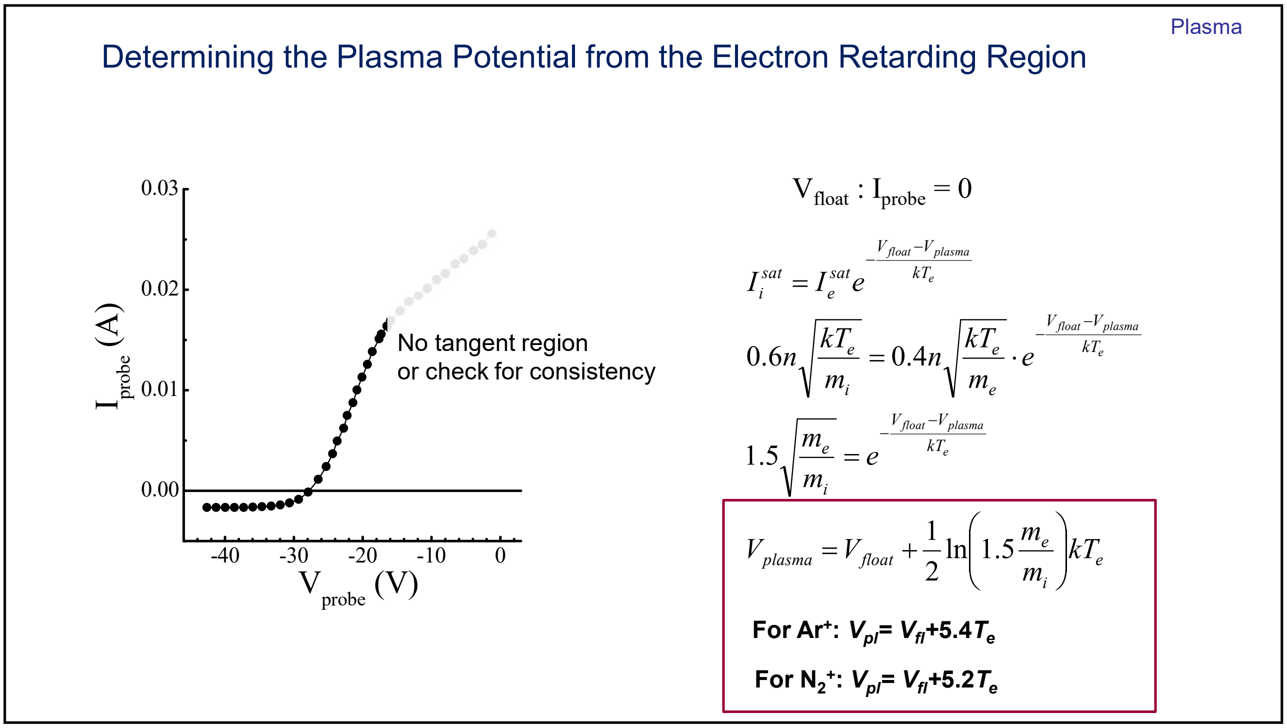

Determining the Plasma Potential from the Electron Retarding Region

No tangent region
or check for consistency

$$V_{float} : I_{probe} = 0$$

$$I_i^{sat} = I_e^{sat} e^{-\frac{V_{float}-V_{plasma}}{kT_e}}$$

$$0.6n\sqrt{\frac{kT_e}{m_i}} = 0.4n\sqrt{\frac{kT_e}{m_e}} \cdot e^{-\frac{V_{float}-V_{plasma}}{kT_e}}$$

$$1.5\sqrt{\frac{m_e}{m_i}} = e^{-\frac{V_{float}-V_{plasma}}{kT_e}}$$

$$V_{plasma} = V_{float} + \frac{1}{2}\ln\left(1.5\frac{m_e}{m_i}\right)kT_e$$

For Ar^+: $V_{pl} = V_{fl} + 5.4T_e$

For N_2^+: $V_{pl} = V_{fl} + 5.2T_e$

Small probe – experimental data

The ion saturation region – how can we use it? difficult

Plasma

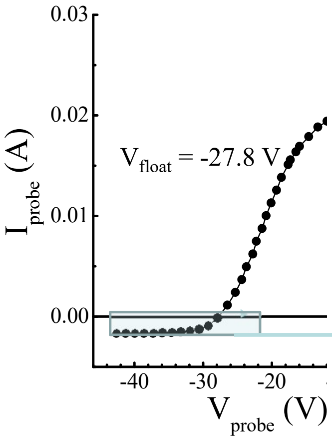

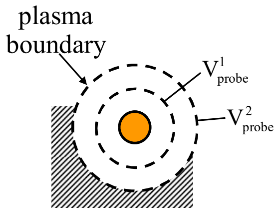

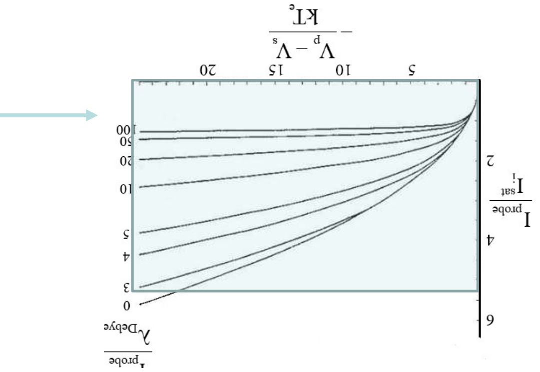

Laframboise, J.G. - numerical calculations:
Ion Saturation (Wire Probe)

Laframboise, J.G. - numerical calculations: Ion Saturation (Wire Probe)

Plasma

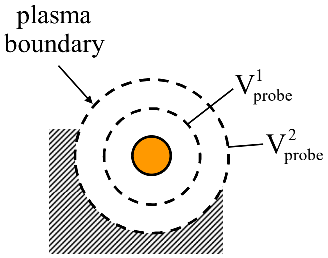

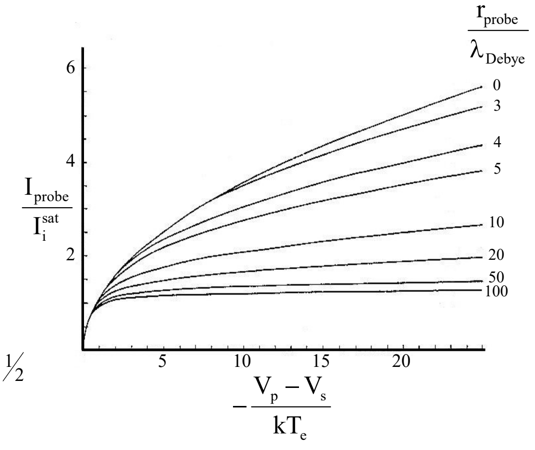

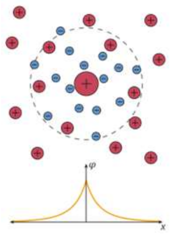

$$\text{Debye length; } \lambda_D = \left(\frac{\varepsilon_o k T_e}{e^2 n}\right)^{1/2}$$

characteristic length over which plasma screens electric field

r_p = probe radius

T_e, n_i, V_s needed - iterations

Complicated procedure to determine ion fluxes from wire probe characteristics

Experimental Set-up for Flat Probe

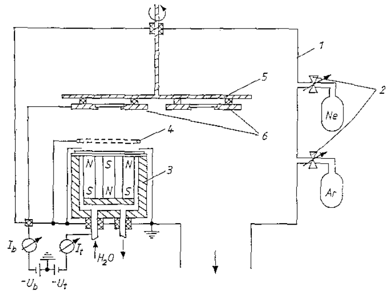

(a) Vacuum chamber with the magnetron assembly and the substrate holder

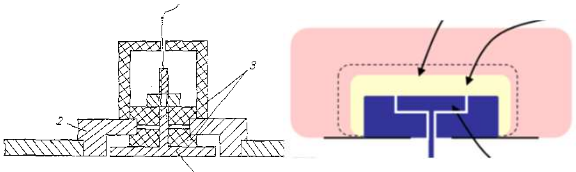

(b) Electrostatic flat probe – embedded in the substrate holder at the same plane with minimal spacing ~ ¼ mm

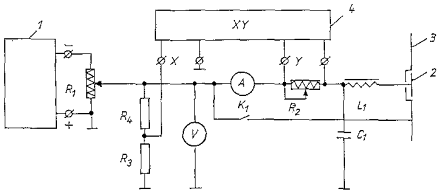

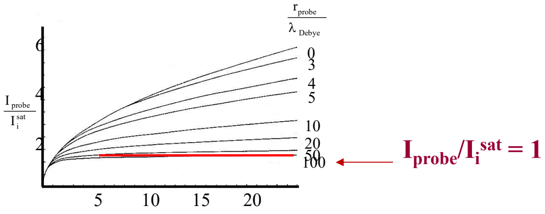

(c) Apply the same potential to the probe and the substrate holder

I. Petrov et al *Contrib. Plasma Phys.*, 30 223 (1990).

Flat Probe, best to measure the ion saturation current

- Directly measure ion flux; $I_{probe} = \frac{eJ^{sat}_{ion}}{1-\gamma}$

γ : Secondary electron emission coefficient

γ correction of the order ~ 10%

- Big probe

- Electron saturation disturbs the plasma (acts as an anode).
- Tangent method cannot be used.
- Plasma potential and electron temperature can still be estimated

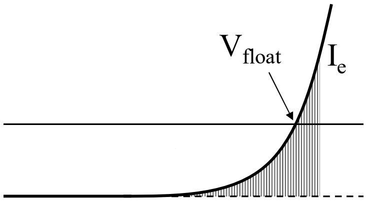

T_e can be determined from the initial portion of the exponential rise of I_e

$$V_{plasma} = V_{float} + \text{const. } T_e$$

Plasma

For film growth we need to know the ion flux J_i and ion energy $E_i \approx e(V_{substrate} - V_{plasma})$

$$I_{probe} = \frac{eJ_{ion}^{sat}}{1-\gamma}$$

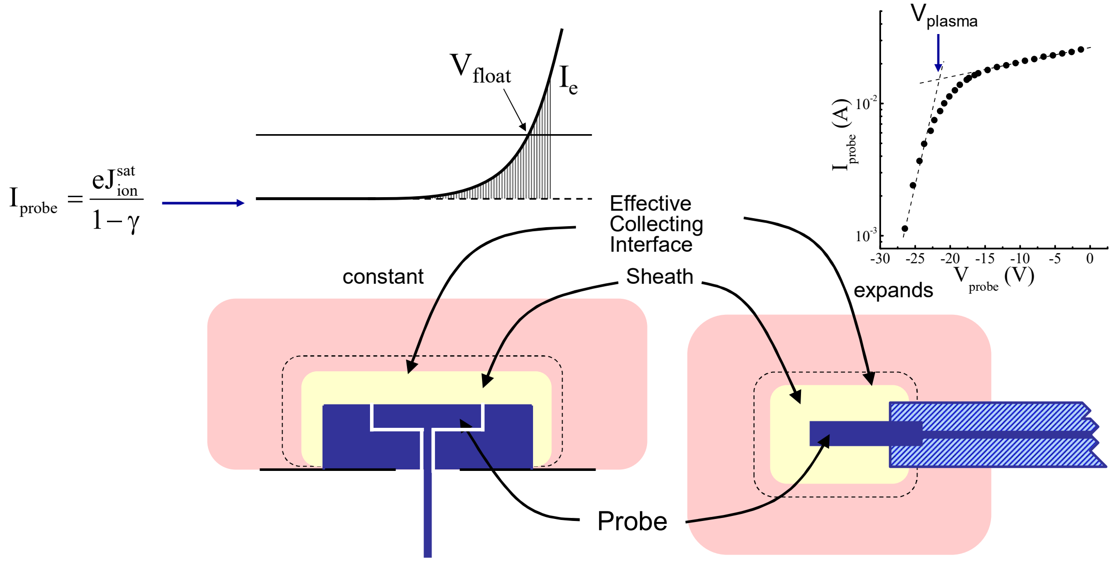

Best: a combination of a flat probe for J_i and a small probe for V_s

---

Example: plasma measurement in unbalanced magnetrons

Ion current measured by flat probe, plasma potential by wire probe

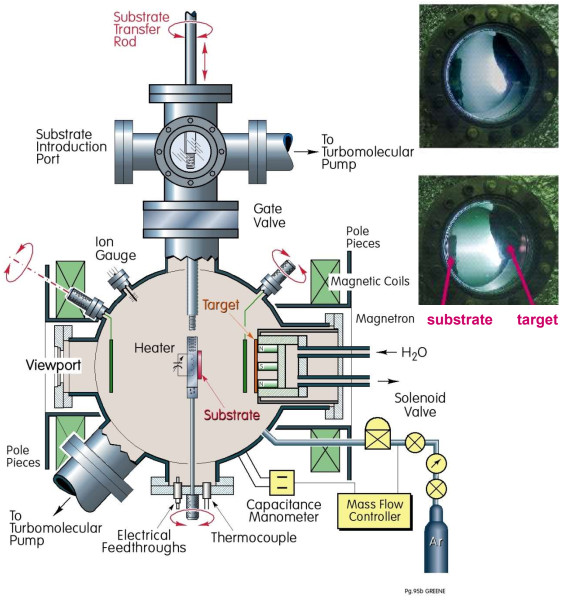

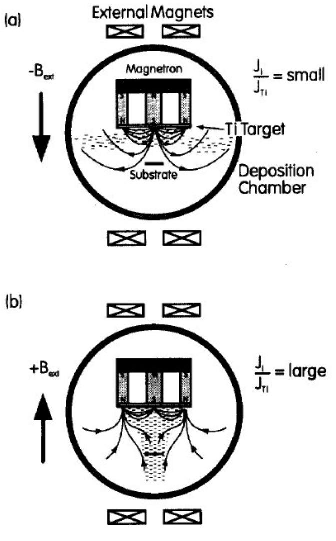

I. Petrov, F. Adibi, J.E. Greene, W.D. Sproul, and W.-D. Münz, *JVST* A10, 3283 (1992).

Example: plasma measurement in unbalanced magnetrons

Ion current measured by flat probe, plasma potential by wire probe

Unbalancing by external coils

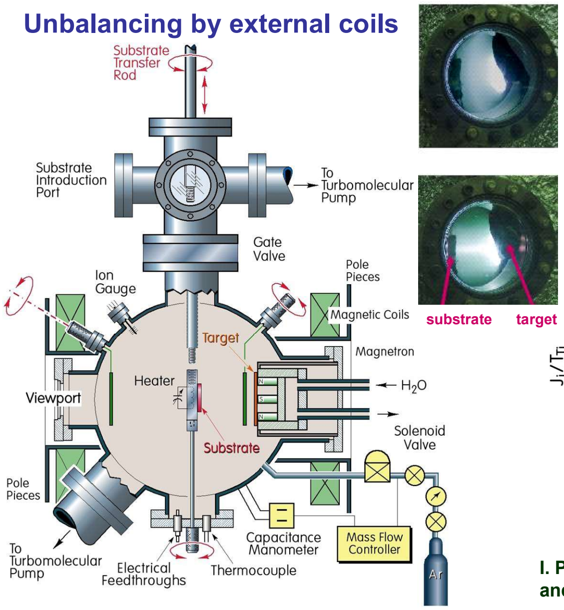

$E_i = e(V_{plasma} - V_{bias})$

$J_i = f(B_{ext})$

J_{Ti} remains approximately constant as a function of B_{ext}.

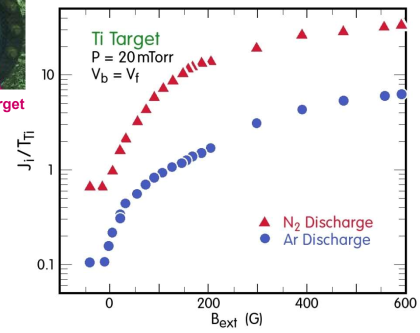

I. Petrov, F. Adibi, J.E. Greene, W.D. Sproul, and W.-D. Münz, *JVST* A10, 3283 (1992).

Plasma potential and density in unbalanced magnetrons (type II) depends on whether the substrate is grounded or not

I. Petrov, F. Adibi, J.E. Greene, W.D. Sproul, and W.-D. Münz, *JVST* A10, 3283 (1992).

Floating or (-) bias

Grounded substrate

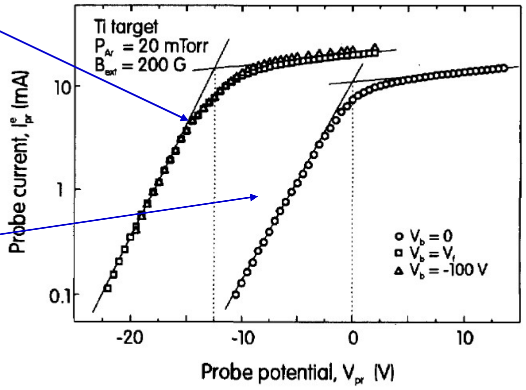

FIG. 7. Probe current I^e_{pr} due to electrons vs the applied probe potential V_{pr} during sputtering of Ti in a 20 mTorr Ar discharge with $B_{ext} = 200$ G and the applied substrate bias $V_b = 0$, V_f, and -100 V. The plasma potential V_p (dotted lines) is 0 for $V_b = 0$ and -12.5 V for $V_b = V_f$ and -100 V.

Plasma potential and density in unbalanced magnetrons (type II) depends on whether the substrate is grounded or not

Penning-type configuration

Floating or (-) bias

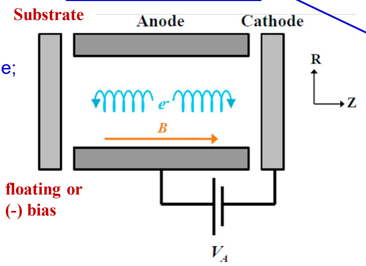

The substrate is NOT an anode;
Collects no/few electrons

Grounded substrate

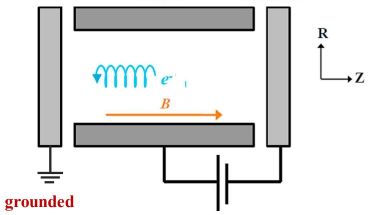

The substrate is the anode;
collects all electrons

I. Petrov, F. Adibi, J.E. Greene, W.D. Sproul, and W.-D. Münz, *JVST* A10, 3283 (1992).

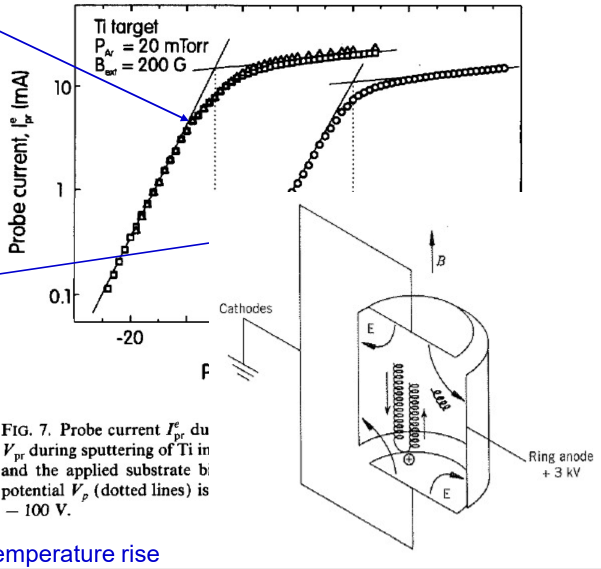

FIG. 7. Probe current I^e_{pr} du
V_{pr} during sputtering of Ti in
and the applied substrate bi
potential V_p (dotted lines) is
− 100 V.

NB significant heating by electrons – measure substrate temperature rise

More on the Electron Energy Distribution Functions

Maxwell electron energy distribution functions
Elastic collision between electrons dominate

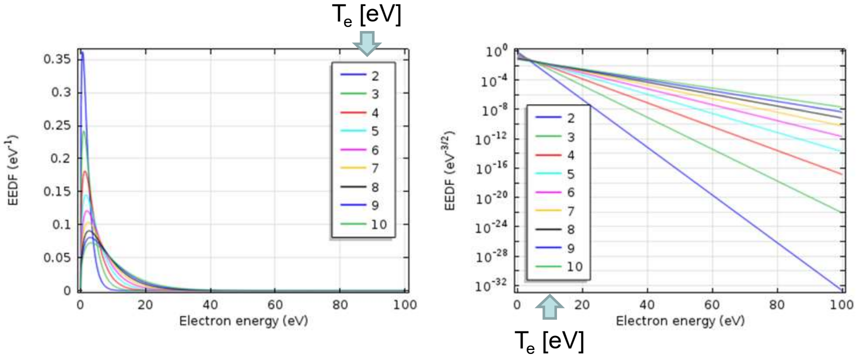

$$f(\epsilon) = \frac{2}{(kT)^{\frac{3}{2}}}\sqrt{\frac{\epsilon}{\pi}}\exp\left(\frac{-\epsilon}{kT}\right)$$

More on the Electron Energy Distribution Functions

Druyvesteyn EEDF
Elastic collision between electrons and cold atoms included

$$f_D(\epsilon) = \frac{0.5648 n_e}{(kT)^{\frac{3}{2}}}\sqrt{\epsilon}\exp\left[-0.243\left(\frac{\epsilon}{kT}\right)^2\right]$$

Maxwell EEDF
Elastic collision between electrons dominate

$$f(\epsilon) = \frac{2}{(kT)^{\frac{3}{2}}}\sqrt{\frac{\epsilon}{\pi}}\exp\left(\frac{-\epsilon}{kT}\right)$$

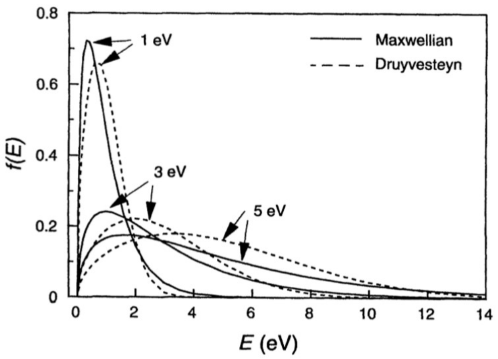

A. Grill, Cold Plasma Materials Fabrication: From Fundamentals to Applications. Wiley, 1994.

More on the Electron Energy Distribution Functions

Boltzmann EEDF includes inelastic collisions

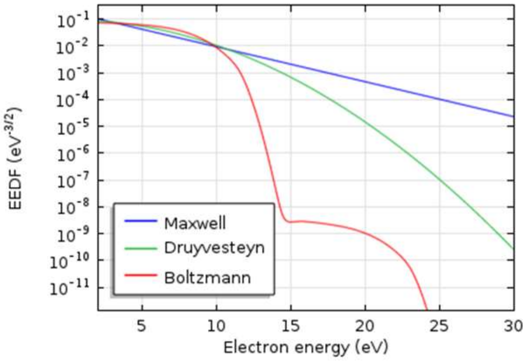

Computational example from:
https://www.comsol.com/

Measured Electron Energy Distribution Functions

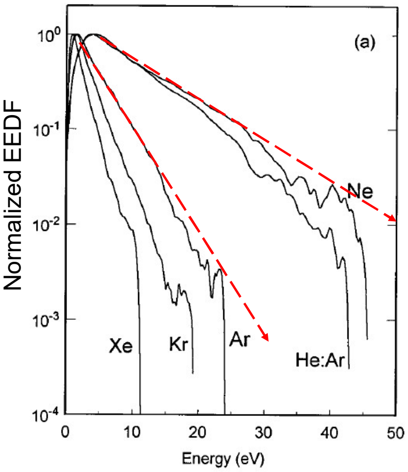

- The linear portion corresponds to Maxwell-like energy distribution
- Electron temperature T_e is the slope of the linear portion of the curve
- T_e decreases as the ionization potential of the inert gas decreases
- In the area of inelastic collisions the high-energy tail is underpopulated
- extrapolation of the EEDF from the elastic energy range into the inelastic energy range may cause a significant error in the calculation of excitation and ionization rates
- **Metal dominated plasmas in HIPIMS lack high energy electron needed to ionize the inert gas**.

A. Schwabedissen et al Physical review E, 55 (1997) 3450

Measured Electron Energy Distribution Functions

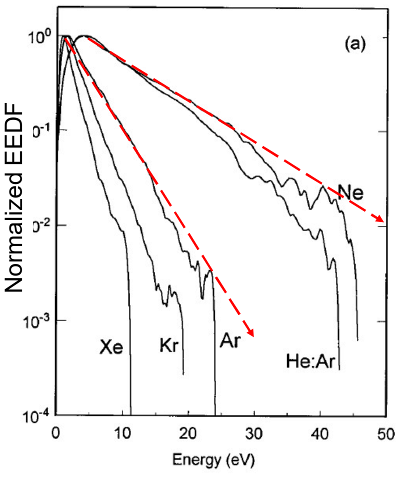

- The linear portion corresponds to Maxwell-like energy distribution
- Electron temperature T_e is the slope of the linear portion of the curve
- T_e decreases as the ionization potential of the inert gas decreases
- In the area of inelastic collisions the high-energy tail is underpopulated
- extrapolation of the EEDF from the elastic energy range into the inelastic energy range may cause a significant error in the calculation of excitation and ionization rates
- **Metal dominated plasmas in HIPIMS lack high energy electron needed to ionize the inert gas**.

Electron impact ionization

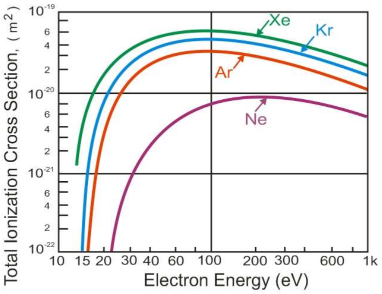

Ionization potentials

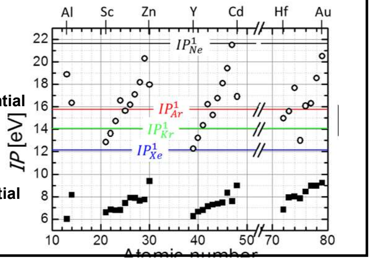

○ 2nd ionization potential

▪ 1st ionization potential

A. Schwabedissen et al Physical review E, 55 (1997) 3450

Cooling of the electrons in metal-rich phase of HIPIMS discharges

Alena Vetushka and Arutiun P Ehiasarian
J. Phys. D: Appl. Phys. 41 (2008) 015204

P Poolcharuansin and J W Bradley
Plasma Sources Sci. Technol. 19 (2010) 025010

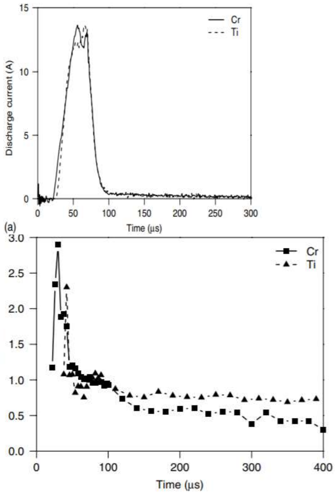

Figure 6. Effective electron temperature as a function of time for Cr and Ti targets at a pressure of 0.28 Pa.

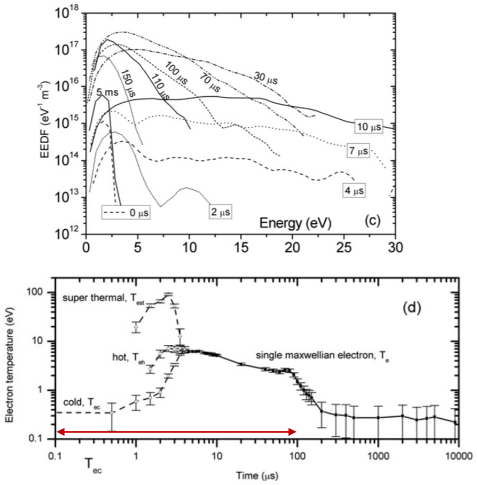

100µs, 100 Hz,

Plasmas: practical example

$$d^2[cm] = 8.64x10^{-6}\frac{V^{3/2}[V]}{j\left[\frac{mA}{cm^2}\right]}$$

$$\lambda_{CE} = \frac{kT}{p[Pa]\sigma[m^2]\sqrt{2}}$$

$$\sigma_{CE}^{Ar} = 4\times10^{-19}\left[m^2\right]$$

Cross-section for charge exchange collisions for Ar

Sputtering system		Voltage	Current density	Sheath width	λ_{Ar}
Diode p_{Ar} = 70 mTorr	target	3000 V	1 mA cm^{-2}	12 mm	0.7 mm
	substrate	100 V	0.1 mA cm^{-2}	3 mm	0.7 mm
magnetron p_{Ar} = 3 mTorr	target	500 V	50 mA cm^{-2}	**0.5 mm**	**16 mm**
	substrate	100 V	1 mA cm^{-2}	**0.9 mm**	**16 mm**

For magnetron sputtering λ_{Ar} > sheath width -> $E_i \approx e(V_{electrode} - V_{plasma})$

Cold Cathode Discharge

Ion surface interactions

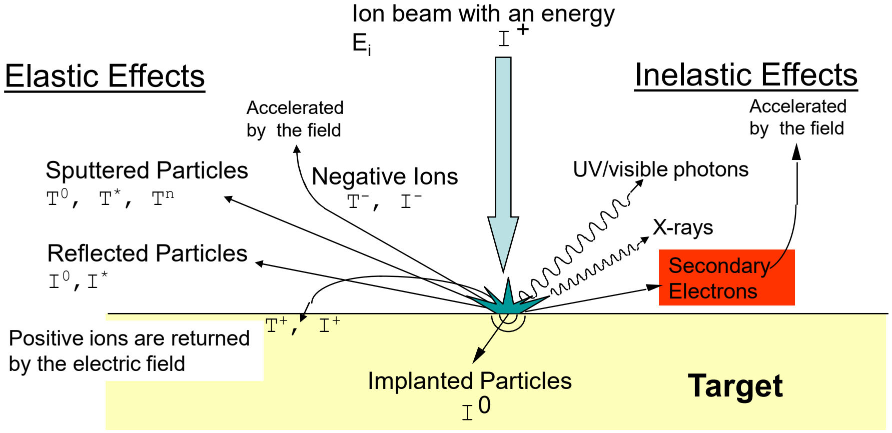

Ion beam with an energy E_i I^+

Elastic Effects

Inelastic Effects

Accelerated by the field

Sputtered Particles T^0, T^*, T^n

Negative Ions T^-, I^-

Reflected Particles I^0, I^*

Positive ions are returned by the electric field

T^+, I^+

Implanted Particles I^0

Accelerated by the field

UV/visible photons

X-rays

Secondary Electrons

Target

Figure after G.M. McCracken, Rep. Prog Phys. **28**, 241 (1975).

Discharge

Glow Discharge Voltage

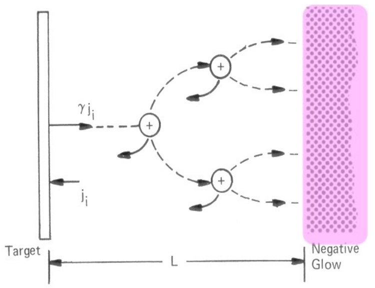

On the average, a secondary electron emitted from the cathode must acquire energy sufficient to produce a number of ions to release one further electron from the cathode.

$$\gamma_i \frac{V_T}{E_o} = 1$$

$$\boxed{\frac{V_T}{E_o} = \frac{1}{\gamma_i\, \varepsilon_i\, \varepsilon_e}}$$

E_o – the average energy to produce an ion (for Ar ~ 30 eV)
γ_I – the secondary ion-electron yield (for Ar ~ 0.1)
ε_I – ion collection efficiency (fraction of created ions that strike the target)
ε_e – fraction of the secondary electrons participating in ionization
$\varepsilon_i\, \varepsilon_e$ – characterizes the effectiveness of the ionization system; for magnetrons ~ 1

John A. Thornton and Alan S. Penfold, in *Thin Film Processes*, Ed. by John L. Vossen and Werner Kern (Academic Press, New York, 1978) p. 86.

Glow Discharge Maintenance

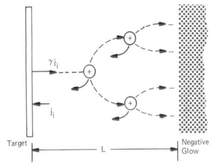

Electron impact ionization

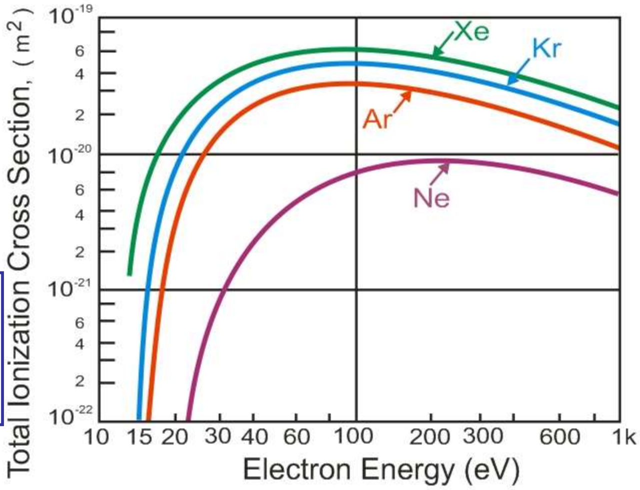

Ionization potentials
Ne - 21.56 eV
Ar - 15.76 eV
Kr – 14.00 eV
Xe - 12.13 eV

$$\boxed{\frac{V_T}{E_o} = \frac{1}{\gamma_i \, \varepsilon_i \, \varepsilon_e}}$$

Figure after John A. Thornton and Alan S. Penfold, in *Thin Film Processes*, Ed. by John L. Vossen and Werner Kern (Academic Press, New York, 1978) p. 84.

Secondary ion-electron yield γ_i

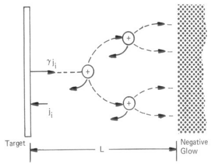

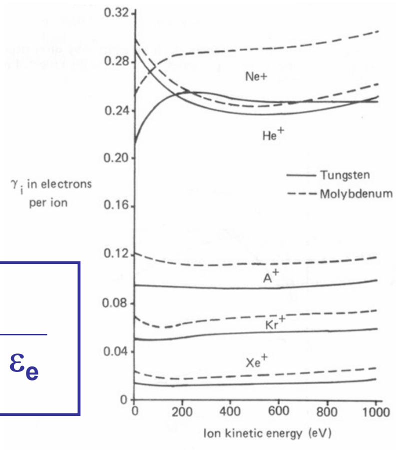

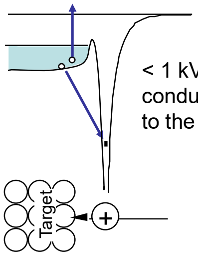

< 1 kV, electrons emitted from the conduction band of the target due to the potential energy of the ion

$$\boxed{\frac{V_T}{E_o} = \frac{1}{\gamma_i \, \varepsilon_i \, \varepsilon_e}}$$

Ionization potentials
Ne - 21.56 eV
Ar - 15.76 eV
Kr – 14.00 eV
Xe - 12.13 eV

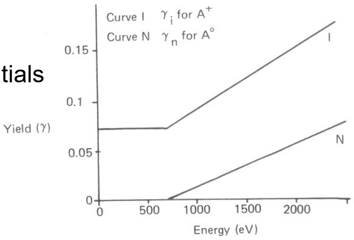

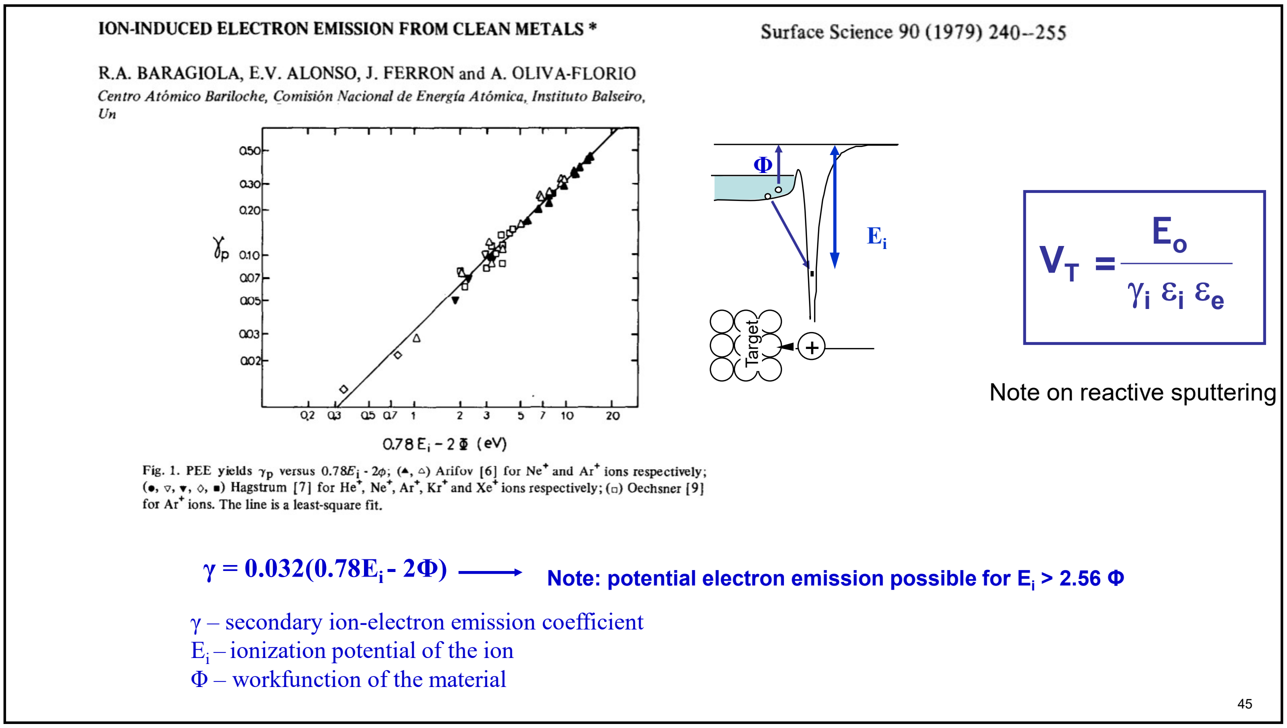

ION-INDUCED ELECTRON EMISSION FROM CLEAN METALS *

Surface Science 90 (1979) 240--255

R.A. BARAGIOLA, E.V. ALONSO, J. FERRON and A. OLIVA-FLORIO

Centro Atómico Bariloche, Comisión Nacional de Energía Atómica, Instituto Balseiro, Un

Fig. 1. PEE yields γ_p versus $0.78E_i - 2\phi$; (▲, △) Arifov [6] for Ne^+ and Ar^+ ions respectively; (●, ▽, ▼, ◇, ■) Hagstrum [7] for He^+, Ne^+, Ar^+, Kr^+ and Xe^+ ions respectively; (□) Oechsner [9] for Ar^+ ions. The line is a least-square fit.

$$V_T = \frac{E_o}{\gamma_i\, \varepsilon_i\, \varepsilon_e}$$

Note on reactive sputtering

$\gamma = 0.032(0.78E_i - 2\Phi)$ ⟶ **Note: potential electron emission possible for $E_i > 2.56\ \Phi$**

γ – secondary ion-electron emission coefficient

E_i – ionization potential of the ion

Φ – workfunction of the material

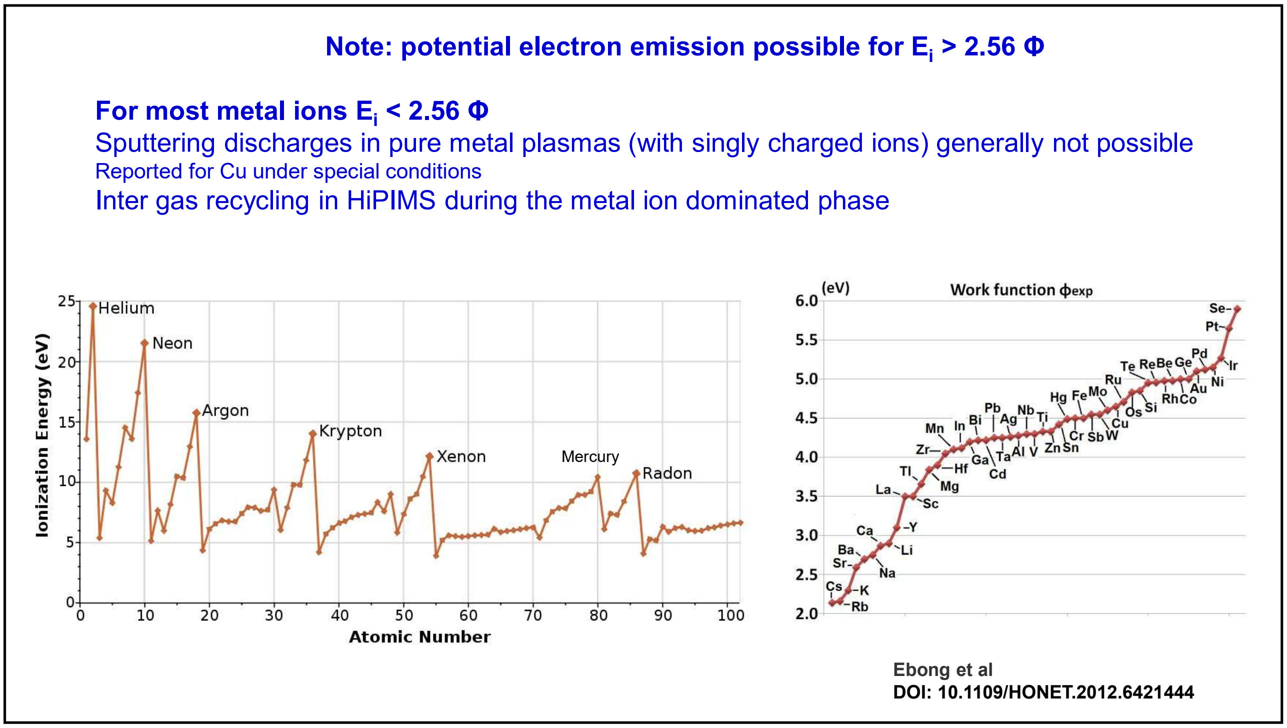

Note: potential electron emission possible for $E_i > 2.56\ \Phi$

For most metal ions $E_i < 2.56\ \Phi$

Sputtering discharges in pure metal plasmas (with singly charged ions) generally not possible

Reported for Cu under special conditions

Inter gas recycling in HiPIMS during the metal ion dominated phase

Ebong et al

DOI: 10.1109/HONET.2012.6421444

Example of DC magnetron discharge characteristics

The interplay between ionization cross section and the secondary ion-electron emission coefficient

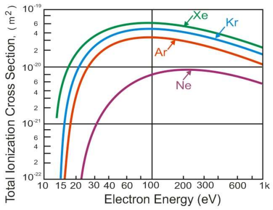

$$V_T = \frac{E_o}{\gamma_i \; \varepsilon_i \; \varepsilon_e}$$

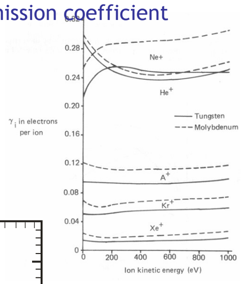

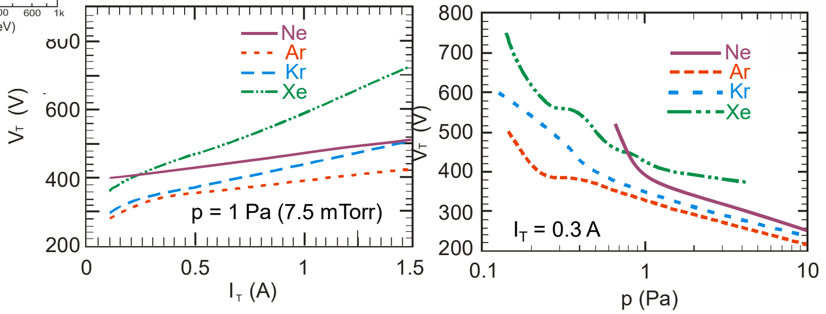

Argon is the best

Example: 50 mm Vanadium target, planar magnetron

Comparison of magnetron sputter deposition conditions in neon, argon, krypton, and xenon discharges

I. Petrov,[a] I. Ivanov,[b] and V. Orlinov
Institute of Electronics, Bulgarian Academy of Sciences, Sofia 1784, Bulgaria
J.-E. Sundgren
Thin Film Division, Department of Physics, Linköping University, S-581 83 Linköping, Sweden

J. Vac. Sci. Technol, 11 2733 (1993)

Sputtering Yield

Ion surface interactions

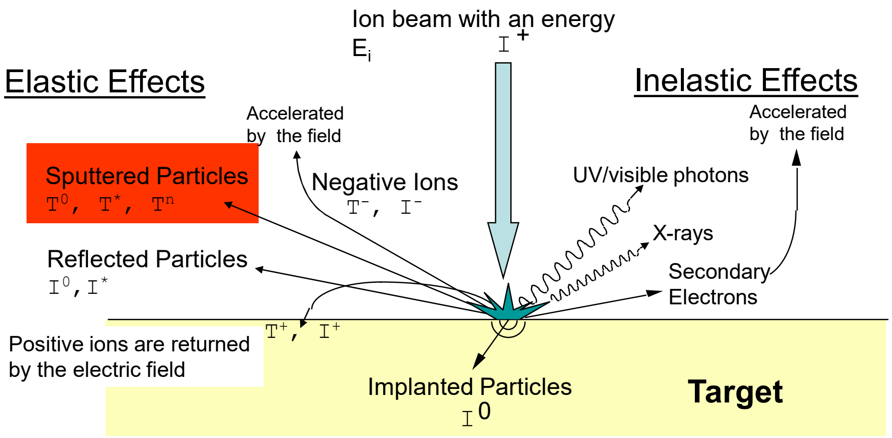

Ion beam with an energy E_i

I^+

Elastic Effects

Inelastic Effects

Accelerated by the field

Accelerated by the field

Sputtered Particles

T^0, T^*, T^n

Negative Ions

T^-, I^-

UV/visible photons

X-rays

Reflected Particles

I^0, I^*

Secondary Electrons

Positive ions are returned by the electric field

T^+, I^+

Implanted Particles

I^0

Target

Figure after G.M. McCracken, Rep. Prog Phys. **28**, 241 (1975).

Collision Cascade

Energy increasing (dependent on M_i/M_t)

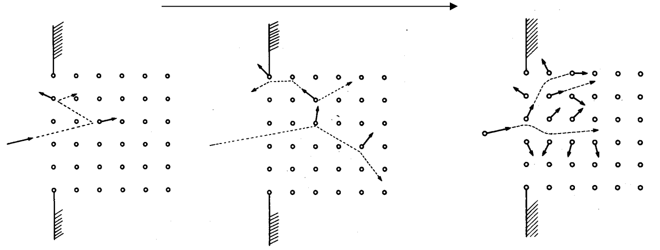

Threshold regime
recoils sputtered, but no (limited) cascades

Linear cascade
a series of binary collisions

Spike regime
high density of recoils

- Ions striking a surface interact with a number of atoms in a series collisions.
- recoiled target atoms in turn collide with atom at rest generating a collision cascade.
- The initial ion energy and momentum are distributed to among the target recoil atoms.
- When $E_i > 1$ keV, the cascade is “linear”, i.e. approximated by a series of binary collisions in a stationary matrix.

P.Sigmund, “Sputtering by ion bombardment: theoretical concepts”, in *Sputtering by particle bombardment* I, edited by R. Behrish, Springer-Verlag, 1981

Stopping cross section

$$\frac{dE}{dx} = -NS(E) = -N\left[S_n(E) + S_e(E)\right]$$

$S_n(E)$ - nuclear stopping
$S_e(E)$ - electronic stopping

$$Range = \int_0^E \frac{dE'}{NS(E')}$$

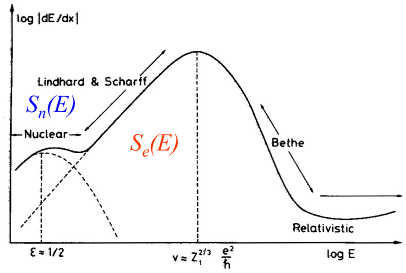

P.Sigmund, "Sputtering by ion bombardment: theoretical concepts", in *Sputtering by particle bombardment* I, edited by R. Behrish, Springer-Verlag, 1981

Stopping cross section

$$\frac{dE}{dx} = -NS(E) = -N\left[S_n(E) + S_e(E)\right]$$

$$Range = \int_0^E \frac{dE'}{NS(E')}$$

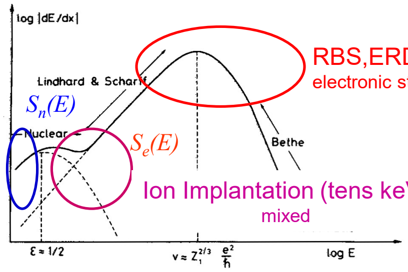

RBS,ERDA,NRA (MeV)
electronic stopping dominates

Sputter Deposition (keV)
nuclear stopping dominates

Ion Implantation (tens keV)
mixed

P.Sigmund, "Sputtering by ion bombardment: theoretical concepts", in *Sputtering by particle bombardment* I, edited by R. Behrish, Springer-Verlag, 1981

SRIM/TRIM simulation

Monte-Carlo simulation of ion implantation, reflection, recoil cascades, and sputtering

200 impacts

1 keV Ar -> Be

2 impacts

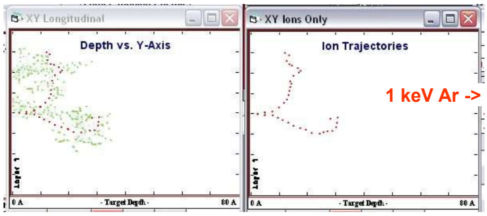

1 keV Ar -> Ti

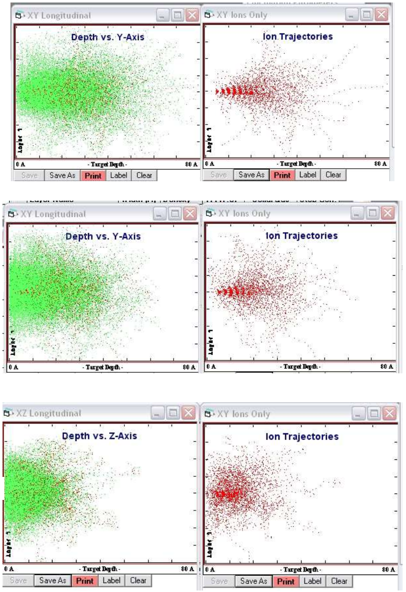

ion trajectories in red
recoils in green

1 keV Ar -> W

James F. Ziegler, IBM : http://www.srim.org/

Sputtering Yield (Y)

- Sputtering begins at an energy threshold and increases rapidly
- **Then nearly linearly**
- As the energy increases the curve levels off.

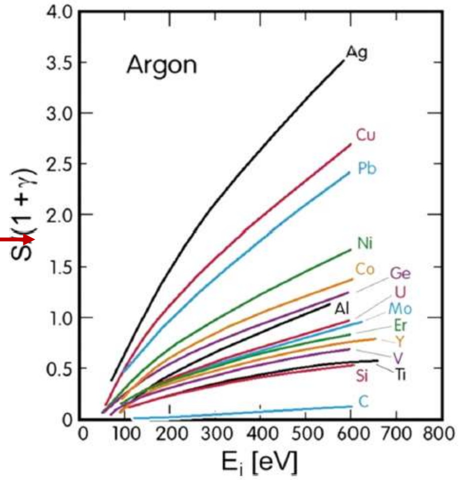

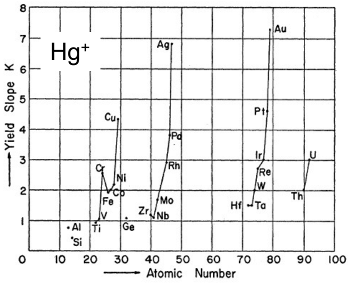

Fig. 7. Yield slopes *vs* atomic number.

Slope of linear portion vs atomic number

Data from R.Y. Stuart and G.K. Wehner, J. Appl. Phys. 33, 2351 (1962); G.K. Wehner, Phys Rev, 112, 1120, 1958
D. Rosenberg and G.K. Wehner, J. Appl. Phys. 33, 1842 (1962);

JOURNAL OF APPLIED PHYSICS VOLUME 33, NUMBER 7 JULY 1962

Sputtering Yields at Very Low Bombarding Ion Energies*

Gottfried Karl Wehner
23 September 1910 (Dresden)
13 June 1996 (Munich)

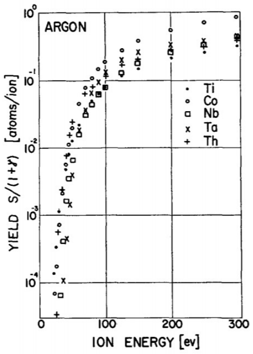

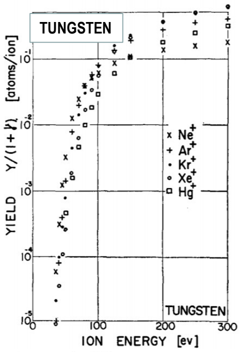

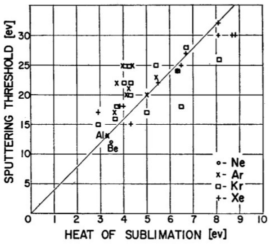

FIG. 13. Thresholds vs heats of sublimation.

TABLE II. Threshold energies. Circled values are those for which the energy transfer factor $4m_1m_2/(m_1+m_2)^2$ is 0.9 or higher.

	Ne	Ar	Kr	Xe	Hg		Ne	Ar	Kr	Xe	Hg
Be	⑫	15	15	15		Mo	24	24	㉘	㉗	32
Al	⑬	⑬	15	18	18	Rh	25	24	㉕	㉕	
Ti	㉒	⑳	⑰	18	25	Pd	20	20	⑳	⑮	20
V	21	㉓	㉕	28	25	Ag	12	15	⑮	⑰	
Cr	22	㉒	⑱	20	23	Ta	25	26	30	㉚	30
Fe	22	⑳	㉕	23	25	W	35	33	30	㉚	30
Co	20	㉕	㉒	22		Re	35	35	25	㉚	35
Ni	23	㉑	㉕	20		Pt	27	25	22	㉒	25
Cu	17	⑰	⑯	15	20	Au	20	20	20	⑱	
Ge	23	㉕	㉒	⑱	25	Th	20	24	25	㉕	
Zr	23	22	⑱	㉕	30	U	20	23	25	㉒	27
Nb	27	25	㉖	㉜							

JOURNAL OF APPLIED PHYSICS VOLUME 32, NUMBER 3 MARCH, 1961

Sputtering Yields of Metals for Ar+ and Ne+ Ions with Energies from 50 to 600 ev*†

To this day:
the most comprehensive set of
low-energy sputtering yields data

NILS LAEGREID AND G. K. WEHNER
Mechanical Division of General Mills, Incorporated, Minneapolis, Minnesota

(August 24, 1960)

Sputtering yields for polycrystalline metal and semiconductor targets under normally incident Ar^+ and Ne^+ ion bombardment were measured in the energy range from 50 to 600 ev. The yields (atoms/ion) were determined by measuring the weight loss of spherical targets immersed like large negative Langmuir probes

TABLE I. Sputtering yields for 28 elements under Ne^+ and Ar^+ ion bombardment.

	Neon				Yield at lowest ion energy		Argon			
Target	100 (ev)	200 (ev)	300 (ev)	600 (ev)	Y	E (ev)	100 (ev)	200 (ev)	300 (ev)	600 (ev)
Be	0.012	0.10	0.26	0.56	0.05	80	0.074	0.18	0.29	0.80
Al	0.031	0.24	0.43	0.83	0.11	100	0.11	0.35	0.65	1.24
Si	0.034	0.13	0.25	0.54	0.06	80	0.07	0.18	0.31	0.53
Ti	0.08	0.22	0.30	0.45	0.081	100	0.081	0.22	0.33	0.58
V	0.06	0.17	0.36	0.55	0.03	60	0.11	0.31	0.41	0.70
Cr	0.18	0.49	0.73	1.05	0.026	40	0.30	0.67	0.87	1.30
Fe	0.18	0.38	0.62	0.97	0.064	60	0.20	0.53	0.76	1.26
Co	0.084	0.41	0.64	0.99	0.048	60	0.15	0.57	0.81	1.36
Ni	0.22	0.46	0.65	1.34	0.067	60	0.28	0.66	0.95	1.52
Cu	0.26	0.84	1.20	2.00	0.10	60	0.48	1.10	1.59	2.30
Ge	0.12	0.32	0.48	0.82	0.017	30	0.22	0.50	0.74	1.22
Zr	0.054	0.17	0.27	0.42	0.027	60	0.12	0.28	0.41	0.75
Nb	0.051	0.16	0.23	0.42	0.017	60	0.068	0.25	0.40	0.65
Mo	0.10	0.24	0.34	0.54	0.027	60	0.13	0.40	0.58	0.93
Ru	0.078	0.26	0.38	0.67	0.012	60	0.14	0.41	0.68	1.30
Rh	0.081	0.36	0.52	0.77	0.19	100	0.19	0.55	0.86	1.46
Pd	0.14	0.59	0.82	1.32	0.033	50	0.42	1.00	1.41	2.39
Ag	0.27	1.00	1.30	1.98	0.22	60	0.63	1.58	2.20	3.40
Hf	0.057	0.15	0.22	0.39	0.004	40	0.16	0.35	0.48	0.83
Ta	0.056	0.13	0.18	0.30	0.01	60	0.10	0.28	0.41	0.62
W	0.038	0.13	0.18	0.32	0.008	60	0.068	0.29	0.40	0.62
Re	0.04	0.15	0.24	0.42	0.034	80	0.10	0.37	0.56	0.91
Os	0.032	0.16	0.24	0.41	0.057	100	0.057	0.36	0.56	0.95
Ir	0.069	0.21	0.30	0.46	0.019	60	0.12	0.43	0.70	1.17
Pt	0.12	0.31	0.44	0.70	0.032	60	0.20	0.63	0.95	1.56
Au	0.20	0.56	0.84	1.18	0.035	50	0.32	1.07	1.65	2.43 (500)
Th	0.028	0.11	0.17	0.36	0.017	60	0.097	0.27	0.42	0.66
U	0.063	0.20	0.30	0.52	0.14	100	0.14	0.35	0.59	0.97

To this day:
the most comprehensive set of
low-energy sputtering yields data

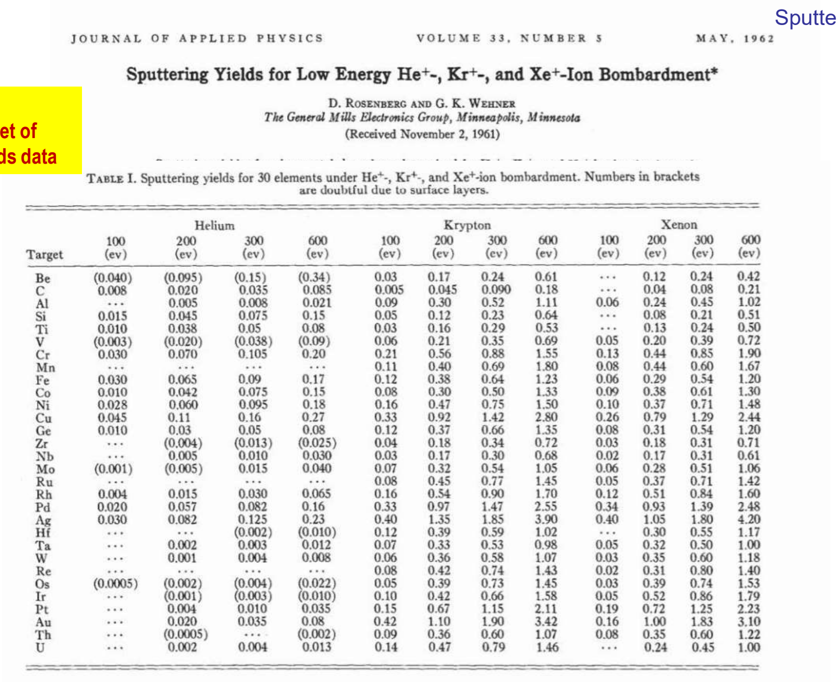

JOURNAL OF APPLIED PHYSICS VOLUME 33, NUMBER 5 MAY, 1962

Sputtering Yields for Low Energy He$^+$-, Kr$^+$-, and Xe$^+$-Ion Bombardment*

D. Rosenberg and G. K. Wehner
The General Mills Electronics Group, Minneapolis, Minnesota
(Received November 2, 1961)

Table I. Sputtering yields for 30 elements under He$^+$-, Kr$^+$-, and Xe$^+$-ion bombardment. Numbers in brackets are doubtful due to surface layers.

	Helium				Krypton				Xenon			
Target	100 (ev)	200 (ev)	300 (ev)	600 (ev)	100 (ev)	200 (ev)	300 (ev)	600 (ev)	100 (ev)	200 (ev)	300 (ev)	600 (ev)
Be	(0.040)	(0.095)	(0.15)	(0.34)	0.03	0.17	0.24	0.61	···	0.12	0.24	0.42
C	0.008	0.020	0.035	0.085	0.005	0.045	0.090	0.18	···	0.04	0.08	0.21
Al	···	0.005	0.008	0.021	0.09	0.30	0.52	1.11	0.06	0.24	0.45	1.02
Si	0.015	0.045	0.075	0.15	0.05	0.12	0.23	0.64	···	0.08	0.21	0.51
Ti	0.010	0.038	0.05	0.08	0.03	0.16	0.29	0.53	···	0.13	0.24	0.50
V	(0.003)	(0.020)	(0.038)	(0.09)	0.06	0.21	0.35	0.69	0.05	0.20	0.39	0.72
Cr	0.030	0.070	0.105	0.20	0.21	0.56	0.88	1.55	0.13	0.44	0.85	1.90
Mn	···	···	···	···	0.11	0.40	0.69	1.80	0.08	0.44	0.60	1.67
Fe	0.030	0.065	0.09	0.17	0.12	0.38	0.64	1.23	0.06	0.29	0.54	1.20
Co	0.010	0.042	0.075	0.15	0.08	0.30	0.50	1.33	0.09	0.38	0.61	1.30
Ni	0.028	0.060	0.095	0.18	0.16	0.47	0.75	1.50	0.10	0.37	0.71	1.48
Cu	0.045	0.11	0.16	0.27	0.33	0.92	1.42	2.80	0.26	0.79	1.29	2.44
Ge	0.010	0.03	0.05	0.08	0.12	0.37	0.66	1.35	0.08	0.31	0.54	1.20
Zr	···	(0.004)	(0.013)	(0.025)	0.04	0.18	0.34	0.72	0.03	0.18	0.31	0.71
Nb	···	0.005	0.010	0.030	0.03	0.17	0.30	0.68	0.02	0.17	0.31	0.61
Mo	(0.001)	(0.005)	0.015	0.040	0.07	0.32	0.54	1.05	0.06	0.28	0.51	1.06
Ru	···	···	···	···	0.08	0.45	0.77	1.45	0.05	0.37	0.71	1.42
Rh	0.004	0.015	0.030	0.065	0.16	0.54	0.90	1.70	0.12	0.51	0.84	1.60
Pd	0.020	0.057	0.082	0.16	0.33	0.97	1.47	2.55	0.34	0.93	1.39	2.48
Ag	0.030	0.082	0.125	0.23	0.40	1.35	1.85	3.90	0.40	1.05	1.80	4.20
Hf	···	···	(0.002)	(0.010)	0.12	0.39	0.59	1.02	···	0.30	0.55	1.17
Ta	···	0.002	0.003	0.012	0.07	0.33	0.53	0.98	0.05	0.32	0.50	1.00
W	···	0.001	0.004	0.008	0.06	0.36	0.58	1.07	0.03	0.35	0.60	1.18
Re	···	···	···	···	0.08	0.42	0.74	1.43	0.02	0.31	0.80	1.40
Os	(0.0005)	(0.002)	(0.004)	(0.022)	0.05	0.39	0.73	1.45	0.03	0.39	0.74	1.53
Ir	···	(0.001)	(0.003)	(0.010)	0.10	0.42	0.66	1.58	0.05	0.52	0.86	1.79
Pt	···	0.004	0.010	0.035	0.15	0.67	1.15	2.11	0.19	0.72	1.25	2.23
Au	···	0.020	0.035	0.08	0.42	1.10	1.90	3.42	0.16	1.00	1.83	3.10
Th	···	(0.0005)	···	(0.002)	0.09	0.36	0.60	1.07	0.08	0.35	0.60	1.22
U	···	0.002	0.004	0.013	0.14	0.47	0.79	1.46	···	0.24	0.45	1.00

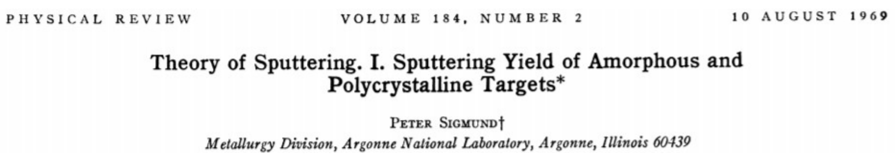

PHYSICAL REVIEW VOLUME 184, NUMBER 2 10 AUGUST 1969

Theory of Sputtering. I. Sputtering Yield of Amorphous and Polycrystalline Targets*

Peter Sigmund†
Metallurgy Division, Argonne National Laboratory, Argonne, Illinois 60439

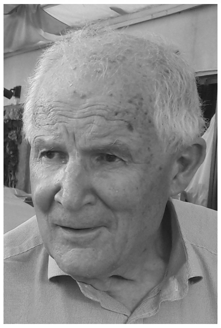

$$Y(E) = \frac{0.04}{U}\alpha(M_t/M_i)S_n(E)$$

α - dimensionless coefficient
α – sublimation energy
$S_n(E)$, nuclear stopping cross-section
E – incident ion energy
Note: the sputtering yield is proportional to the nuclear stopping at the point of entry

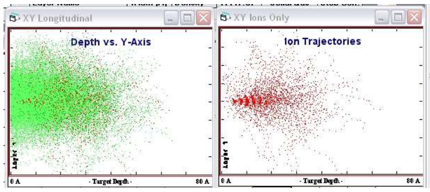

Peter Sigmund
University of Southern Denmark
PhD. 1962, TU Aachen, under Prof. Guenter Leibfried
1967-9 Visiting scientist, Argonne National Lab
1965-7 Scientist, Research Center Jülich

Sigmund’s linear cascade formula for Y(E)

$$\boxed{Y(E) = \frac{0.04}{U}\alpha(M_t/M_i)S_n(E)}$$

α - dimensionless coefficient

$S_n(E)$, collisional energy at the surface (nuclear energy loss function)

U – sublimation energy

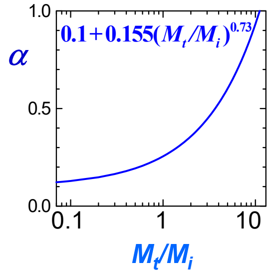

$$S_n(E) = 85\frac{Z_iZ_t}{(Z_i^{2/3}+Z_t^{2/3})^{0.5}}\frac{M_i}{M_t+M_i}s_n(\varepsilon)$$

$s_n(\varepsilon)$ – function of the reduced energy which is the same for all ion-target combination

$$\boxed{s_n(\varepsilon) = \frac{3.441\sqrt{\varepsilon}\ln(\varepsilon+2.718)}{1+6.355\sqrt{\varepsilon}+\varepsilon(6.882\sqrt{\varepsilon}-1.708)}}$$

Curve 1

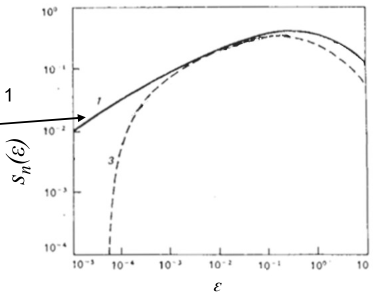

ε – reduced energy

$$\varepsilon = \frac{0.03255}{Z_iZ_t(Z_i^{2/3}+Z_t^{2/3})^{0.5}}\frac{M_t}{M_t+M_i}E$$

Sigmund formula: good agreement in the 10s keV, poor in the < 1 keV

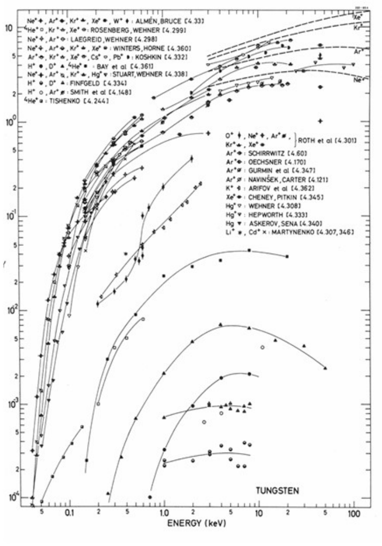

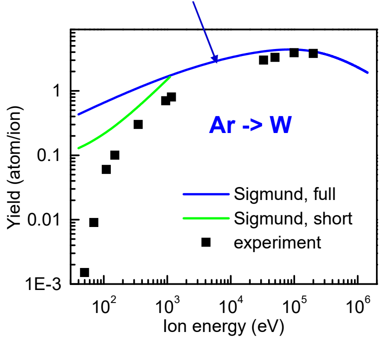

0.1 < E < 1kV, Sigmund derives a remarkably simple formula

$$\boxed{\begin{aligned} Y(E) &= \frac{3}{4\pi^2}\alpha(M_t/M_i)\frac{\gamma E}{U} \\ \gamma &= \frac{4M_tM_i}{(M_t+M_i)^2} \end{aligned}}$$

HH Anderson and HL Bay, “Sputtering yield measurements”, in *Sputtering by particle bombardment* I, edited by R. Behrish, Springer-Verlag, 1981

Formulas introducing Sputtering Threshold Energy, E_{TH}

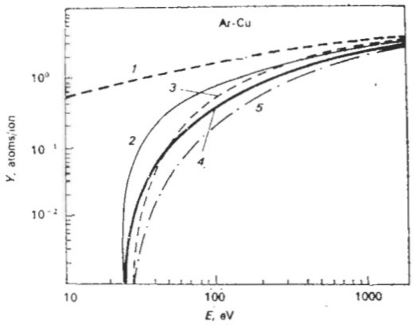

Fig. 2. Energy dependence of the sputtering yield: curve 1 — Sigmund's expression, curve 2 — Matsunami I, curve 3 — Bohdansky, curve 4 — Yamamura, curve 5 — Matsunami II

$Y(E) = Y_{Sigmund}(E).f(E)$,

$f(E) = 0$, $E = E_{TH}$
$f(E) = 1$, $E >> E_{TH}$

Each formula comes with its choice of E_{TH}

3. Matsunami, N., Y. Yamamura, Y. Itikava, N. Itoh, Y. Kazumata, S. Miyagawa. K. Morita, R. Shimizu. — Rad. Eff. Letters, 57, 1980, p. 15.
4. Yamamura. Y., N. Matsunami, N. Itoh. — Rad. Eff., 71, 1983, p. 65.
5. Bohdansky, J. — Nucl. Instr. Meth., B2. 1984, p. 587.
6. Matsunami, N., Y. Yamamura, Y. Itikawa, N. Itoh, Y. Kazumata, S. Niyagawa, K. Morita, R. Shimizu, H. Tawara. — Atomic Data and Nucl. Data Tables, 31, 1984, p. 1.

Petrov, V. Orlinov, S. Grudeva, Comparison of the Low-Energy Sputtering Yield Formulas, *Bulg. J. Phys*., 19 102 (1991).

The best formula for low energy sputtering yield: Y. Yamamura et al formula

Sputtering begins at an energy threshold that depends on the efficiency of momentum transfer to the target. This depends on the mass match. It also depends on the surface binding energy of atoms in the target.

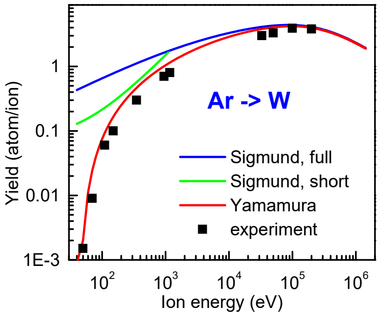

Petrov et al:
Y. Yamamura's correction for f(E), E_{TH} is best for Sputter-deposition combinations ion/target

$$Y(E) = \frac{0.04}{U}\alpha(M_t/M_i)QS_n(E)\left(1-\left(\frac{E_{TH}}{E}\right)^{0.5}\right)^2$$

$$Q = \frac{q_T}{1+s_e(\varepsilon)}$$

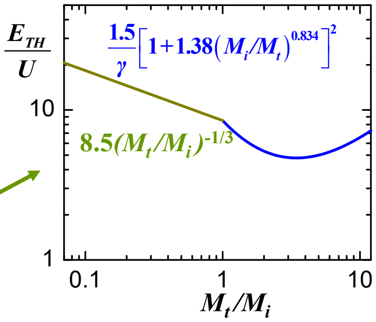

Y. Yamamura et al, Rad.Eff.,11 65 (1983)
I. Petrov et al, Bulg.J.Phys., 18 203(1991)

“Simple” Y(E) formula

Sputtering

for E < 1 keV , M_i > 15 amu

$$Y(E) = \frac{1.8}{U}\alpha(M_t/M_i)\frac{(Z_iZ_t)^{0.5}}{(Z_i^{2/3}+Z_t^{2/3})^{0.5}}\frac{(M_iM_t)^{0.5}}{(1+M_t/M_i)^{0.5}}E^{0.5}\left(1-\left(\frac{E_{TH}}{E}\right)^{0.5}\right)^2$$

Eqn. A

$$Y(E) = \frac{3}{4\pi^2}\alpha(M_t/M_i)\frac{\gamma E}{U}$$

$$\gamma = \frac{4M_tM_i}{(M_t+M)^2}$$

Petrov, unpublished

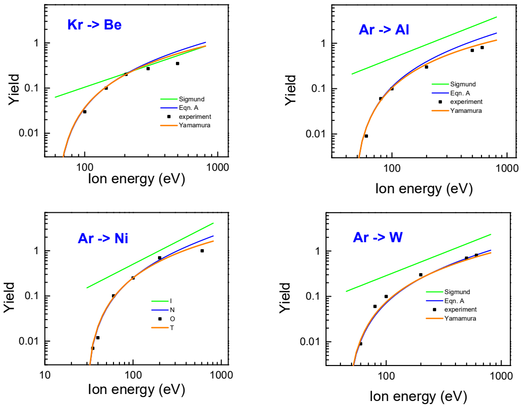

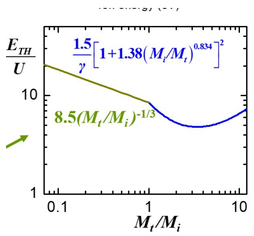

Note: Works for pure metal targets, including self-sputtering $Y_{selfsp}(E) = (0.9/U)Z^{2/3}M\,E^{1/2}(1-(8.5U/E)^{1/2})^2$

Energy efficiency of sputtering

Sputtering

Power of the ion beam - $P_{ion\ flux} = J*E$

Power used for sputtering - $P_{sp}=U*J*Y(E)$

Sputtering efficiency $\eta = P_{sp}/P_{ion\ flux}$

$\eta = U*Y(E)/E$

Yamamura formula: ⇨

η_{max} at $E=7*E_{th}$

For $3E_{TH} \le E \le 10E_{TH}, \eta \ge 0.8\eta_{max}$

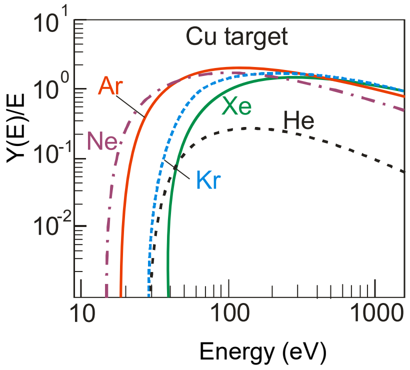

Typical example:

U = 4 eV, E_{TH} = 30 eV, η_{max} at E=210 eV
0.8 η_{max} E = 90 – 300 eV

Magnetrons work at or slightly
above the optimum energy

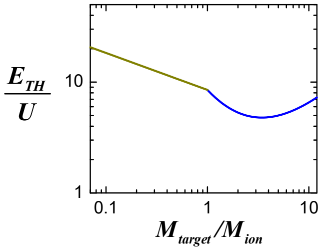

I. Petrov et al, Bulg.J.Phys., 18 2013(1991)

Energy efficiency of sputtering

The maximum sputtering efficiency between 0.5 and 5 %

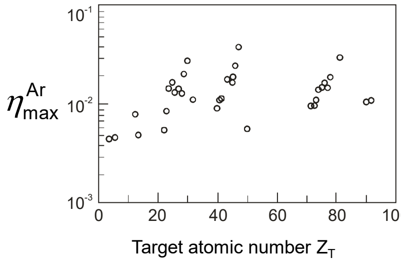

Ar provides high sputtering efficiency for a large number of metal targets (from Al to La)

Ne has ~ 20% advantage for Be and C

Kr ~ 40-60% advantage for targets heavier than Ta

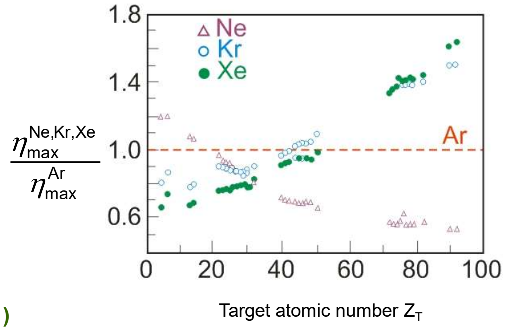

I. Petrov et al, Bulg.J.Phys., 18 2013(1991)

Energy of Sputtered Particles

Sputtered atom energy has a maximum at ~ U/2 (several eV) and tail extending to tens and hundreds of eV, depending on the ion energy.

Energy (Sigmund-Thompson) distribution:

$$F(E) \propto \frac{E}{(E+U)^3}\left(1-\left(\frac{E+U}{\gamma E_{ion}}\right)^{1/2}\right) \approx \frac{E}{(E+U)^3}$$

Has a maximum ~ U/2

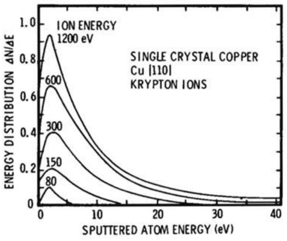

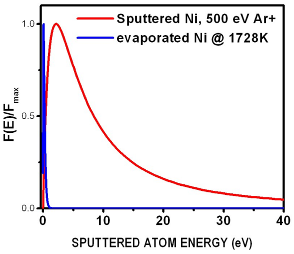

Comparison with thermal evaporation energies

Energetic particles in sputterdepostion
Thermalization

Sputtering Yield: Other Species

Distribution of types of sputtered species:
[Example for Ar sputtering of Cu]

Single atoms sputtered	100
Diatoms	1
Resputtered trapped gas	5
Single ions	0.1
Diatomic ions	0.001
Reflected incident species	3
Secondary electrons	10

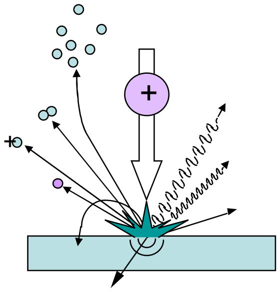

Prof. Angus Rocket

Energetic bombardment

Source of energetic particles bombardment

Reflection of Primary Ions

Incident ions may be reflected from the target surface.

Reflection coefficient = #reflected ions/#incident ions

Case study: TRIM simulation of 500 eV Ar ion scattering

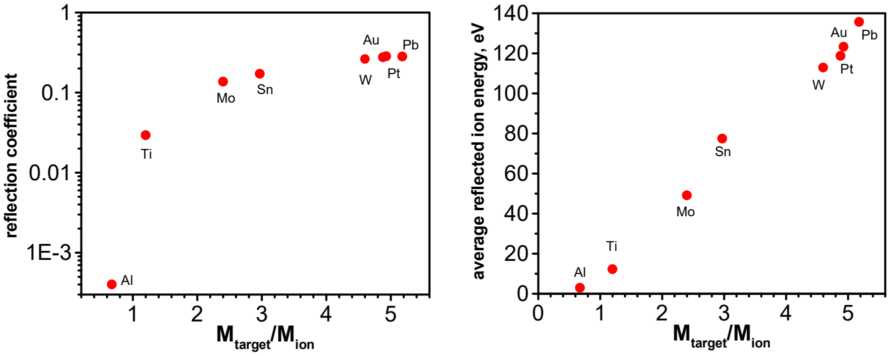

Both reflection coefficient and the average energy of the reflected ions increase when the target atom is heavier than the ion

Petrov, unpublished

Energetic bombardment

Reflection of Primary Ions, cont.

Incident ions may be reflected from the target surface.

Reflection coefficient = #reflected ion/#incident ion

Case study: TRIM simulation of 500 eV , **Xe**, **Ar**, and **N** ion scattering

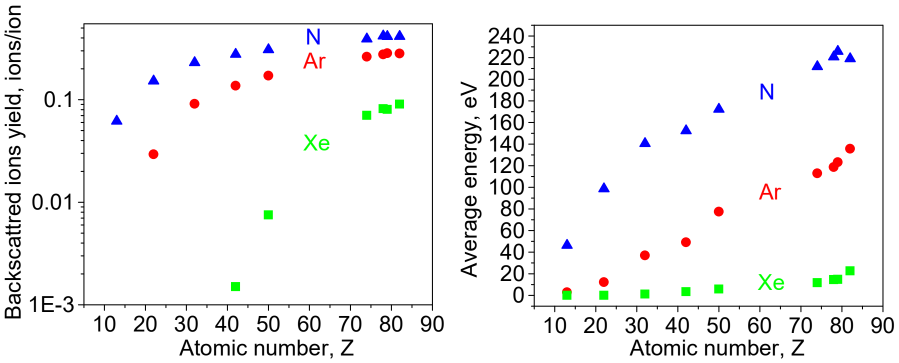

Both reflection coefficient and the average energy of the reflected ions for a given target decrease when heavier ions are used.

Petrov, unpublished

Reflection of Primary Ions, cont.

Case study: TRIM simulation of 500 eV , Xe, Ar, and N ion scattering

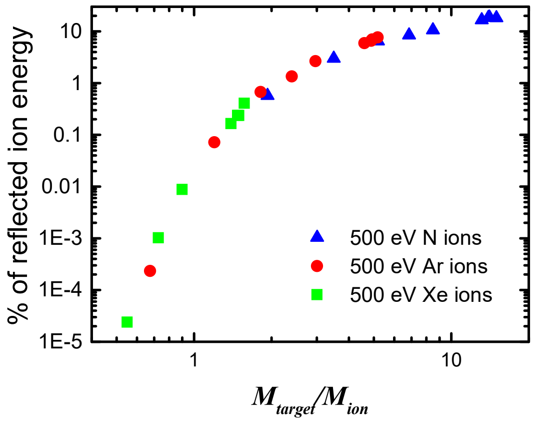

A significant fraction of the incident ion energy (> 10%) is reflected back when ions are much lighter than the target atoms

Petrov, unpublished

Another source of energetic particle bombardment

The role of negative ions during sputter-deposition of oxides

Note: Oxygen has an electron affinity of 1.461 eV

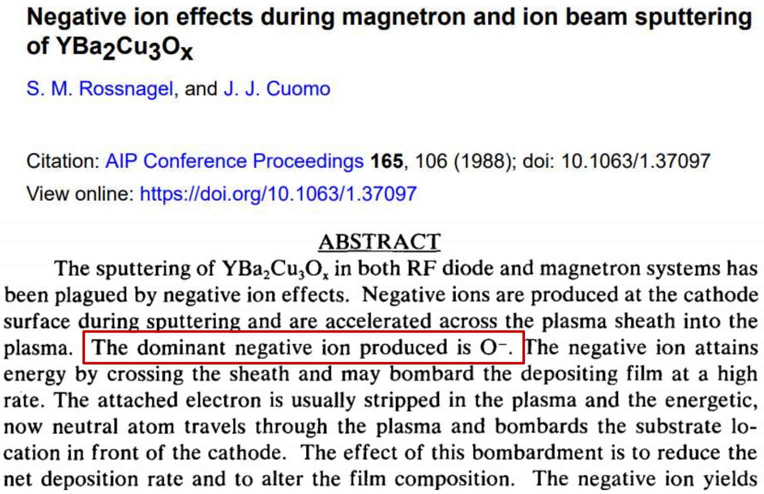

Negative ion effects during magnetron and ion beam sputtering of $YBa_2Cu_3O_x$

S. M. Rossnagel, and J. J. Cuomo

Citation: AIP Conference Proceedings **165**, 106 (1988); doi: 10.1063/1.37097
View online: https://doi.org/10.1063/1.37097

ABSTRACT

The sputtering of $YBa_2Cu_3O_x$ in both RF diode and magnetron systems has been plagued by negative ion effects. Negative ions are produced at the cathode surface during sputtering and are accelerated across the plasma sheath into the plasma. The dominant negative ion produced is O^-. The negative ion attains energy by crossing the sheath and may bombard the depositing film at a high rate. The attached electron is usually stripped in the plasma and the energetic, now neutral atom travels through the plasma and bombards the substrate location in front of the cathode. The effect of this bombardment is to reduce the net deposition rate and to alter the film composition. The negative ion yields

Another source of energetic particle bombardment

The role of negative ions during sputter-deposition of oxides

JAPANESE JOURNAL OF APPLIED PHYSICS
VOL. 20, NO. 3, MARCH, 1981 pp. 519–526

High-Energy Neutral Atoms in the Sputtering of ZnO

Kikuo TOMINAGA, Nozomu UESHIBA, Yoshihiro SHINTANI and Osamu TADA

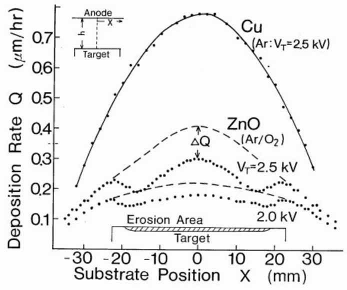

Fig. 1. Distributions of deposition rates at 0.05 Torr in DC diode sputtering, where V_T and ΔQ represent discharge voltage and drop in deposition rate, respectively.

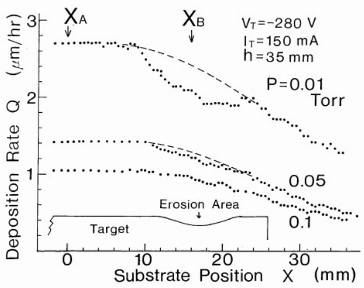

Fig. 2. Distributions of deposition rates at several gas pressures in planar magnetron sputtering.

The role of negative ions during sputter-deposition of oxides

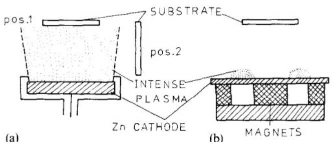

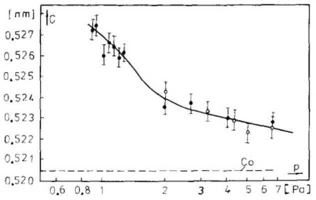

Fig. 6. Variation in the lattice parameter c of ZnO films magnetron sputtered at different total pressures and for constant Q = 80%: ●, P = 55 W; ○, P = 110 W.

Placing the substrates to the side of the target and increasing the deposition pressure eliminate the adverse effect of energetic oxygen bombardment

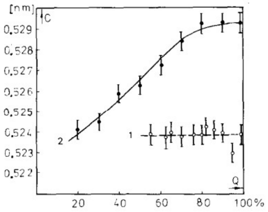

Fig. 7. Variation in the lattice parameter c of ZnO films with Q at two different total pressures and discharge powers: ●, p = 0.4 Pa, P = 20 W; ○, p = 6.6 Pa, P = 110 W.

I Petrov, V.Orlinov, A. Misiuk, Thin Solid Films, 120 (1984) 55

Transport of sputtered species in the gas phase

I. Petrov, I. Ivanov, V. Orlinov, and J.E. Sundgren, J. Vac. Sci. Technol, 11 2733 (1993)

Transport in the gas phase

Measured and calculated deposition fluxes

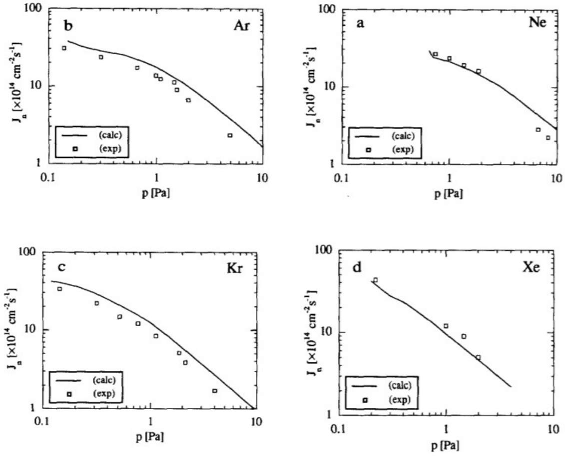

Vanadium target, 50 mm dia

$D_{target\text{-}substrate}$ = 10 cm

I_T = 0.3 A

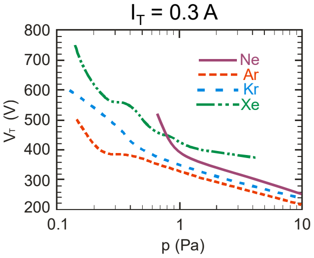

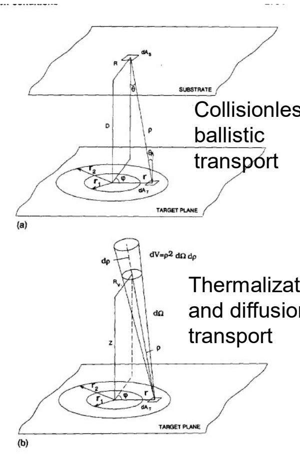

Collisionless/ ballistic transport

Thermalization and diffusion transport

FIG. 1. Geometry used in the calculations for the ballistics transport (a), and thermalization in the gas phase (b).

Calculated curves follow pressure dependence for all gases, **only after accounting for diffusion**

Comparison of magnetron sputter deposition conditions in neon, argon, krypton, and xenon discharges

I. Petrov,[a] I. Ivanov,[b] and V. Orlinov
Institute of Electronics, Bulgarian Academy of Sciences, Sofia 1784, Bulgaria
J.-E. Sundgren
Thin Film Division, Department of Physics, Linköping University, S-581 83 Linköping, Sweden

J. Vac. Sci. Technol, 11 2733 (1993)

Thermalization of sputtered species

In typical pressure range for magnetron sputter deposition, both collisionless and diffusive transport are effective

Note: to get the relatively good agreement at low pressures several adjustments to the mean free path had to be made
To get agreement at high pressures diffusive transport had to be taken into account

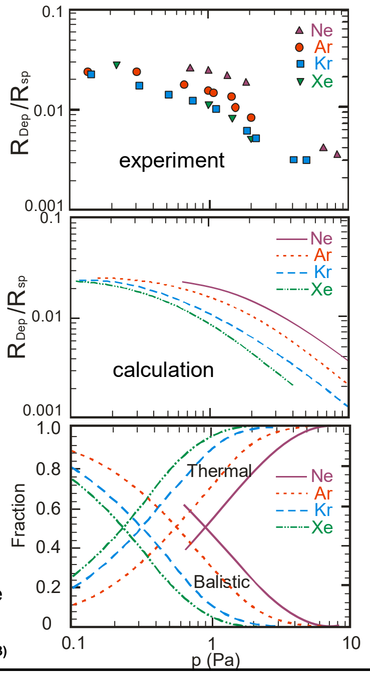

flux fractions in the calculation

I. Petrov, I. Ivanov, V. Orlinov, and J.E. Sundgren, J. Vac. Sci. Technol, 11 2733 (1993)

---

http://emaps.mrl.uiuc.edu/casandra/ **N!B! the site no longer works**

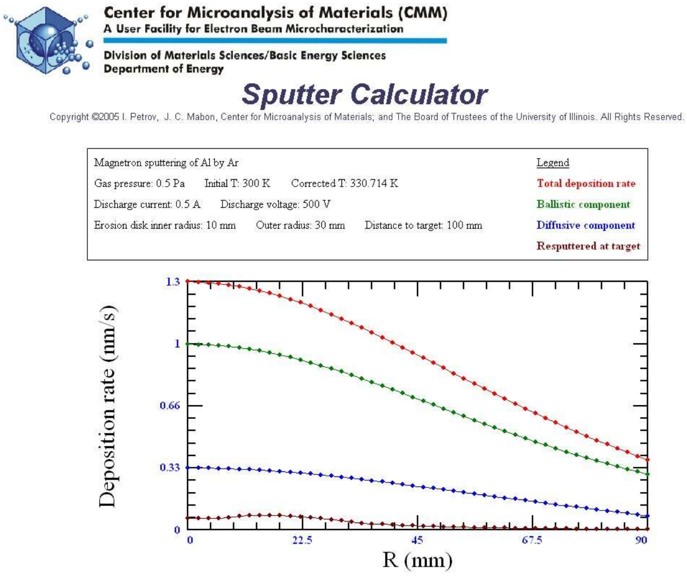

Center for Microanalysis of Materials (CMM)
A User Facility for Electron Beam Microcharacterization
Division of Materials Sciences/Basic Energy Sciences
Department of Energy

Sputter Calculator

```
Magnetron sputtering of Al by Ar                                                    Legend
Gas pressure: 0.5 Pa    Initial T: 300 K    Corrected T: 330.714 K                  Total deposition rate
Discharge current: 0.5 A    Discharge voltage: 500 V                                Ballistic component
Erosion disk inner radius: 10 mm    Outer radius: 30 mm    Distance to target: 100 mm   Diffusive component
                                                                                    Resputtered at target
```

Classic paper

Calculation of deposition rates in diode sputtering systems

W. D. Westwood

Journal of Vacuum Science and Technology **15**, 1 (1978); https://doi.org/10.1116/1.569429

Mean free path

$$\lambda^{-1} = 8.34 \times 10^{14} \rho \frac{(\sigma_s + \sigma_g)^2}{4} (1 + M_s/M_g)^{1/2},$$

ρ – pressure [Pa], σ_s, σ_g diameters [cm],
Author did not specify the temperature; it is 273 K

Number of collisions to thermalize the atom

An alternative approach is to use the concept of "persistence" introduced by Jeans.[13] This is the expectation that an atom of velocity ν will have velocity ν^1 in the direction of ν after the collision and is given by

$$\frac{\nu^1}{\nu} = \frac{1-M}{1+M} + \frac{2M}{1+M} \frac{\ln[1+M)^{1/2} + M^{1/2}]}{4M^{3/2}(1+M)^{1/2}} + \frac{2M^4 + 5M^3 + 3M^2 - M - 1}{4M(1+M)^3}. \quad (7)$$

The number of collisions required to reduce the initial velocity ν_o to the thermal velocity ν_g is

$$\eta^1 = \ln(\nu_g/\nu_o)/\ln(\nu^1/\nu). \quad (8)$$

---

[13] J. H. Jeans, in *The Dynamical Theory of Gases* (Dover New York, 1954).

Thermalization distance

$$D_3 = \eta^1 \lambda$$

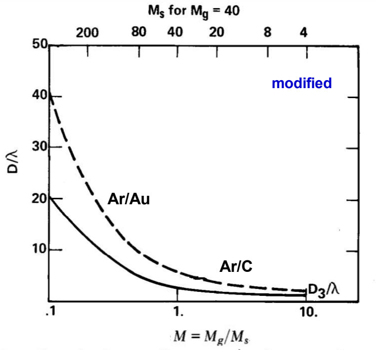

FIG. 4. The number of average collisions required to reduce a sputtered atom of mass M_s with initial energy of 5 (full lines) and 1000 eV (dashed lines) to thermal energies by collision with gas atoms, mass M_g.

The thermalization of energetic atoms during the sputtering process

Cite as: Journal of Vacuum Science & Technology A **2**, 1285 (1984); https://doi.org/10.1116/1.572396
Submitted: 11 July 1983 . Accepted: 19 February 1984 . Published Online: 04 June 1998

R. E. Somekh

Department of Metallurgy and Materials Science, University of Cambridge, Pembroke Street, Cambridge, CB2 3QZ England

(Received 11 July 1983; accepted 19 February 1984)

We consider the sputter deposition process and present a calculation of the rate of energy loss of sputtered atoms and reflected neutrals due to elastic collisions with the sputtering gas atoms. Compared to previous calculations we have explicitly taken into account the strong energy dependence of the scattering cross section recently reported by Robinson. The results suggest a much less efficient energy loss rate than previously envisaged using the classical thermal cross sections. Such thermal cross sections have been used in previous calculations to explain the high sputtering pressure required for preparing high critical transition temperature superconductors Nb_3Ge and Nb_3Sn.

Transport the gas phase

The thermalization of energetic atoms during the sputtering process

Cite as: Journal of Vacuum Science & Technology A **2**, 1285 (1984); https://doi.org/10.1116/1.572396
Submitted: 11 July 1983 . Accepted: 19 February 1984 . Published Online: 04 June 1998

R. E. Somekh

In order to estimate the collision cross section between sputtered metal atoms (atomic number Z_1) and the inert sputtering gas atom (atomic number Z_2) a simple interpolation scheme has been used. We interpolate linearly using the cross sections $\sigma(E)$ based on Robinson's original calculations for Ar, Kr, and Xe ($Z_2 = 18, 36, 54$, respectively). Thus, the scattering cross section $\sigma(E)$ is given by

$$\sigma(E) = \sigma_{\mathrm{Ar}}(E) + [\sigma_{\mathrm{Kr}}(E) - \sigma_{\mathrm{Ar}}(E)]\,\frac{(Z_1 - Z_2)}{(Z_{\mathrm{Kr}} - Z_{\mathrm{Ar}})},$$

for the case with a mean atomic number $[(Z_1 + Z_2)/2]$ lying between 18 and 36.

Sputtered atoms

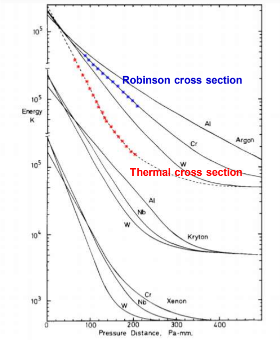

FIG. 2. The variation of sputtered atom energy with distance of sputtered atoms in Ar, Kr, and Xe; (---) earlier thermal cross-section calculation of Meyer *et al.*[7]

Back scattered gas atoms

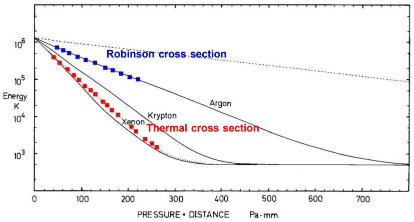

FIG. 3. The variation of energy with distance of reflected ne Ar, Kr, and Xe for initial e 110 ± 55 eV; (---) calculation of Gilbert *et al.*[10] (O–Ar); (···) calculation of Wu *et al.*[5] (Ar–Ar).

Thermal cross-sections severely underestimate thermalization distances

Transport the gas phase

Energetic binary collisions in rare gas plasmas

Cite as: Journal of Vacuum Science and Technology **16**, 185 (1979); https://doi.org/10.1116/1.569903
Published Online: 04 June 1998

R. S. Robinson

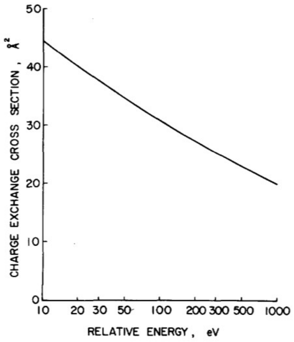

FIG. 1. Total resonance charge exchange cross section for argon as a function of relative energy.

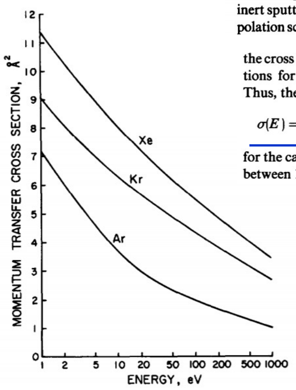

FIG. 4. Momentum transfer (diffusion) cross section for Ar, Kr, and Xe as a function of energy.

In order to estimate the collision cross section between sputtered metal atoms (atomic number Z_1) and the inert sputtering gas atom (atomic number Z_2) a simple interpolation scheme has been used. We interpolate linearly using the cross sections $\sigma(E)$ based on Robinson's original calculations for Ar, Kr, and Xe ($Z_2 = 18, 36, 54$, respectively). Thus, the scattering cross section $\sigma(E)$ is given by

$$\sigma(E) = \sigma_{\mathrm{Ar}}(E) + [\sigma_{\mathrm{Kr}}(E) - \sigma_{\mathrm{Ar}}(E)]\,\frac{(Z_1 - Z_2)}{(Z_{\mathrm{Kr}} - Z_{\mathrm{Ar}})},$$

for the case with a mean atomic number $[(Z_1 + Z_2)/2]$ lying between 18 and 36.

For metal atom Somekh extrapolated between Robinson data for inert gases

Faster atoms have smaller scattering cross-sections -> larger mean free path

Transport the gas phase

Thermalization of sputtered species

Good agreement obtained using both
Westwood and Somekh approaches
x10 over thermal cross-section

In typical pressure range for magnetron sputter deposition, both collisionless and diffusive transport are effective

We can use pressure to tune the average energy of the sputtered species and to control the energy of the reflected ions

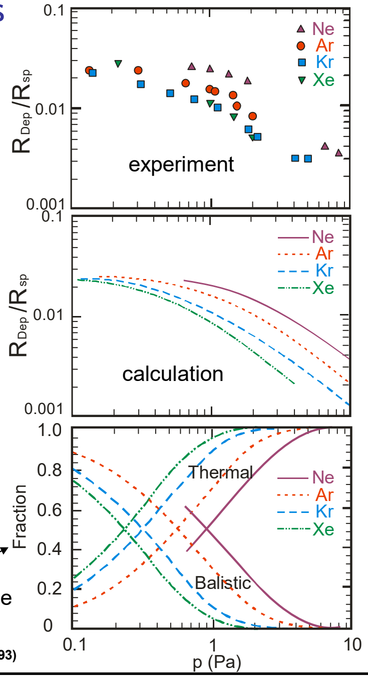

flux fractions in the calculation

I. Petrov, I. Ivanov, V. Orlinov, and J.E. Sundgren, J. Vac. Sci. Technol, 11 2733 (1993)

Contents lists available at SciVerse ScienceDirect

Thin Solid Films
Thin Solid Films 520, 6337–6354 (2012)
journal homepage: www.elsevier.com/locate/tsf

ELSEVIER

Special feature

Magnetron sputter deposition as visualized by Monte Carlo modeling

D. Depla *, W.P. Leroy

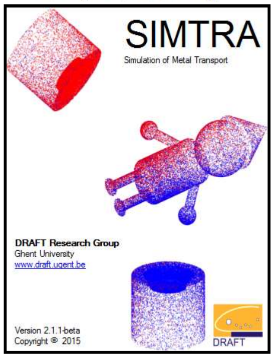

SIMTRA
Simulation of Metal Transport

DRAFT Research Group
Ghent University
www.draft.ugent.be

Version 2.1.1-beta
Copyright © 2015

DRAFT

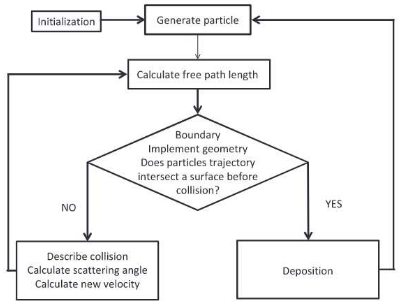

Fig. 1. Flow chart of the Monte Carlo model SIMTRA, showing the important steps in the calculation of a deposition profile.

Diederik Depla
Ghent University, Belgium

https://www.ugent.be/we/solidstatesciences/draft/en/services/software#SiMTRA
watch the YouTube video

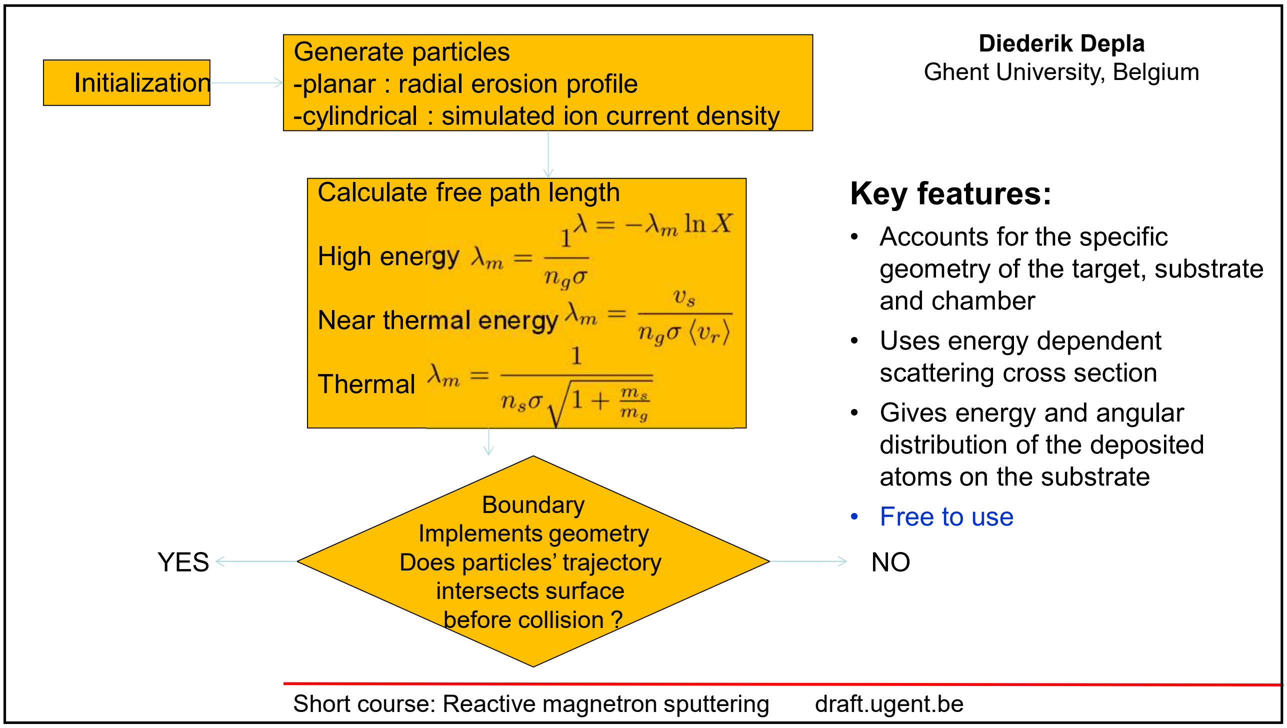

Diederik Depla
Ghent University, Belgium

Initialization

Generate particles
-planar : radial erosion profile
-cylindrical : simulated ion current density

Calculate free path length

$$\lambda = -\lambda_m \ln X$$

High energy $\lambda_m = \frac{1}{n_g \sigma}$

Near thermal energy $\lambda_m = \frac{v_s}{n_g \sigma \langle v_r \rangle}$

Thermal $\lambda_m = \frac{1}{n_s \sigma \sqrt{1 + \frac{m_s}{m_g}}}$

Boundary
Implements geometry
Does particles' trajectory
intersects surface
before collision ?

YES

NO

Key features:

- Accounts for the specific geometry of the target, substrate and chamber
- Uses energy dependent scattering cross section
- Gives energy and angular distribution of the deposited atoms on the substrate
- Free to use

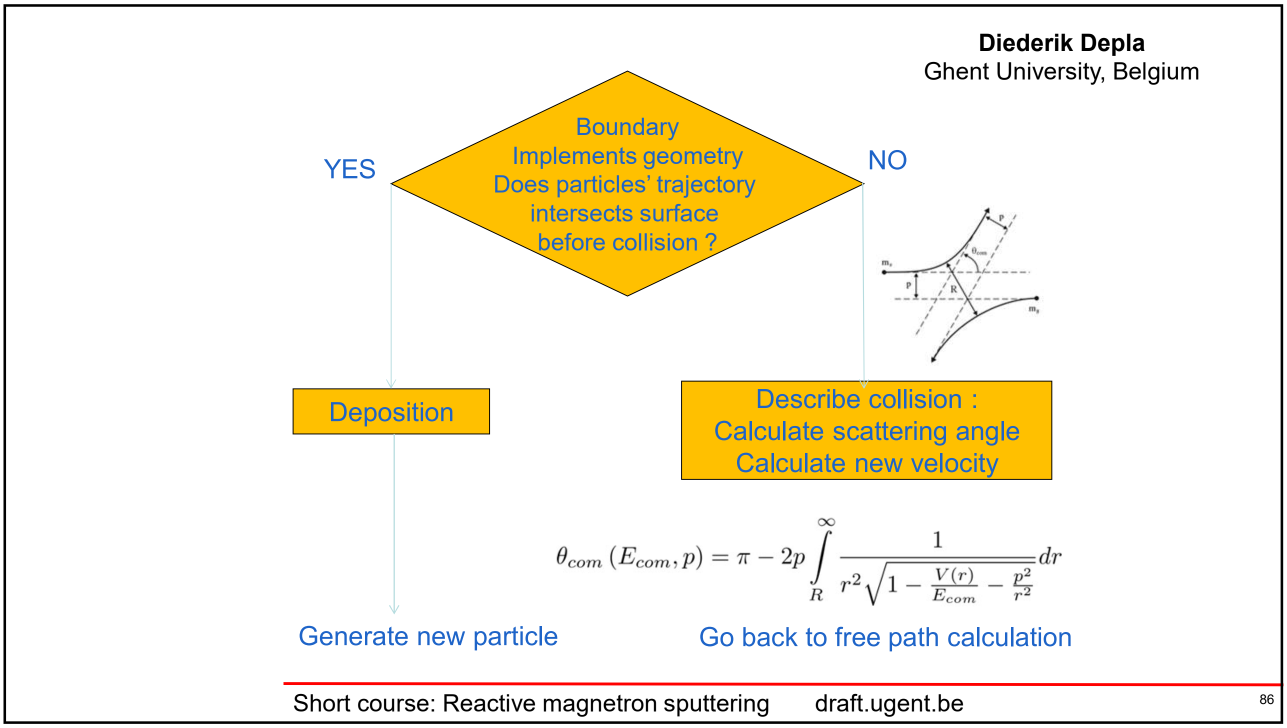

Diederik Depla
Ghent University, Belgium

Boundary
Implements geometry
Does particles' trajectory
intersects surface
before collision ?

YES

NO

Deposition

Describe collision :
Calculate scattering angle
Calculate new velocity

$$\theta_{com}(E_{com}, p) = \pi - 2p \int_R^\infty \frac{1}{r^2 \sqrt{1 - \frac{V(r)}{E_{com}} - \frac{p^2}{r^2}}} dr$$

Generate new particle

Go back to free path calculation

Influence of the sputtering gas on the deposition rate: SiMTRA comparison with literature data

unpublished

D. Depla
Department of Solid State Sciences, Ghent University, Krijgslaan 281 (S1), 9000 Gent, Belgium

(Dated: April 26, 2023)

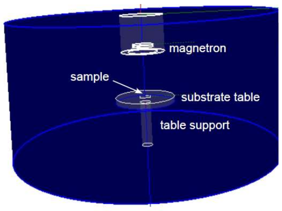

Figure 1. Used geometry. The vacuum chamber (blue) is a cylir with a radius and a height of 0.25 m.

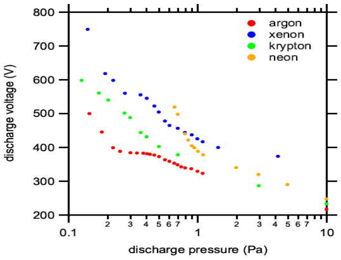

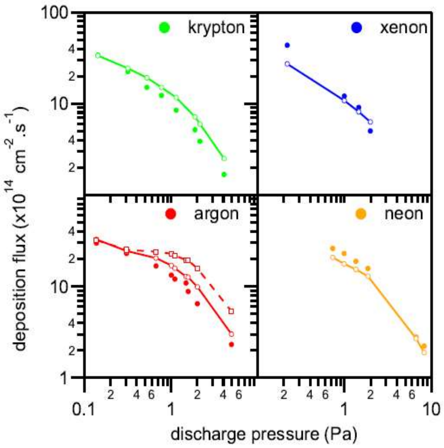

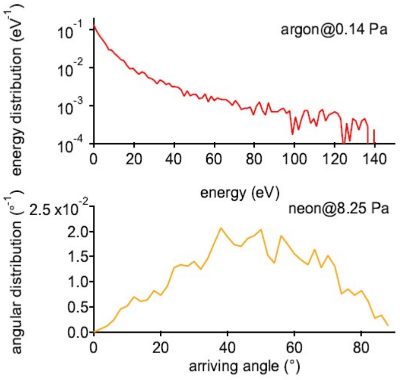

Exp. Data from: I. Petrov, I. Ivanov, V. Orlinov, and J.E. Sundgren, J. Vac. Sci. Technol, 11 2733 (1993)

Variations of sputtering systems
Magnetron sputtering
Unbalanced magnetrons

Diode sputter deposition system

Components and typical parameters

V_T ~ 2-5 kV
J_T ~ 1 mA/cm^2
p ~ 50-80 mTorr
$\lambda << d_{TS}$

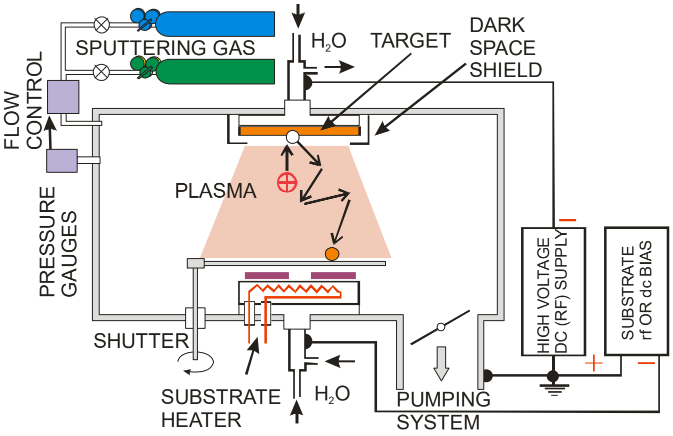

Triode sputter deposition system

Components and typical parameters

V_T ~ 1 kV
J_T ~ 5 mA/cm^2
p ~ 10-20 mTorr
λ ~ d_{TS}

Thermionic arc; V_{arc} ~ 10-30 V, I_{arc} ~ several Amps
Independent control of ion flux and energy
The presence of a hot filament hampers reactive deposition

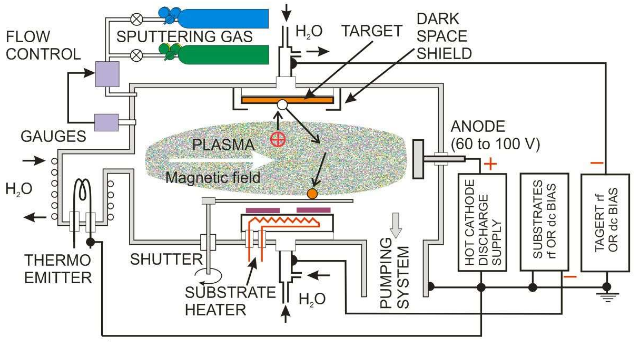

Magnetron sputter deposition system

Components and typical parameters

$V_T \sim 0.3\text{-}0.5$ kV
$J_T \sim 10\text{-}100$ mA/cm^2
$P_T \sim 3\text{-}50$ W/cm^2
p ~ 2-20 mTorr
$\lambda > d_{TS,,}$, $\lambda < d_{TS}$

ExB field near target enhances ionization efficiency, thus reducing both V_T and p

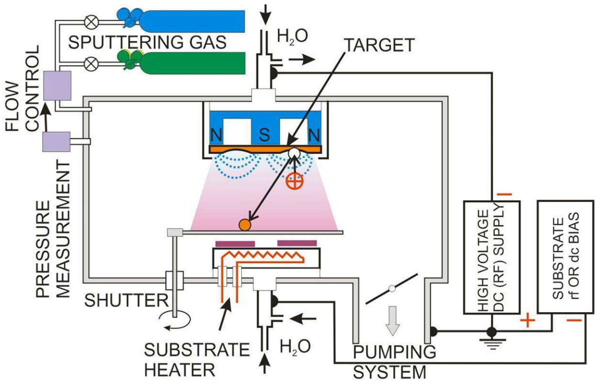

Magnetron discharge characteristics

MATSE,
University of Illinois

Thornton, cylindrical magnetrons

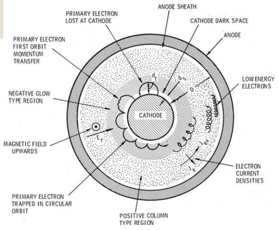

Conventional DC sputtering: kV, tens mTorr

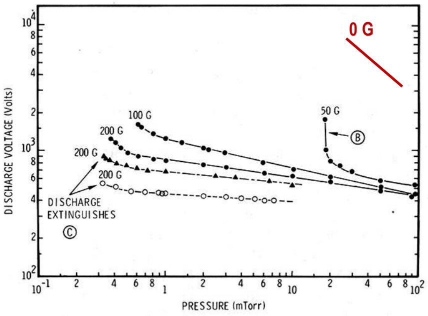

J.A. Thornton and A.S. Penfold, "Cylindrical Magnetron Sputtering," in *Thin Film Processes*, edited by J.L. Vossen and W. Kern, Academic Press, NY 1978.

ExB configurations

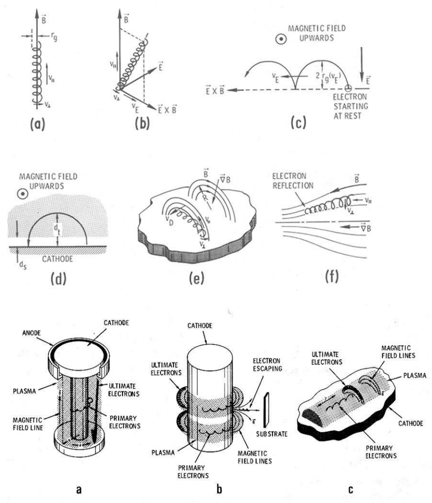

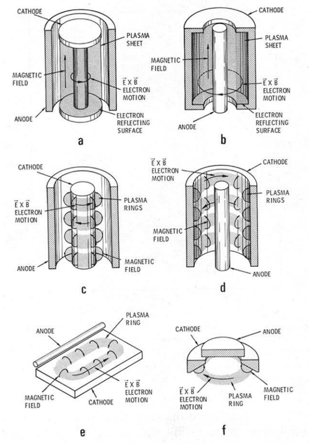

$$\frac{V_T}{E_o} = \frac{1}{\gamma_i\ \varepsilon_i\ \varepsilon_e}$$

$$\varepsilon_i\ \varepsilon_e \approx 1$$

J.A. Thornton and A.S. Penfold, “Cylindrical Magnetron Sputtering,” in *Thin Film Processes*, edited by J.L. Vossen and W. Kern, Academic Press, NY 1978.

Reactive sputtering

Target surface reaction, transition from Ar sputtering pure metal to nitride

Transition from discharge in Ar to a discharge in N_2

Sputtering of Ti target in Ar+N2

I. Petrov, A. Myers, J.E. Greene, and J.R. Abelson, JVST A 12, 2846 (1994)

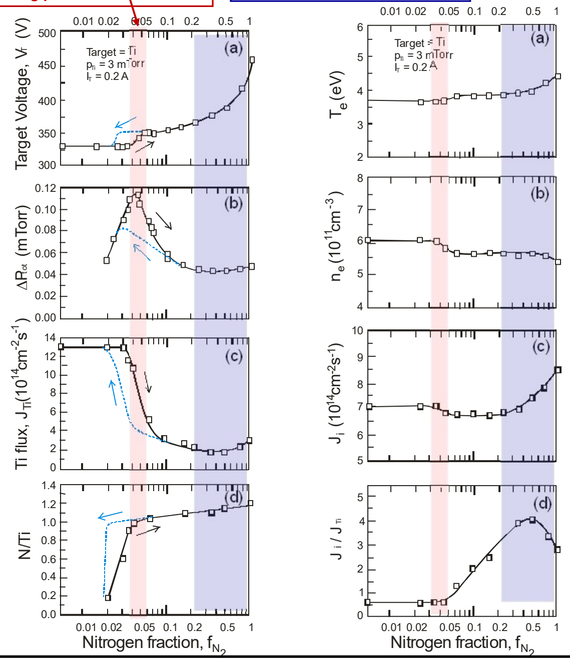

$$\frac{V_T}{E_o} = \frac{1}{\gamma_i\ \varepsilon_i\ \varepsilon_e}$$

$$Y(E) = \frac{0.04}{U}\alpha(M_t/M_i)S_n(E)$$

Reactive sputtering

Magnetron sputter deposition: Linking discharge voltage with target properties

D. Depla *, S. Mahieu, R. De Gryse

Thin Solid Films 517 (2009) 2825–2839

Department of Solid State Sciences, Ghent University, Krijgslaan 281(S1) 9000 Gent, Belgium

Relative change of the effective secondary
ion-electron emission coefficient upon target reaction “poisoning”

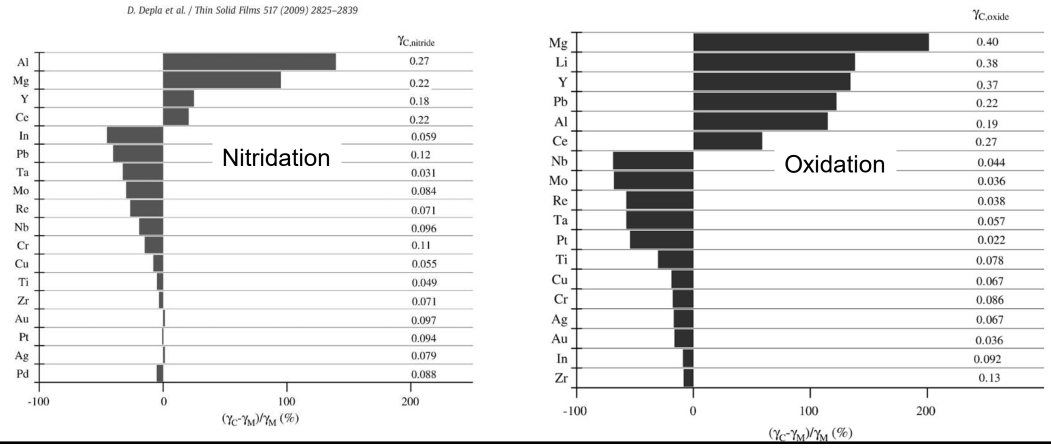

Ion distribution at the substrate

DC magnetron sputtering

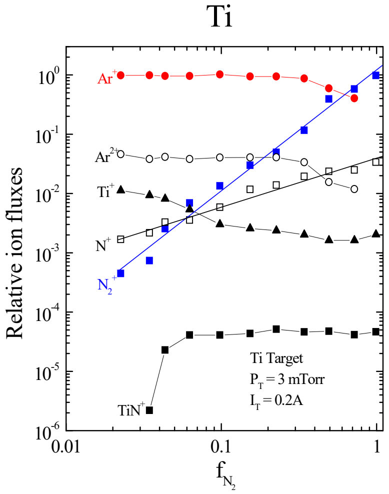

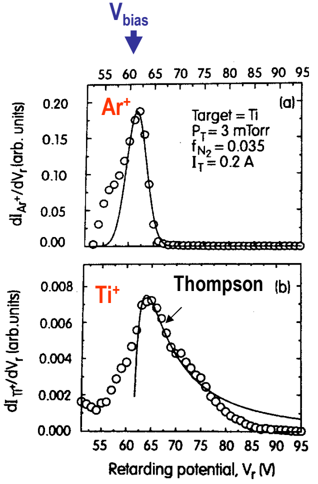

Gas ions dominate:
Ar^+ in most of the range, N_2^+ in pure Nitrogen

Gas ions energy corresponds to the applied bias
TI^+ extend to higher energies due to being sputter ejected

I. Petrov, A. Myers, J.E. Greene, and J.R. Abelson, JVST A **12**, 2846 (1994)

Reactive sputtering, the big names

Modeling reactive magnetron sputtering: Opportunities and challenges

D. Depla*, K. Strijckmans, A. Dulmaa, F. Cougnon, R. Dedoncker, R. Schelfhout, I. Schramm, F. Moens, R. De Gryse

Department of Solid State Sciences, Ghent University, Krijgslaan 281 (S1), 9000 Gent, Belgium

Thin Solid Films 688 (2019) 137326

Fundamental understanding and modeling of reactive sputtering processes

S. Berg*, T. Nyberg

The Angstrom Laboratory, Uppsala University, Box 534, 751 21 Uppsala, Sweden

Thin Solid Films 476 (2005) 215–230

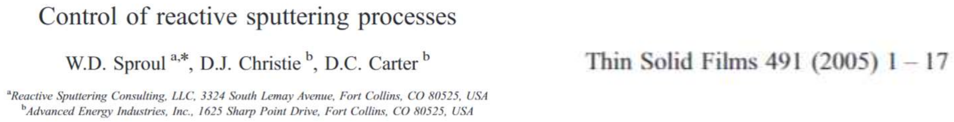

Control of reactive sputtering processes

W.D. Sproul [a,*], D.J. Christie [b], D.C. Carter [b]

[a]*Reactive Sputtering Consulting, LLC, 3324 South Lemay Avenue, Fort Collins, CO 80525, USA*
[b]*Advanced Energy Industries, Inc., 1625 Sharp Point Drive, Fort Collins, CO 80525, USA*

Thin Solid Films 491 (2005) 1 – 17

A parametric model for reactive high-power impulse magnetron sputtering of films

Tomáš Kozák[1,2] **and Jaroslav Vlček**[1]

J. Phys. D: Appl. Phys. **49** (2016) 055202 (18pp)

Magnetron sputter deposition
High Power Pulse Magnetron Sputtering (HPPMS)
High Power Impulse MS (HiPIMS)

Main new features:
- Source of metal ions
- Time separation between the gas and the metal ions
- Higher energy ions
- Lower deposition rates

Magnetron sputter deposition system
High Power Pulse MS (HPPMS)
High Power Impulse MS (HIPIMS)

Frequency ~ 50-500 Hz
Duty cycle < 10%
peak values
V_T ~ 0.7-2 kV
J_T ~ 100-1000 mA/cm^2
P_T ~ 70-2000 W/cm^2
p ~ 2-20 mTorr
$\lambda > d_{TS}$, $\lambda < d_{TS}$

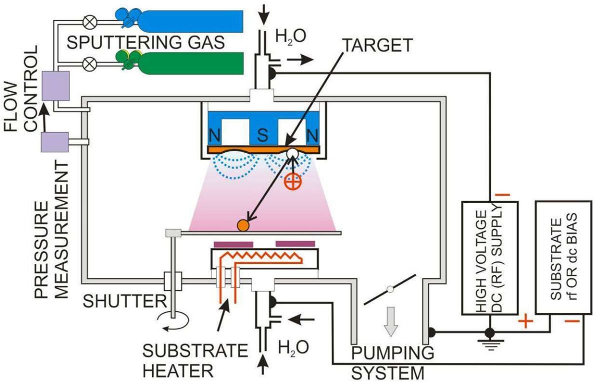

Main new features:
- Source of metal ions
- Time separation between the gas and the metal ions
- Higher energy ions
- Lower deposition rates

DCMS vs HiPIMS

Same average power
Same hardware

V_T ~ 0.3-0.5 kV
P_T ~ 10-50 W/cm^2
p ~ 2-20 mTorr

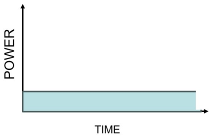

peak values
V_T ~ 0.7-2 kV
P_T ~ 500-3000 W/cm^2
p ~ 2-20 mTorr

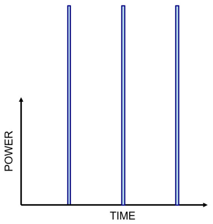

Frequency ~ 100-500 Hz
Duty cycle < 1-4 %

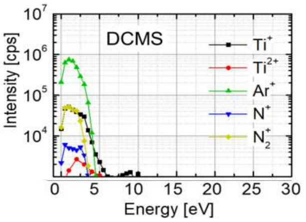

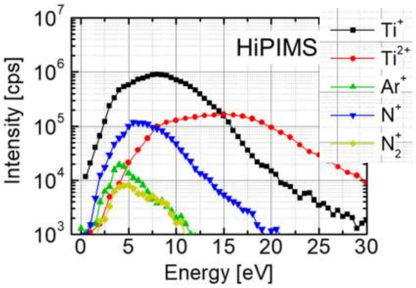

1. Thermal gas ions
2. Neutral deposited atoms
3. High deposition rate

Hybrid HiPIMS/DCMS

1. Energetic metal ions
2. Gas and metal ions separated in time
3. Lower deposition rates

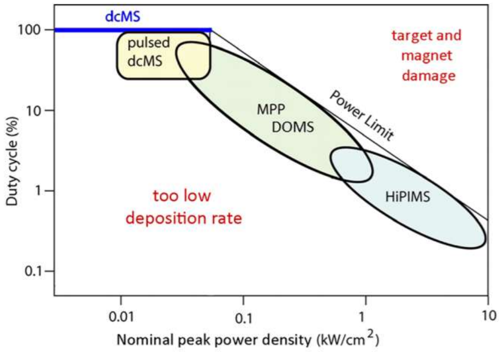

FIG. 36. Schematic showing various forms of magnetron sputtering in a duty-cycle—nominal peak power density diagram. Reprinted with permission from Gudmundsson *et al*., J. Vac. Sci. Technol. A **30**, 030801 (2012). Copyright 2012 AIP Publishing LLC (Fig. 1 from Ref. 140).

Gudmundsson, Brenning, Lundin, Helmersson,
J. Vac. Sci. Technol. A 30 (2012) 030801

Andre Anders, Tutorial: Reactive high power impulse magnetron sputtering (R-HiPIMS) JAP 121, 171101 (2017)
https://doi.org/10.1063/1.4978350

High Power Impulse Magnetron Sputtering

Surface and Coatings Technology 122 (1999) 290–293

A novel pulsed magnetron sputter technique utilizing very high target power densities

Vladimir Kouznetsov [a,*], Karol Macák [a], Jochen M. Schneider [a], Ulf Helmersson [a], Ivan Petrov [b]

Using a novel pulsed power supply in combination with a standard circular flat magnetron source, operated with a Cu target, a peak power density of 2800 W cm^{-2} was achieved. This results in a very intense plasma with peak ion current densities of up to 3.4 A cm^{-2} at the substrate situated 10 cm from the target. The ionized fraction of the deposited Cu flux was estimated to be approximately 70% from deposition rate measurements. The potential for high-aspect-ratio trench filling applications by high

Source of metal ions

Both May 1999

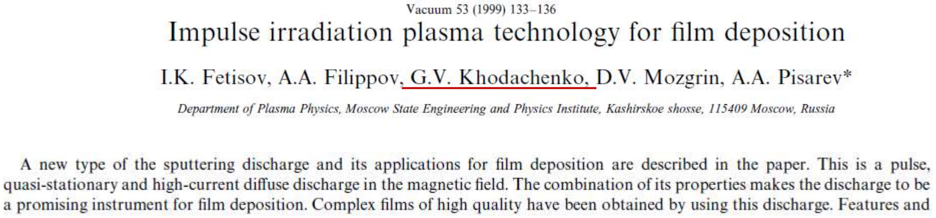

Vacuum 53 (1999) 133–136

Impulse irradiation plasma technology for film deposition

I.K. Fetisov, A.A. Filippov, G.V. Khodachenko, D.V. Mozgrin, A.A. Pisarev*

Department of Plasma Physics, Moscow State Engineering and Physics Institute, Kashirskoe shosse, 115409 Moscow, Russia

A new type of the sputtering discharge and its applications for film deposition are described in the paper. This is a pulse, quasi-stationary and high-current diffuse discharge in the magnetic field. The combination of its properties makes the discharge to be a promising instrument for film deposition. Complex films of high quality have been obtained by using this discharge. Features and

High Power Impulse Magnetron Sputtering

Surface and Coatings Technology 122 (1999) 290–293

A novel pulsed magnetron sputter technique utilizing very high target power densities

Vladimir Kouznetsov [a,*], Karol Macák [a], Jochen M. Schneider [a], Ulf Helmersson [a], Ivan Petrov [b]

Using a novel pulsed power supply in combination with a standard circular flat magnetron source, operated with a Cu target, a peak power density of 2800 W cm^{-2} was achieved. This results in a very intense plasma with peak ion current densities of up to 3.4 A cm^{-2} at the substrate situated 10 cm from the target. The ionized fraction of the deposited Cu flux was estimated to be approximately 70% from deposition rate measurements. The potential for high-aspect-ratio trench filling applications by high

Source of metal ions

Both May 1999

Vacuum 53 (1999) 133–136

Impulse irradiation plasma technology for film deposition

I.K. Fetisov, A.A. Filippov, G.V. Khodachenko, D.V. Mozgrin, A.A. Pisarev*

Department of Plasma Physics, Moscow State Engineering and Physics Institute, Kashirskoe shosse, 115409 Moscow, Russia

A new type of the sputtering discharge and its applications for film deposition are described in the paper. This is a pulse, quasi-stationary and high-current diffuse discharge in the magnetic field. The combination of its properties makes the discharge to be a promising instrument for film deposition. Complex films of high quality have been obtained by using this discharge. Features and

---

Surface & Coatings Technology 293 (2016) 42–47

High-current impulse magnetron discharge with liquid target

Alexander V. Tumarkin *, Andrey V. Kaziev, Maxim M. Kharkov, Dobrynya V. Kolodko,
Igor V. Ilychev, Georgy V. Khodachenko [1]

Department of Plasma Physics, National Research Nuclear University MEPhI (Moscow Engineering Physics Institute), 31 Kashirskoye Shosse, Moscow 115409, Russia

1. Introduction

The HiPIMS technology has been extensively developed over the recent two decades, and nowadays it is widely used for the deposition of superior thin films. The coatings prepared by HiPIMS find their applications in advanced areas of industry [1]. The HiPIMS technique emerged in 1999 [2] and quickly attracted major attention both among the industries and the academia. However, the pioneering studies in the field of the high power pulsed magnetron sputtering were carried out in the beginning of 1990s [3–5]. In particular, Mozgrin et al. [4] originally described the high-current impulse magnetron sputtering discharge (HCIMD), whose distinguishing feature is the behaviour of the voltage and current waveforms exhibiting the quasi-stationary stage duration up to tens ms (see Fig. 1). The pulsed discharge regimes are superior to di-

[2] V. Kouznetsov, K. Macák, J.M. Schneider, U. Helmersson, I. Petrov, A novel pulsed magnetron sputter technique utilizing very high target power densities, Surf. Coat. Technol. 122 (1999) 290–293.

[3] I.K. Fetisov, G.V. Khodachenko, D.V. Mozgrin, Quasi-stationary High Current Forms of Low Pressure Discharge in Magnetic Field, Proc. ICPIG-XX, Piza, Italy, 1991 476–478.

[4] D.V. Mozgrin, I.K. Fetisov, G.V. Khodachenko, High-current low-pressure quasi-stationary discharge in a magnetic field: experimental research, Plasma Phys. Rep. 21 (1995) 422–433.

[5] S.P. Bugaev, N.N. Koval, N.S. Sochugov, A.N. Zakharov, Investigation of a high-current pulsed magnetron discharge initiated in the low-pressure diffuse arc plasma, Proc. XVII Int. Symp. on Disch. and Electr. Insulation in Vac., Berkeley, USA 1996, pp. 1074–1076.

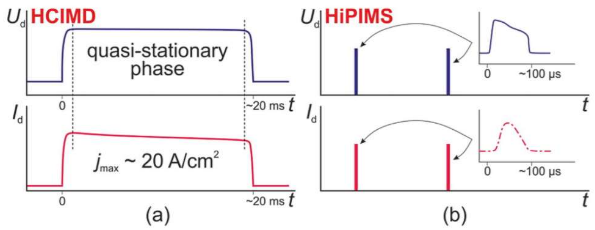

Fig. 1. Typical voltage and current traces of HCIMD (a) and HiPIMS (b).

Average discharge power P

$P_{HIPIMS} \approx P_{DCMS}$
$P_{HCIMD} >> P_{DCMS}$

Molten and hot trgets

petrov@illinois.edu

To properly exploit the advantages of HiPIMS it is necessary to know the energy and time evolution of the gas and metal ions

DCMS vs HiPIMS

Same average power
Same hardware

V_T ~ 0.3-0.5 kV
P_T ~ 10-50 W/cm^2
p ~ 2-20 mTorr

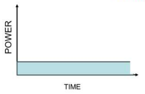

peak values
V_T ~ 0.7-2 kV
P_T ~ 500-3000 W/cm^2
p ~ 2-20 mTorr

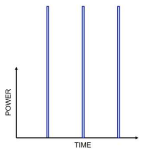

Frequency ~ 100-500 Hz
Duty cycle < 1-4 %

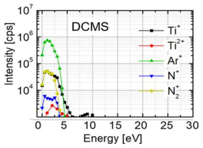

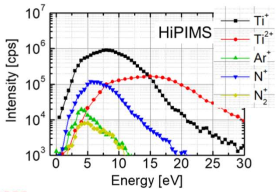

1. Thermal gas ions
2. Neutral deposited atoms
3. High deposition rate

Hybrid HiPIMS/DCMS

1. Energetic metal ions
2. Gas and metal ions separated in time
3. Lower deposition rates

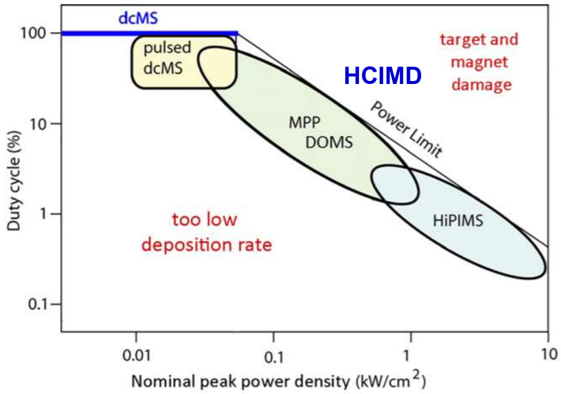

FIG. 36. Schematic showing various forms of magnetron sputtering in a duty-cycle—nominal peak power density diagram. Reprinted with permission from Gudmundsson *et al.*, J. Vac. Sci. Technol. A **30**, 030801 (2012). Copyright 2012 AIP Publishing LLC (Fig. 1 from Ref. 140).

Gudmundsson, Brenning, Lundin, Helmersson,
J. Vac. Sci. Technol. A 30 (2012) 030801

Andre Anders, Tutorial: Reactive high power impulse magnetron sputtering (R-HiPIMS) JAP 121, 171101 (2017)
https://doi.org/10.1063/1.4978350

Roman Chistyakov and Bassam Abraham, Zpulser, LLC

Lin et al, Surface and Coatings Technology (2009) 203 3676

Modulated Pulse Power Magnetron Sputtering MPPMS

J. Lin et al. / Surface & Coatings Technology 203 (2009) 3676–3685 3677

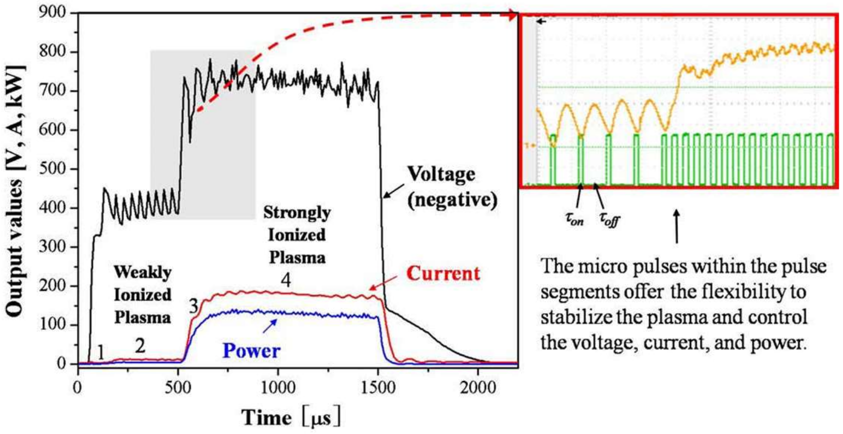

Fig. 1. Typical MPP pulse showing four steps of the target voltage, current and power evolutions during one modulated pulse (1500 µs overall pulse length in this example): 1) ignition of the weakly ionized plasma; 2) duration of the weakly ionized plasma; 3) transition stage from the weakly ionized plasma to the strongly ionized plasma; (4) duration of the strongly ionized plasma. The inserted figure on the right side shows the micro pulses within the pulse with adjustable voltage on (τ_{on}) and off (τ_{off}) times.

Roman Chistyakov and Bassam Abraham, Zpulser, LLC

Deep Oscillation Magnetron Sputtering DOMS

Lin et al, Surface and Coatings Technology (2015) 276, pp. 70-76

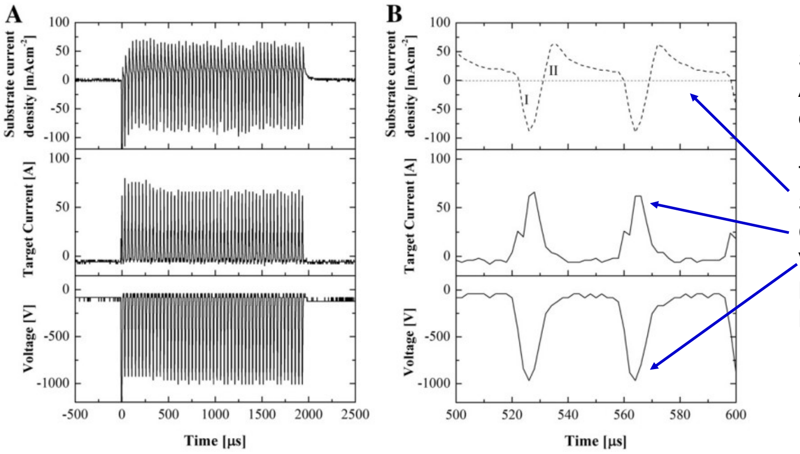

Scopus:
A few dozen of publications
on MPP and DOMS

Typical parameters:
Substrate current
Current
Voltage
Macropulses - ~0.5-1.5 ms, 100s Hz
Micropulses ~20-30 kHz

“The DOMS technique offers virtually **arc-free conditions** for reactive sputtering of many **insulating films** e.g. AlN, Al_2O_3, Si_3N_4, SiO_2 etc.”

Ionized sputter deposition using an extremely high plasma density pulsed magnetron discharge

Karol Macák, Vladimir Kouznetsov, Jochen Schneider, and Ulf Helmersson[a)]
Department of Physics, Linköping University, SE-581 83 Linköping, Sweden

Ivan Petrov
Materials Science Department and Materials Research Laboratory, University of Illinois,

1533 J. Vac. Sci. Technol. A 18(4), Jul/Aug 2000

Transition from gas to metal vapor discharge/gas rarefaction;
Time separation between the gas and the metal ions

Ar gas rarefaction > 80%
Metal plasma density > 10^{12} cm^{-3}

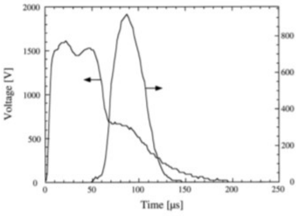

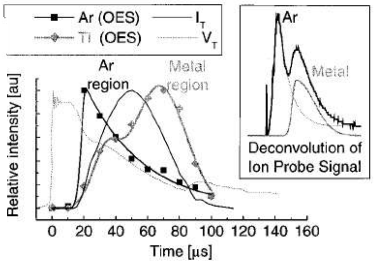

FIG. 3. Comparison of target current I_T and voltage V_T wave forms and

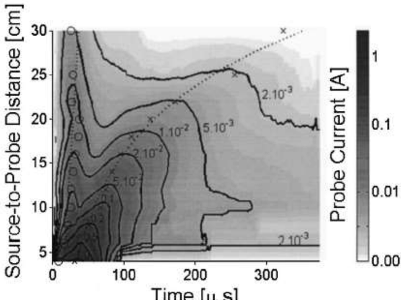

The existence of time separation between the Ar and metal-ion dominated fluxes at the substrate opens the possibility for selection one of the components for ion-assisted by using a pulsed bias voltage with suitable synchronization

Phases of the HIPIMS discharge

1. **Ignition/discharge breakdown**
2. **Current rise**
3. **Gas depletion/rarefaction**
4. **Metal mode***
5. **Afterglow**

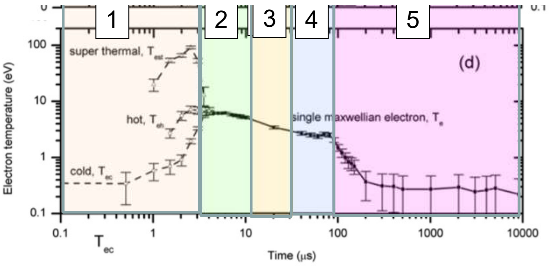

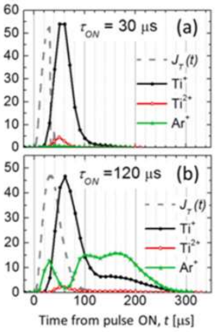

P Poolcharuansin and J W Bradley
Plasma Sources Sci. Technol. 19 (2010) 025010

Time- and Species-Resolved Plasma Imaging as a New Diagnostic Approach for HiPIMS Discharge Characterization

Matěj Hála, Oleg Zabeida, Bill Baloukas, Jolanta E. Klemberg-Sapieha, and Ludvik Martinu

Page 3035

IEEE TRANSACTIONS ON PLASMA SCIENCE, VOL. 38, NO. 11, NOVEMBER 2010

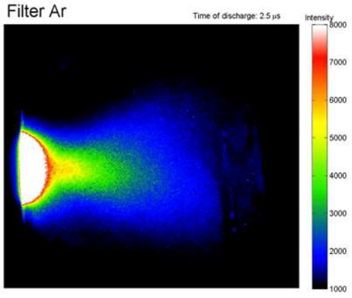

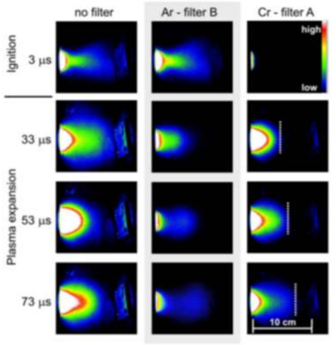

Fig. 4. Images taken during 200-µs HiPIMS discharge pulses in pure Ar at 4 Pa with no filter on the camera objective (left column), and with an optical bandpass filter specific for emission from neutral Ar (middle column - filter B), and from neutral Cr (right column - filter A). The images were recorded at different times after the pulse initiation as indicated in Fig. 3. For clarity purposes, different colors are assigned to different emission intensities, according to the scale depicted in the upper right image. The position of the Cr emission wavefront is highlighted by a dashed line. Please note that a movie of the discharge can be downloaded at http://ieeexplore.ieee.org.

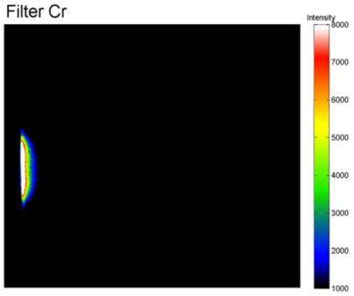

Lower deposition rates in HiPIMS due to back attraction of positive ions of the sputtered materials back to the target

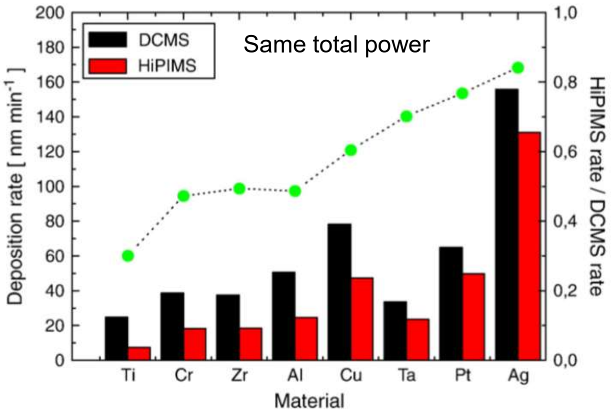

Fig. 1. The deposition rates for DCMS and HiPIMS discharges plotted as bars for the different target materials used (left axis). The deposition rate of HiPIMS over DCMS deposition rate is shown as a scatter plot (right axis).

M. Samuelsson, D. Lundin, J. Jensen, M. A. Raadu, J. T. Gudmundsson, and U. Helmersson, Surf. Coat. Technol. 202, 591 (2010).

Note: This is just typical example

The reduction of deposition rate may vary significantly for a given material depending on the experimental set-up and the HiPIMS characteristics, as discussed later

Gas sputtering and recycling, metal self-sputtering

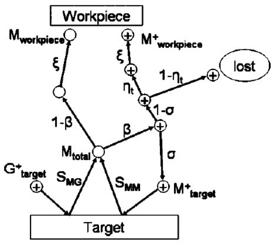

DJ Christie, JVST A 23,330, 2005

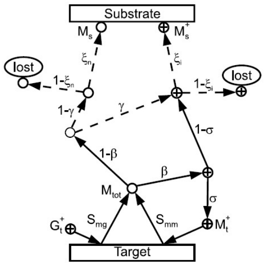

J Vlcek K Burkalova
Plasma Sources Sci Techn 19, 065010, 2010

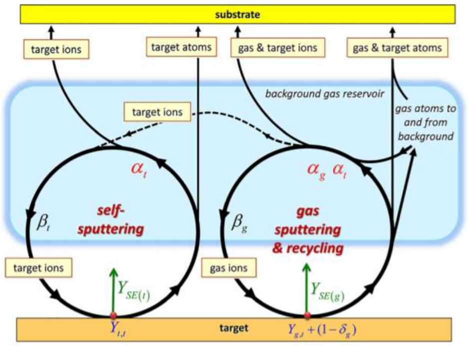

FIG. 19. Illustration of fluxes including self-sputtering, sputtering by gas, and repeated use ("recycling") of gas atoms. Figures like that illustrate a system of nonlinear rate equations. Reprinted with permission from Anders *et al.*, J. Phys. D: Appl. Phys. **45**, 012003 (2012). Copyright 2012 the IOP Publishing Ltd. (Fig. 1 from Ref. 84).

A Anders, J Capek, M Hala and L Martinu
J Phys D 45, 012003 (2012)

A unified treatment of self-sputtering, process gas recycling, and runaway for high power impulse sputtering magnetrons

Plasma Sources Sci. Technol. **26** (2017) 125003 (13pp)

N Brenning[1,2,3], **J T Gudmundsson**[1,2,4], **M A Raadu**[1], **T J Petty**[2], **T Minea**[2] **and D Lundin**[2,5]

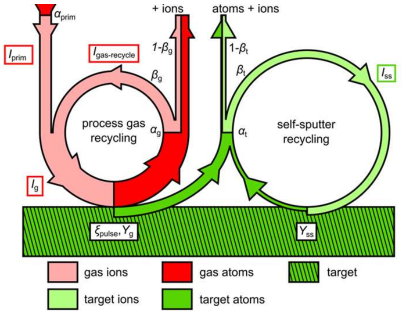

Figure 1. A schematic illustration, revised from Anders *et al* [9], of the combined processes of process gas recycling and self-sputter recycling. The widths of the flow arrows are drawn to scale with a parameter combination $\alpha_{prim} = 1$, $\xi_{pulse} = 1$, $\alpha_g = 0.7$, $\beta_t = 0.7$, $Y_g = 0.4$, $\alpha_t = 0.8$, $\beta_t = 0.7$, and $Y_{SS} = 0.5$. This combination is arbitrarily chosen as suitable to illustrate combined gas-recycling and SS-recycling.

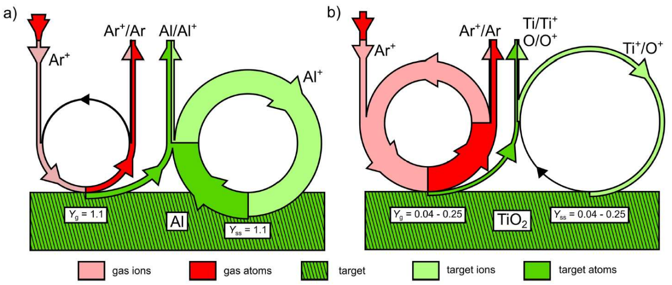

Figure 7. Recycling loops such as in figure 1, with the widths of the arrows drawn to scale for two cases from figure 6: one (a) showing the discharge with an Al target where SS-recycling dominates, and one (b) showing the discharge with a TiO_2 target where gas-recycling dominates.

Inert gas sputtering and self-sputtering yield important

Time evolution and the energy distribution of the gas and metal ion fluxes in HiPIMS
by in-situ ion mass spectrometry measurements

- Time separation between the gas and the metal ions (gas rarefaction)
  important for HiPIMS with metal ions synchronized bias and bipolar HiPIMS
- Control of doubly charged ions in HIPIMS
  important for metastable films synthesis (examples tomorrow)
- High energy metal ions in HIPIMS

Prof. Greg Greczynski

Gas rarefaction effects during high power pulsed magnetron sputtering of groups IVb and VIb transition metals in Ar **JVST A, 35, 060601 (2017)**

Grzegorz Greczynski, Igor Zhirkov, Ivan Petrov, J. E. Greene, and Johanna Rosen

Time separation between the gas and the metal ions

Depends on the peak current, on the material (next slide), and on the pulse length

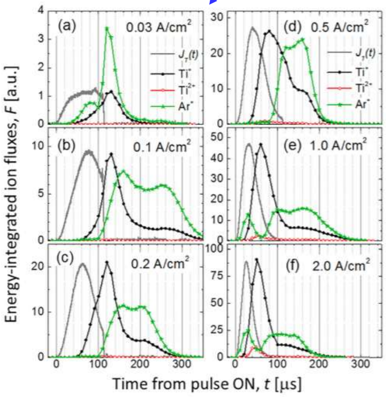

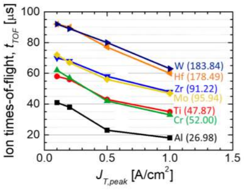

Time of flight (average ion velocity) depends on the peak current and ion mass

The HiPIMS pulse length is 120 µs at a frequency of 300 Hz.

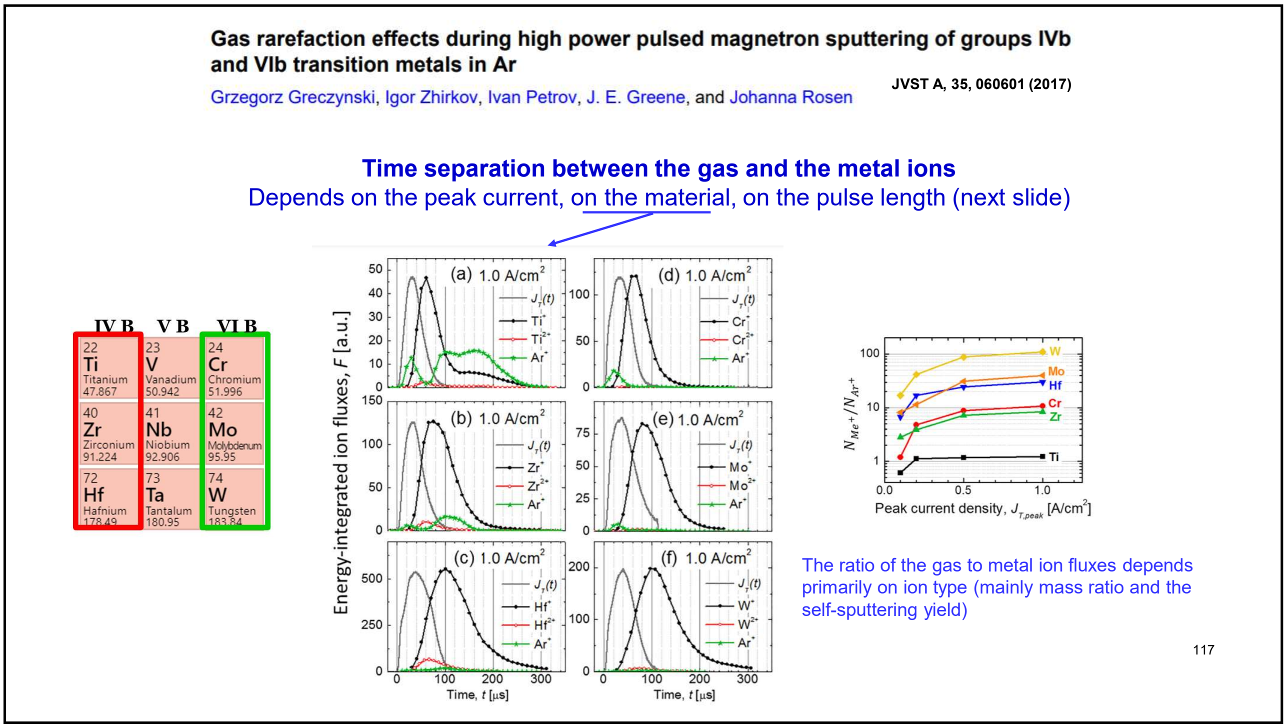

Gas rarefaction effects during high power pulsed magnetron sputtering of groups IVb and VIb transition metals in Ar

Grzegorz Greczynski, Igor Zhirkov, Ivan Petrov, J. E. Greene, and Johanna Rosen

JVST A, 35, 060601 (2017)

Time separation between the gas and the metal ions

Depends on the peak current, on the material, on the pulse length (next slide)

The ratio of the gas to metal ion fluxes depends primarily on ion type (mainly mass ratio and the self-sputtering yield)

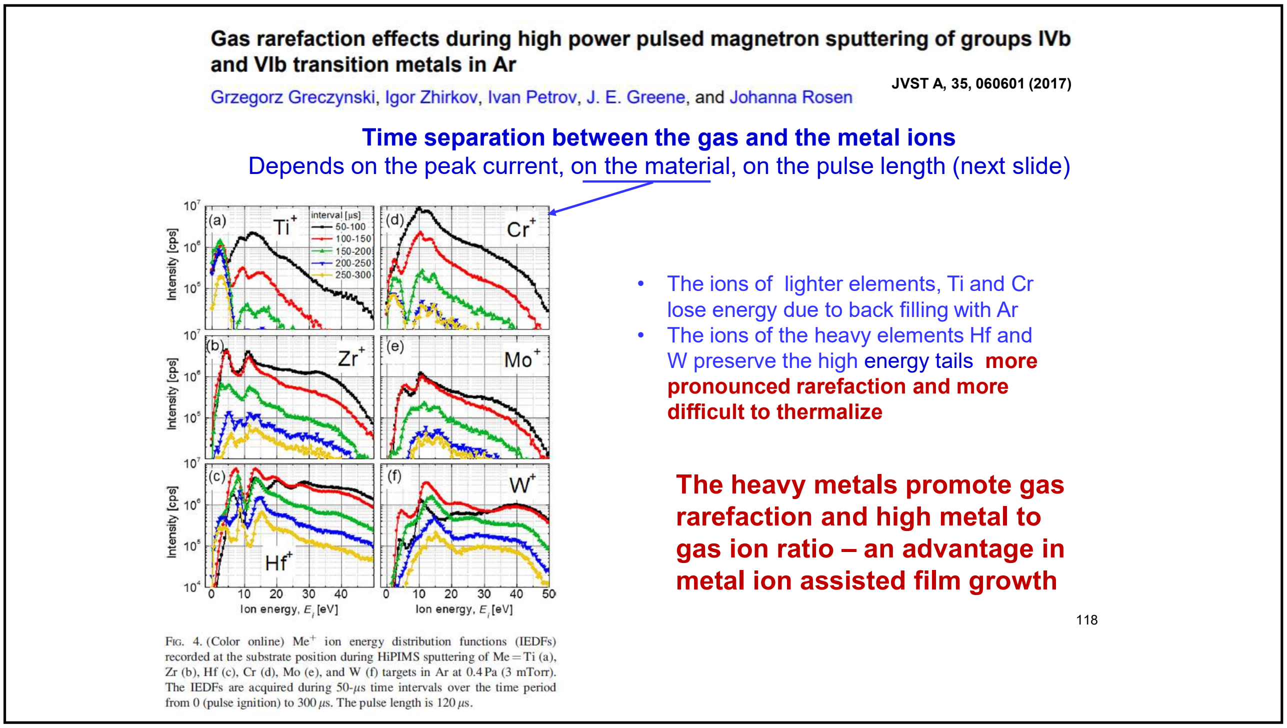

Gas rarefaction effects during high power pulsed magnetron sputtering of groups IVb and VIb transition metals in Ar

Grzegorz Greczynski, Igor Zhirkov, Ivan Petrov, J. E. Greene, and Johanna Rosen

JVST A, 35, 060601 (2017)

Time separation between the gas and the metal ions

Depends on the peak current, on the material, on the pulse length (next slide)

FIG. 4. (Color online) Me⁺ ion energy distribution functions (IEDFs) recorded at the substrate position during HiPIMS sputtering of Me = Ti (a), Zr (b), Hf (c), Cr (d), Mo (e), and W (f) targets in Ar at 0.4 Pa (3 mTorr). The IEDFs are acquired during 50-µs time intervals over the time period from 0 (pulse ignition) to 300 µs. The pulse length is 120 µs.

- The ions of lighter elements, Ti and Cr lose energy due to back filling with Ar
- The ions of the heavy elements Hf and W preserve the high energy tails **more pronounced rarefaction and more difficult to thermalize**

The heavy metals promote gas rarefaction and high metal to gas ion ratio – an advantage in metal ion assisted film growth

Control of the metal/gas ion ratio incident at the substrate plane during high-power impulse magnetron sputtering of transition metals in Ar

G. Greczynski[a,*], I. Zhirkov[a], I. Petrov[a,b], J.E. Greene[a,b,c], J. Rosen[a] Thin Solid Films 642 (2017) 36–40

Time separation between the gas and the metal ions
Depends on the peak current, on the material, on the pulse length)

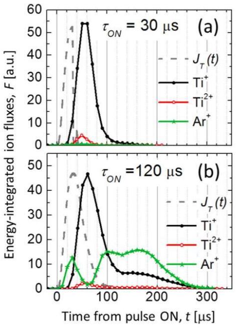

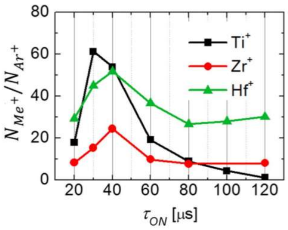

Reactive sputtering: Ion mass spectrometry at substrate position to determine the metal ion dominated phase

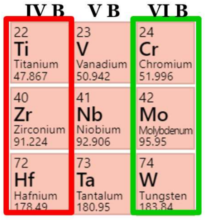

IV B	V B	VI B
22 Ti Titanium 47.867	23 V Vanadium 50.942	24 Cr Chromium 51.996
40 Zr Zirconium 91.224	41 Nb Niobium 92.906	42 Mo Molybdenum 95.95
72 Hf Hafnium 178.49	73 Ta Tantalum 180.95	74 W Tungsten 183.84

p =3 mTorr; N_2/Ar flow ratio of 0.11
Peak Current 1 A/cm^2

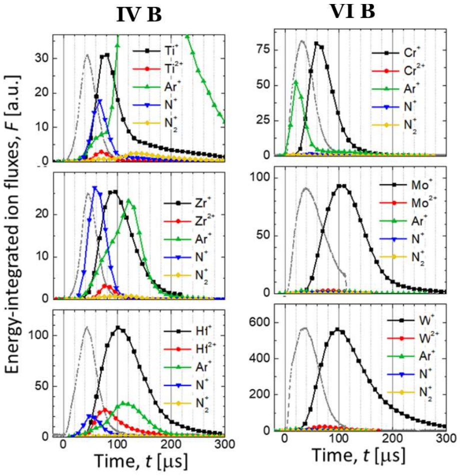

Ar$^+$ overlaps with Me$^+$ Ar$^+$ separated from Me$^+$

Grzegorz Greczynski, Igor Zhirkov, Ivan Petrov, J. E. Greene, and Johanna Rosen, JVST A 36, 020602 (2018);

Reactive sputtering: Ion mass spectrometry at substrate position to determine the metal ion dominated phase

Metal ion synchronized bias

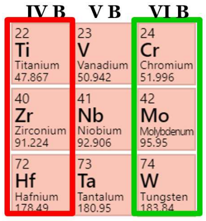

p =3 mTorr; N_2/Ar flow ratio of 0.11
Peak Current 1 A/cm^2

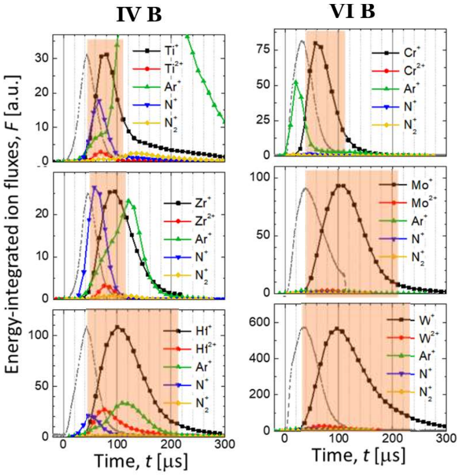

Ar$^+$ overlaps with Me$^+$ Ar$^+$ separated from Me$^+$

Grzegorz Greczynski, Igor Zhirkov, Ivan Petrov, J. E. Greene, and Johanna Rosen, JVST A 36, 020602 (2018);

Changes in the Me^{2+} component

Important for metastable materials synthesis

Ion energy distribution functions for metal ions

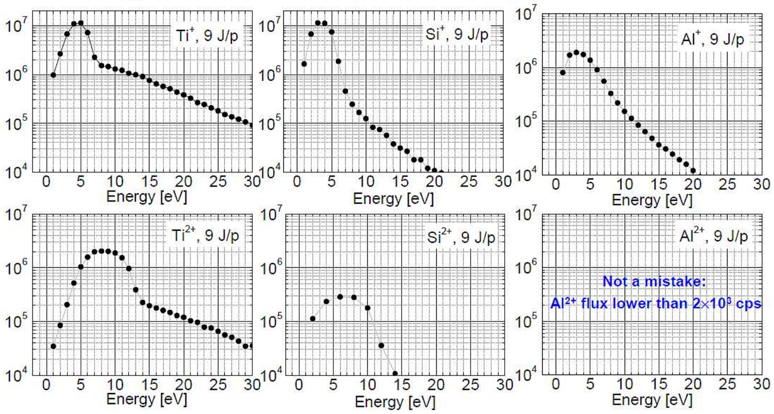

Not a mistake:
Al^{2+} flux lower than 2×10^3 cps

- Second ionization potential: Ti: 13.62 eV, Si: 16.35 eV, Al: 18.89 eV

Ar first ionization potential 15.76 eV

Control of doubly charged ions in HIPIMS

Model system: Ti sputtered in Ne, Ar, Kr, and Xe

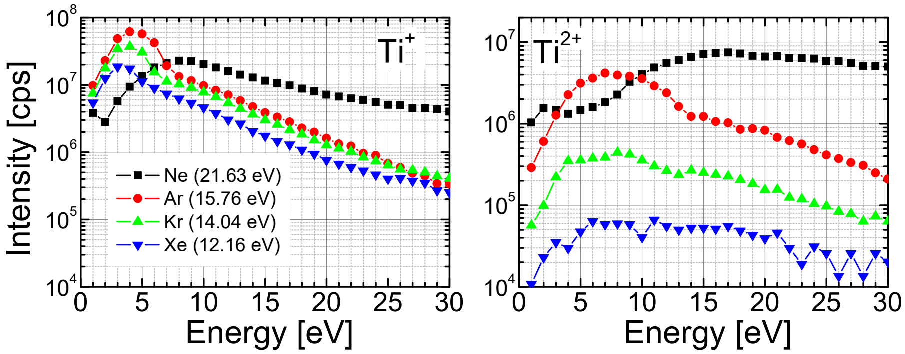

Ionization potentials
Ne - 21.56 eV
Ar - 15.76 eV
Kr – 14.00 eV
Xe - 12.13 eV

- Ti^{2+} detrimental to TiAlN films grown by HIPIMS/DCMS
- Reason for high Ti^{2+} population while sputtering in Ar: $IP^2_{Ti} < IP^1_{Ar}$
- exchanging Ar for lower IP gases (Kr, Xe) decreases T_e and the relative amount of Ti^{2+}, while the opposite is valid for Ne which has highest IP

G. Greczynski, I. Petrov, J.E. Greene, and L. Hultman, *Vacuum* 116 (2015) 36

$J_{Ti^{2+}}/J_{Ti^+}$: comparison for Ne, Ar, Kr and Xe

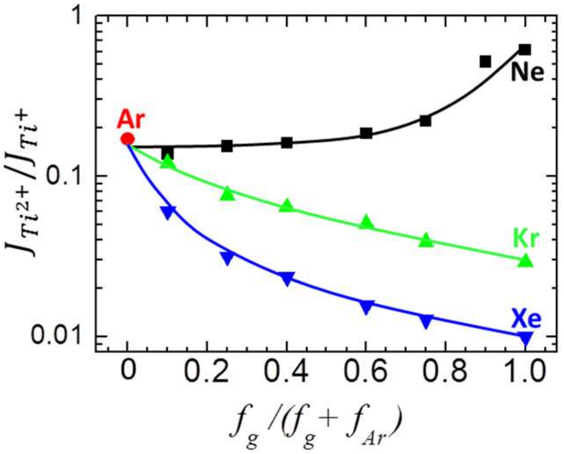

- by changing noble-gas mixtures, $J_{Ti^{2+}}$ varies by more than two orders of magnitude with only a small change in J_{Ti^+}.
- This allows the ratio $J_{Ti^{2+}}/J_{Ti^+}$ to be continuously tuned from 0.01 with Xe to 0.62 with Ne

G. Greczynski, I. Petrov, J.E. Greene, and L. Hultman, *Vacuum* 116 (2015) 36

Extension to other materials

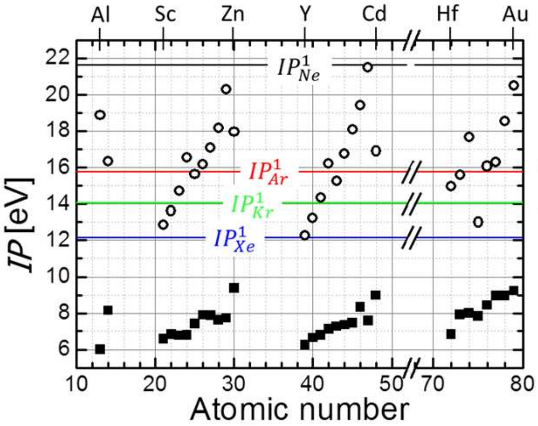

empty circles - second ionization potentials, IP^2_{Me}

$$IP^1_{Xe} < IP^2_{Me} < IP^1_{Ne}$$

$$IP^1_{Me} < IP^1_{Xe}$$

full squares - first ionization potentials, IP^1_{Me}

G. Greczynski, I. Petrov, J.E. Greene, and L. Hultman, *Vacuum* 116 (2015) 36

An example of the importance of the choice of inert sputtering gas

Low temperature epitaxial growth of HfN/MgO(100) via HiPIMS-synchronized pulsed substrate bias

HfN the highest melting point TM nitride: T_M ~ 3520 K

T_S < 70 °C; T_S/T_M < 0.1

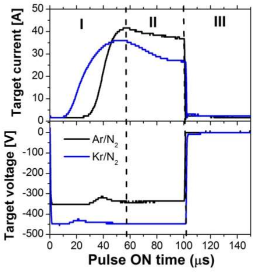

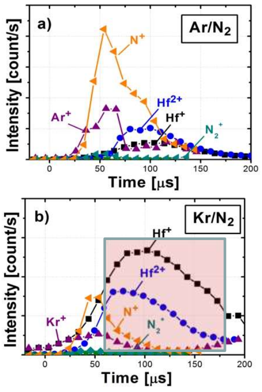

V_s = -100 V

IP_{Ar} = 15.8 eV
IP_N = 14.5 eV
IP_{N2} =15.6 eV
IP_{Kr} = 14.0 eV

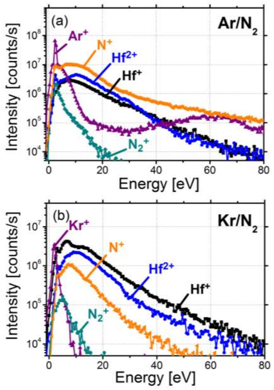

M.M.S. Villamayor,T. Shimizu, J. Keraudy, R.P.B. Viloan, R. Boyd, D. Lundin, J.E. Greene, Ivan Petrov, Ulf Helmersson J. Vac. Sci. Technol. A, Vol. 36 (2018) 06151

An example of the importance of the choice of inert sputtering gas

Low temperature epitaxial growth of HfN/MgO(100) via HiPIMS-synchronized pulsed substrate bias

HfN the highest melting point TM nitride: T_M ~ 3520 K

T_S < 70 °C; T_S/T_M < 0.1

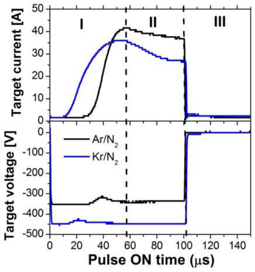

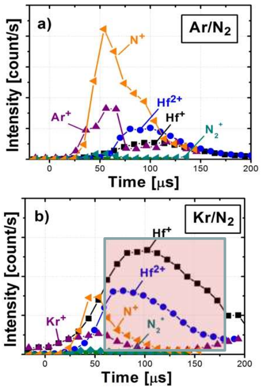

V_s = -100 V

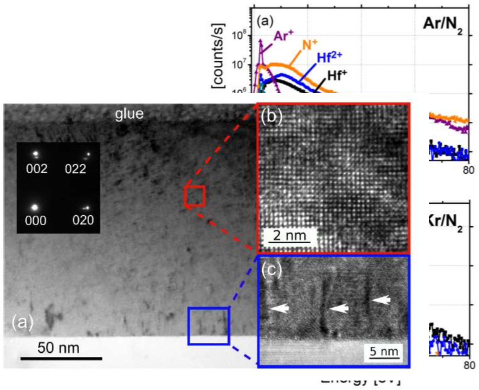

M.M.S. Villamayor,T. Shimizu, J. Keraudy, R.P.B. Viloan, R. Boyd, D. Lundin, J.E. Greene, Ivan Petrov, Ulf Helmersson J. Vac. Sci. Technol. A, Vol. 36 (2018) 06151

HiPIMS: source of energetic metal ions

J. Bohlmark, M. Lattemann, J.T. Gudmundsson, A.P. Ehiasarian,
Y. Aranda Gonzalvo, N. Brenning, U. Helmersson
The ion energy distributions and ion flux composition from a high-power impulse magnetron sputtering discharge
Thin Solid Films 515 (2006) 1522–1526

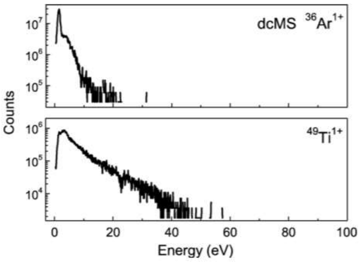

Fig. 2. The ion energy distributions taken from a conventional DC magnetron discharge. The Ar pressure was 0.4 Pa, the applied power 1 kW, and the target material was Ti. The recorded counts have been adjusted with the corresponding isotope abundance.

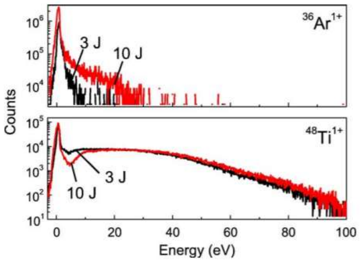

Fig. 3. The ion energy distributions for Ar^{1+} and Ti^{1+} ions measured from a HIPIMS discharge. The Ar pressure was 0.4 Pa, the pulse energy 3 and 10 J, and the target was made of Ti. The recorded counts have been adjusted with the corresponding isotope abundance.

Higher-energy metal ions

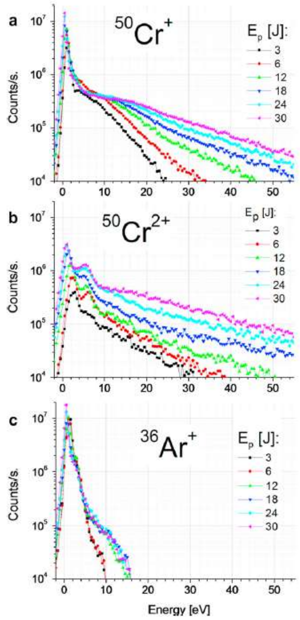

Ion Energy Distribution Functions

high-energy tails due to
- gas rarefaction
- potential humps of associated
with traveling ionization zones – next slide

G. Greczynski, L. Hultman, Vacuum 84 (2010) 1159

Higher-energy metal ions

APPLIED PHYSICS LETTERS **103**, 144103 (2013)

Drifting potential humps in ionization zones: The "propeller blades" of high power impulse magnetron sputtering

André Anders,[1,a)] Matjaž Panjan,[1,2] Robert Franz,[1,3] Joakim Andersson,[1,4] and Pavel Ni[1]

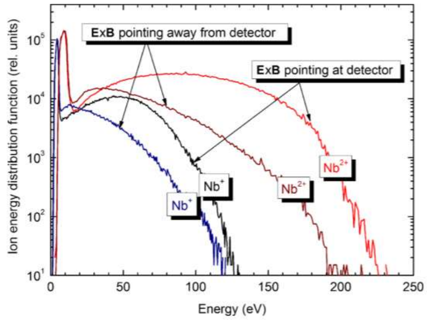

FIG. 2. Ion energy distribution function measured with a Hiden EQP300 energy analyzer at 140 mm distance from the target, recording niobium ions emitted near the target plane tangentially from the racetrack; discharge voltage 350 V, 200 μs pulse length, 100 pulses per second, 275 A peak, in 0.53 Pa of Ar.

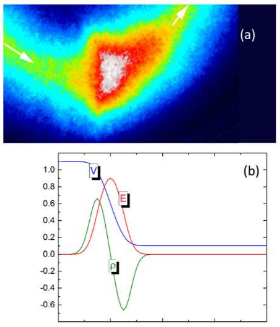

$$E_i = E_0 + \frac{m_i}{2} v_{IZ}^2 + eQV_{hump}, \qquad (8)$$

where E_0 represents the energy from the sputtering and collisional processes, v_{IZ} is the drift velocity of the ionization zone, Q is the ion charge state number, and V_{hump} is the height of the potential hump. Ions moving in the opposite

Andre Anders

Potential humps – double layer

Slide by Andre Anders

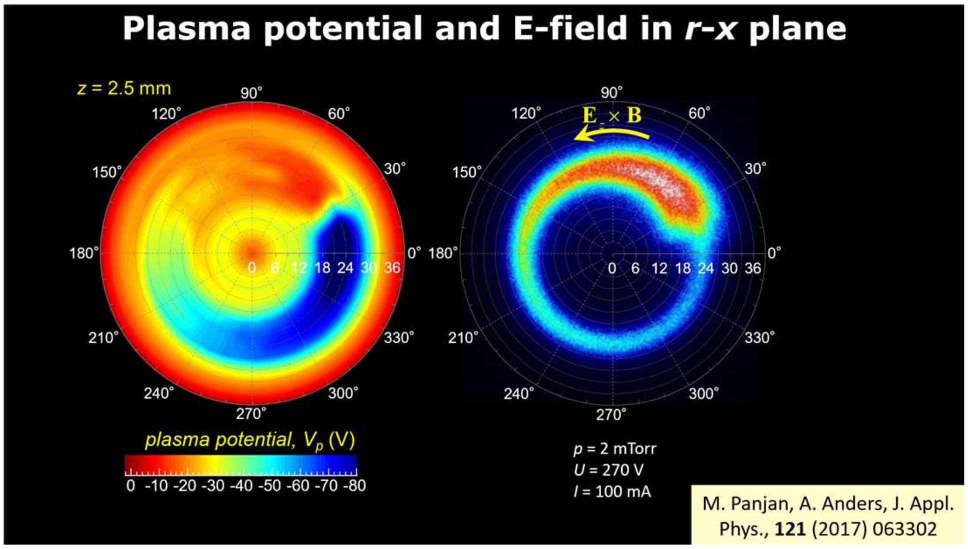

Plasma potential and E-field in *r*-*x* plane

z = 2.5 mm

plasma potential, V_p (V)

p = 2 mTorr
U = 270 V
I = 100 mA

M. Panjan, A. Anders, J. Appl. Phys., **121** (2017) 063302

Further reading on spokes and high energy metal ions in HIPIMS

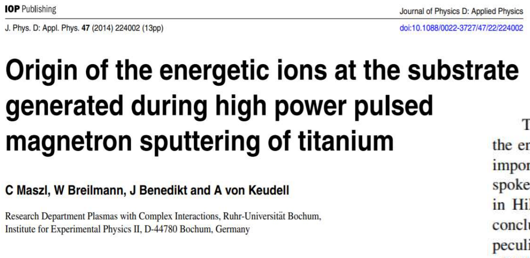

IOP Publishing Journal of Physics D: Applied Physics
J. Phys. D: Appl. Phys. **47** (2014) 224002 (13pp) doi:10.1088/0022-3727/47/22/224002

Origin of the energetic ions at the substrate generated during high power pulsed magnetron sputtering of titanium

C Maszl, W Breilmann, J Benedikt and A von Keudell

Research Department Plasmas with Complex Interactions, Ruhr-Universität Bochum, Institute for Experimental Physics II, D-44780 Bochum, Germany

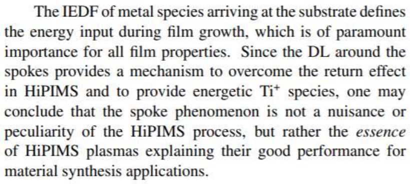

The IEDF of metal species arriving at the substrate defines the energy input during film growth, which is of paramount importance for all film properties. Since the DL around the spokes provides a mechanism to overcome the return effect in HiPIMS and to provide energetic Ti^+ species, one may conclude that the spoke phenomenon is not a nuisance or peculiarity of the HiPIMS process, but rather the *essence* of HiPIMS plasmas explaining their good performance for material synthesis applications.

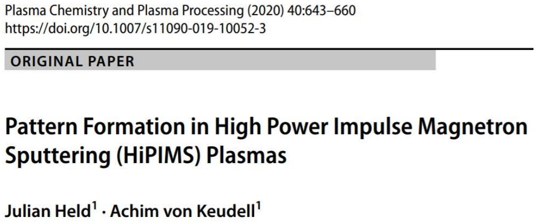

Plasma Chemistry and Plasma Processing (2020) 40:643–660
https://doi.org/10.1007/s11090-019-10052-3

ORIGINAL PAPER

Pattern Formation in High Power Impulse Magnetron Sputtering (HiPIMS) Plasmas

Julian Held[1] · Achim von Keudell[1]

Bipolar pulsed high-power impulse magnetron sputtering

Bipolar pulsed high-power impulse magnetron sputtering

G.Eichenhofer, I Fernandez, A Wennberg
Vakuum in Forschung und Praxis · April 2017

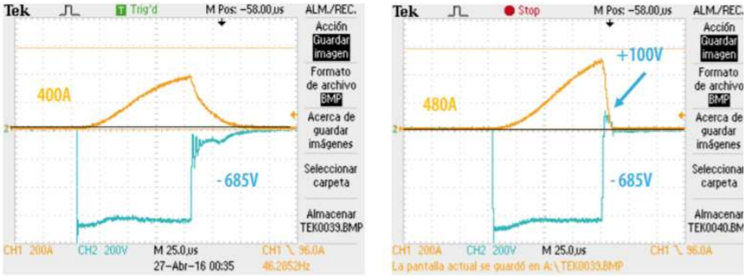

Ivan Fernandez: Nano4Energy

- Novel HIPIMS power supply the hiPV, hiPlus option
- positive voltage reversal for **positive ion assisted deposition on insulating substrates with reducing the tendency to arcing.**

nano4ENERGY

Bipolar pulsed high-power impulse magnetron sputtering

Increased deposition rate

Wu, Haehnlein, Shchelkanov, McLain, Patel, Uhlig, Jurczyk, Leng, Ruzic, *Vacuum, 150, 216* (2018)

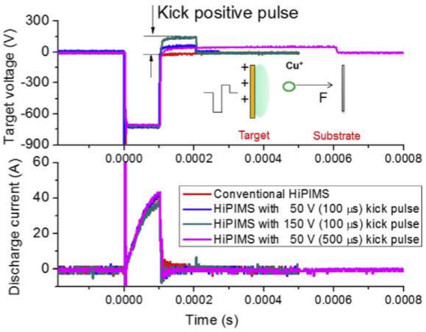

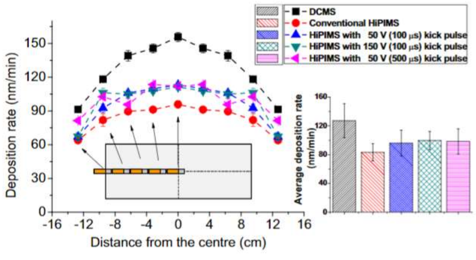

Fig. 3. Deposition rate of Cu films across the center-line length of Cu target. Average deposition rate is the average value of deposition rate of all the samples at different position.

Bipolar pulsed high-power impulse magnetron sputtering

Precise control of ion energy

Velicua,Ianoş, Porosnicu, Mihăilă, Burducea, Velea, Cristea, Munteanu,Tiron, SCT 359, (2019),97-107

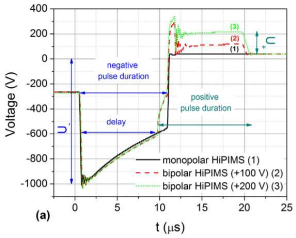

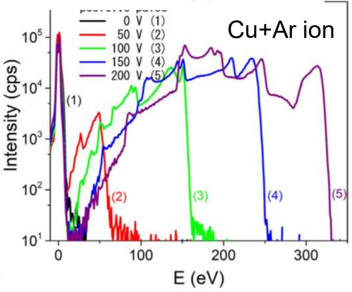

Keraudy, Viloan, Raadu, Brenning, Lundin, Helmersson, SCT 359, (2019),433

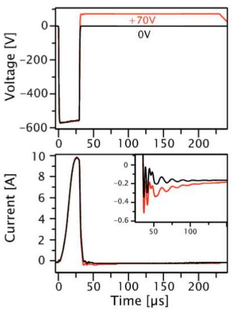

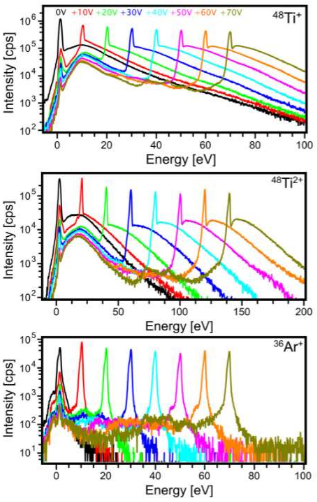

Experimental verification of deposition rate increase, with maintained high ionized flux fraction, by shortening the HiPIMS pulse

Plasma Sources Sci. Technol. **30** (2021) 045006 (8pp)

T Shimizu[1,2], **M Zanáška**[1], **R P Villoan**[1], **N Brenning**[1,3], **U Helmersson**[1] **and Daniel Lundin**[1,4,*]

Plasma Sources Sci. Technol. **30** (2021) 045006 T Shimizu *et al*

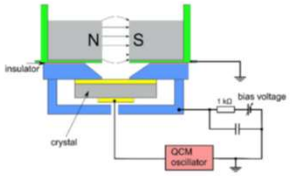

Figure 5. Schematic of the gridless ion meter. Impinging electrons are repelled by a local magnetic field, which prevents the electrons from reaching the biased top QCM electrode.

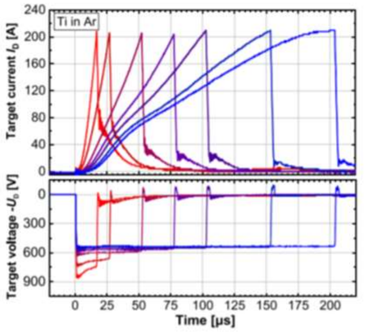

Figure 1. The applied discharge voltage U_D (lower panel) and the resulting discharge current $\langle I_D \rangle$ (upper panel) waveforms of the Ti/Ar discharge when varying the pulse length in the range 15–200 µs. The discharge voltage was adjusted to maintain a peak current of 200 A ($J_{D,peak} = 1.10$ A cm^{-2}). The pulse repetition frequency was adjusted to maintain a constant time-averaged power of 1 kW.

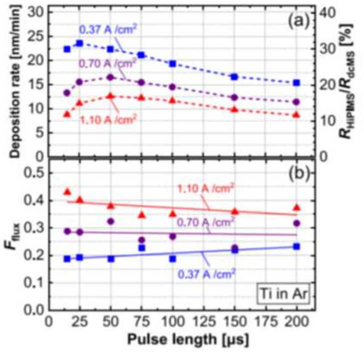

Figure 2. (a) Deposition rate (left axis) with corresponding normalized HiPIMS deposition rate to the dcMS deposition rate, R_{HiPIMS}/R_{dcMS} (right axis), and (b) Ionized flux fraction F_{flux} as a function of pulse length for three different $J_{D,peak}$ of 0.37, 0.70 and 1.10 A cm^{-2}. An averaged power of 1 kW is maintained constant independent of pulse length and $J_{D,peak}$.

Tutorial: Reactive high power impulse magnetron sputtering (R-HiPIMS)

Cite as: J. Appl. Phys. **121**, 171101 (2017); https://doi.org/10.1063/1.4978350
Submitted: 17 November 2016 . Accepted: 18 February 2017 . Published Online: 21 March 2017

André Anders

JOURNAL OF APPLIED PHYSICS **121**, 080901 (2017)

Perspective: Is there a hysteresis during reactive High Power Impulse Magnetron Sputtering (R-HiPIMS)?

K. Strijckmans, F. Moens, and D. Depla
Department of Solid State Sciences, Ghent University, Krijgslaan 281(S1), 9000 Gent, Belgium

Smooth composition control of oxynitrides - TaON (HIPIMS with feedback pulsed reactive gas flow control (RGFC))

J. Rezek, J. Vlcek, J. Houska, R. Cerstvy, Thin Solid Films 566, 70 (2014)

Reactive gas inlets in front of the target and oriented towards the target + dense HIPIMS plasma

⇓

dissociation of O_2 and N_2

~~different reactivities of O_2 and N_2~~

comparable reactivities of O and N

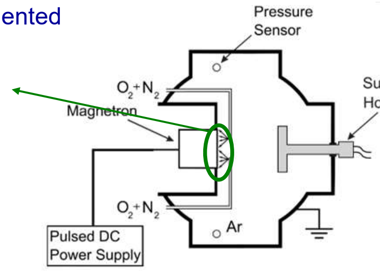

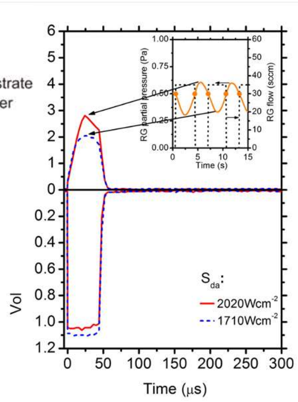

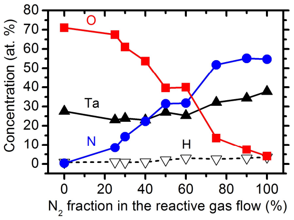

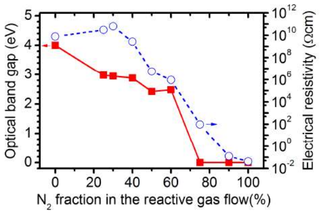

Benefits of the controlled reactive high-power impulse magnetron sputtering of stoichiometric ZrO_2 films

J. Vlček*, J. Rezek, J. Houška, T. Kozák, J. Kohout

Vacuum 114 (2015) 131–141

Department of Physics and NTIS, European Centre of Excellence, University of West Bohemia, Univerzitní 8, 30614 Plzeň, Czech Republic

Major advance: HIPIMS with feedback pulsed reactive gas flow control (RGFC)

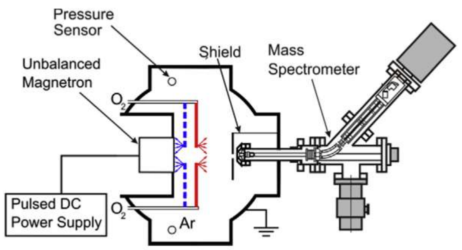

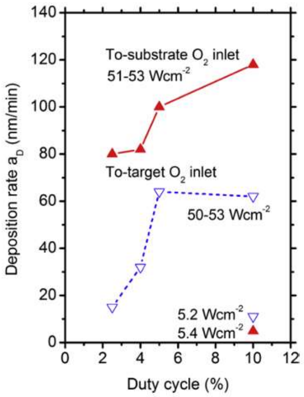

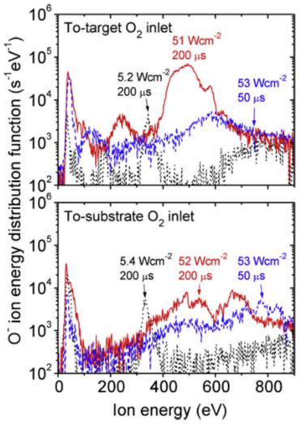

Bibliography

(vacuum, plasmas)

P.A. Redhead, J.P. Hobson, and E.V. Kornelsenn, *The Physical Basis of Ultrahigh Vacuum*, Chapman and Hall, London, 1968.

A. Neugebauer, “Condensation, Nucleation, and Growth of Thin Films,” in *Handbook of Thin Film Technology*, edited by L.I. Maissel and R. Glang, McGraw-Hill, New York 1970.

J.E. Greene, “Physics of Film Growth from the Vapor Phase,” in *Multicomponent and Multilayered Thin Films for Advanced Technologies: Techniques, Fundamentals, and Devices*, ed. by O. Auciello, NATO Advanced Study Institute, Kluwer Academic Publishers, Boston 1993, p. 39.

R. Glang, “Vacuum Evaporation,” in *Handbook of Thin Film Technology*, edited by L. I. Maissel and R. Glang, McGraw-Hill, NY (1970)..

G.K. Wehner and G.S. Anderson, “The Nature of Physical Sputtering” in *Handbook of Thin Film Technology*, edited by L.I. Maissel and R. Glang, McGraw-Hill, NY 1970.

B. Chapman, *Glow Discharge Processes*, Wiley Interscience, New York 1980.

J.A. Thornton and J.E. Greene, “Plasmas in Deposition Process,” in *Deposition Technologies for Films and Coatings*, edited by R.F. Bunshah, Noayes Publications, Park Ridge, New Jersey 1994, p. 29.

S.M. Rossnagel, “Magnetron Plasma Deposition Processes,” in *Handbook of Plasma Processing Technology*, edited by S.M. Rossnagel, J.J. Cuomo, and W.D. Westwood Noyes Publications, Park Ridge, New Jersey 1990.

K.H. Müller, “Film Growth Modification by Concurrent Ion Bombardment: Theory and Simulation,” in *Handbook of Ion-Beam Processing Technology*, edited by J.J. Coumo, S.M. Rossnagel, and H.R. Kaufman, Noyes Publications, Park Ridge, New Jersey 1989, p. 241.

Bibliography

(sputtering, sputter deposition)

P. Sigmund, “Theory of Sputtering I. Sputtering Yield of Amorphous and Polycrystalline Targets,” Physical Review. 184, 383 (1969).

P.Sigmund, “Sputtering by ion bombardment: theoretical concepts”, in *Sputtering by particle bombardment* I, edited by R. Behrish, Springer-Verlag, 1981

HH Anderson and HL Bay, “Sputtering yield measurements”, in *Sputtering by particle bombardment* I, edited by R. Behrish, Springer-Verlag, 1981

G.K. Wehner and G.S. Anderson, “The Nature of Physical Sputtering” in *Handbook of Thin Film Technology*, edited by L.I. Maissel and R. Glang, McGraw-Hill, NY 1970.

J.L. Vossen and J.J. Cuomo, “Glow Discharge Sputter Deposition, “ in *Thin Film Processes*, edited by J.L. Vossen and W. Kern, Academic Press, NY 1978.

J.A. Thornton and A.S. Penfold, “Cylindrical Magnetron Sputtering,” in *Thin Film Processes*, edited by J.L. Vossen and W. Kern, Academic Press, NY 1978.

R.K. Waits, “Planar Magnetron Sputtering,” in *Thin Film Processes*, edited by J.L. Vossen and W. Kern, Academic Press, New York 1978.

B. Chapman, *Glow Discharge Processes*, Wiley Interscience, New York 1980.

J.A. Thornton and J.E. Greene, “Plasmas in Deposition Processes,” in *Deposition Technologies for Films and Coatings*, edited by R.F. Bunshah, Noayes Publications, Park Ridge, New Jersey 1994, p. 29.

S.M. Rossnagel, “Magnetron Plasma Deposition Processes,” in *Handbook of Plasma Processing Technology*, edited by S.M. Rossnagel, J.J. Cuomo, and W.D. Westwood Noyes Publications, Park Ridge, New Jersey 1990.

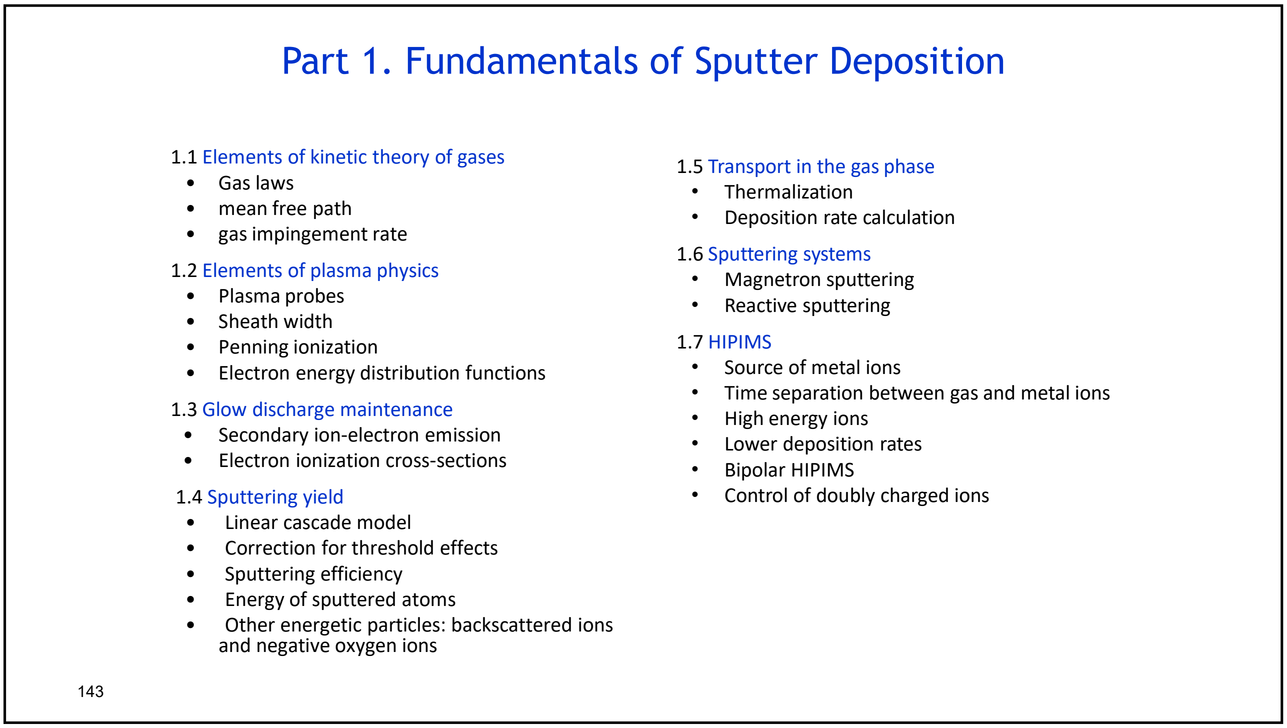

Part 1. Fundamentals of Sputter Deposition

1.1 Elements of kinetic theory of gases
- Gas laws
- mean free path
- gas impingement rate

1.2 Elements of plasma physics
- Plasma probes
- Sheath width
- Penning ionization
- Electron energy distribution functions

1.3 Glow discharge maintenance
- Secondary ion-electron emission
- Electron ionization cross-sections

1.4 Sputtering yield
- Linear cascade model
- Correction for threshold effects
- Sputtering efficiency
- Energy of sputtered atoms
- Other energetic particles: backscattered ions and negative oxygen ions

1.5 Transport in the gas phase
- Thermalization
- Deposition rate calculation

1.6 Sputtering systems
- Magnetron sputtering
- Reactive sputtering

1.7 HIPIMS
- Source of metal ions
- Time separation between gas and metal ions
- High energy ions
- Lower deposition rates
- Bipolar HIPIMS
- Control of doubly charged ions